Synthesis and photophysical properties of neutral and cationic octahedral tungsten iodide clusters

Dissertation

der Mathematisch-Naturwissenschaftlichen Fakultät

der Eberhard Karls Universität Tübingen

zur Erlangung des Grades eines

Doktors der Naturwissenschaften

(Dr. rer. nat.)

vorgelegt von

M. Sc. Florian Pachel

aus Marktredwitz

Tübingen

2023

Gedruckt mit Genehmigung der Mathematisch-Naturwissenschaftlichen Fakultät der Eberhard Karls Universität Tübingen.

Tag der mündlichen Qualifikation:	30.06.2023
Dekan:	Prof. Dr. Thilo Stehle
1. Berichterstatter/-in:	Prof. Dr. Hans-Jürgen Meyer
2. Berichterstatter/-in:	Prof. Dr. Eberhard Schweda

Acknowledgements

First of all, I would like to thank my supervisor Prof. Dr. Hans-Jürgen Meyer for the opportunity to work in his group on this particularly interesting topic. The possibility to work independently, the support whenever needed and the many insightful advice are greatly appreciated.
Moreover, I owe special thanks to Dr. Markus Ströbele for all the helpful suggestions regarding single crystal and powder X-ray diffraction as well as solid state chemistry in general.
I would like to express my gratitude to Prof. Dr. Thomas Jüstel and Dr. David Enseling for many recorded photoluminescence measurements, help and advice on all questions regarding photoluminescence and for the overall productive cooperation.
Similarly, I would like to thank Prof. Dr. Marcus Scheele and Philipp Frech for the enjoyable joint work on the transient absorption spectroscopy on tungsten iodide clusters and the paper we published together.
Furthermore, I thank Dr. Carl Romao for the theoretical calculations and the helpful phrasing advice.
In addition, I would also like to thank Dr. Theo Maulbetsch, Viola Munzert and Prof. Dr. Doris Kunz for the great collaboration on the Cluster-Fe-Carbenaporphyrine compound.
I thank Peter Janoschek for the conducted reflection spectra.
My special thanks go to Patrick Schmidt with whom I worked together during the entire four years of my Ph.D. We were always able to rely on each other for support, ideas and assistance when needed.
Additionally, I would like to thank Dr. Jochen Glaser for the magnetic measurements, the support in their interpretation and helpful advice on many different occasions.
I am grateful to Dr. Wolfgang Leis for recording some photoluminescence spectra and support with the interpretation.
Also, I thank Christian Gienger, Angelika Oswald, Serhat Kilicarslan, and Dr. Nicole Mews for the nice time together supervising the lab course.
Further, profuse thanks go to Dr. Manuel Löber, Dr. Thorsten Hummel, Elaheh Bayat, Fabian Grahlow, Jan Beitlberger, Albert Schwarz, Kai Röseler, Jacqueline Händel, Paula Kallenbach, Catharina Brand, Melena Groß, and Jonas Hiller. It was terrific to work with you and also to spend time with you guys! I could not have asked for better colleagues!
I would also like to thank Jonas von Festenberg, Ronja Wüstefeld, Sophia Westendorf, Arin-Daniel Fuhrmann, Dr. Amira Siai, Albert Kraft, Robert Richter, and Ann-Kathrin Kaiser for their support.

I am equally greatful to all those who supported this work by measuring samples, supplying or disposing of chemicals, purchasing required material, making repairs, blowing glass or organizing work.
Finally, I thank my wonderful girlfriend Franziska Robl and our two families for their constant support.

Table of Contents

List of Abbreviations

DCM	Dichloromethane
DMF	Dimethylformamide
DMSO	Dimethyl Sulfoxide
EA	Elemental Analysis
EDX	Energy Dispersive X-Ray Spectroscopy
ELF	Electron Localization Function
EtOH	Ethanol
FWHM	Full Width at Half Maximum
HOMO	Highest Occupied Molecular Orbital
IC	Internal Conversion
IR	Infrared
ISC	Intersystem Crossing
NMR	Nuclear Magnetic Resonance
OTs	p-Toluene sulfonate
PPN	Bis(triphenylphosphine)iminium
PPh_4	Tetraphenylphosphonium
PXRD	Powder X-Ray Diffraction
RE	Rare-Earth
RhB	Rhodamine B
SEM	Scanning Electron Microscope
TBA	Tetrabutylammonium
TEA	Tetraethylammonium
THF	Tetrahydrofuran
XRD	Single-crystal X-Ray Diffraction

Summary

In the course of this thesis, the first crystal structures of cationic and neutral tungsten iodide clusters were solved and published. In the first step the compound $[(W_6I_8)I_3(CH_3CN)_3]I_7 \cdot I_2$ featuring the heteroleptic cluster cation $[(W_6I_8)I_3(CH_3CN)_3]^+$ was synthesized as bulk material. Follow-up experiments starting from $[(W_6I_8)I_3(CH_3CN)_3]I_7 \cdot I_2$ yielded the two species $[(W_6I_8)I(CH_3CN)_5](I_3)_2(BF_4)$ and $[(W_6I_8)(CH_3CN)_6](I_3)(BF_4)_3 \cdot (H_2O)$. The structures of these two compounds feature the cluster cations $[(W_6I_8)I(CH_3CN)_5]^{3+}$ and $[(W_6I_8)(CH_3CN)_6]^{4+}$. Anions in the three mentioned compounds are either I_3^- or I_7^-, which cause a dark crystal or powder color and no obvious photoluminescence.

Further conducted reactions gave $[W_6I_8(CH_3CN)_6](BF_4)_4 \cdot (CH_3CN)_2$ as a yellow powder or plated-shaped crystals. The crystalline compound shows the typical octahedral metal halide cluster photoluminescence with characteristic broad excitation and emission bands. However, in contrast to species bearing electron-withdrawing ligands, emission lifetimes are short, and no quenching in the presence of molecular oxygen is observed. The calculated Electron Localization Function (ELF) revealed significantly higher d-electron density above the tungsten atoms and reduced ionicity of the W–N bond for $[W_6I_8(CH_3CN)_6](BF_4)_4 \cdot (CH_3CN)_2$ compared to $(TBA)_2[W_6I_8(CO_2C_3F_7)_6]$, which is a strong quencher. This leads to the conclusion that the ionicity of the W–Ligand bond influences the energetic splitting of the emitting triplet sublevels and therefore also emission lifetimes.

Besides the mentioned cationic clusters, the neutral tungsten iodide cluster $[W_6I_{12}(NCC_6H_5)_2]$ was also synthesized and characterized for its properties. Due to two benzonitrile and four iodide as apical ligands, the compound is a heteroleptic cluster species. It shows a good hydrolysis stability and remarkable temperature stability up to 400 °C. Photoluminescence in the solid state is only weakly pronounced with low emission intensity, short lifetime and negligible quantum yield. However, the good hydrolysis and temperature stability as well as the optical band gap of 2.17 eV make the compound a perfect candidate for application in photocatalysis. This was confirmed in an experiment observing the photocatalytic decomposition of Rhodamine B (Rh B) in aqueous solution.

Additional experiments yielded the compounds $[W_6I_8(CH_3CN)_6](ClO_4)_4 \cdot (CH_3CN)_2$ and $[W_6I_8(DMSO)_6](I_3)_4$ featuring cationic clusters in their structures. Further reactions with different solvents suggest a high potential to produce many other cationic and neutral tungsten iodide clusters. This would allow for new insights into the photophysical properties of this type of cluster as well as the possibility to discover other highly stable compounds.

In addition, with the compounds $(^{n}Bu_4N)_2[M_6I_8(NCO)_6]$ (M = Mo, W), new metal iodide clusters are reported. In their structure, NCO^- anions are connected to the $[M_6I_8]$ core as apical ligands via the nitrogen atoms. In solid state, they show the typical cluster photoluminescence with weakly pronounced oxygen quenching.

For comparison of photoluminescence properties with the analogue iodides, the compounds $(PPN)_2[W_6Cl_{14}]\cdot(CH_2Cl_2)_2$ and $(PPh_4)_2[W_6Cl_{14}]\cdot(C_3H_6O)_2$ were synthesized. In solid state, the corresponding octahedral tungsten iodide clusters show high quantum yields. In contrast to this, photoluminescence of the synthesized tungsten chloride species is only weakly pronounced with short lifetimes and unquantifiable quantum yields.

Another contribution of this thesis concerns the synthesis of compounds combining tungsten clusters with metal ions onto which an energy transfer is possible. Reactions with *RE*-chlorides (*RE* = Gd, Tb, Eu) produced GdW_6Cl_{15}, TbW_6Cl_{15} and EuW_6Cl_{14} as products. Magnetic measurements revealed paramagnetism in correspondence to the magnetic moment of the *RE*-ion. Photoluminescence spectra recorded of crystalline samples show no emission of the *RE*-ions.

Cooperation with Dr. T. Maulbetsch lead to the synthesis of the compound $[Fe(CTP)]_2[W_6I_{14}]$. Photoluminescence experiments at room temperature showed no emission. Experiments conducted between 3 K and 100 K in order to clarify if an energy transfer occurs yielded the same results.

Further experiments towards the synthesis of supramolecular $[W_6I_{14}]$-metal complex compounds lead to crystals of $[Fe(CH_3CN)_6][W_6I_{14}]$. They show no sign of luminescence but reveal potential for the synthesis of other compounds based on a metal complex and the $[W_6I_{14}]^{2-}$ anion.

Zusammenfassung

Im Rahmen dieser Arbeit konnten die ersten Kristallstrukturen für kationische und neutrale Wolframiodidcluster gelöst und publiziert werden. Zunächst konnte die Verbindung $[(W_6I_8)I_3(CH_3CN)_3]I_7 \cdot I_2$ mit dem heteroleptischen Clusterkation $[(W_6I_8)I_3(CH_3CN)_3]^+$ als kristallines Pulver hergestellt werden. In weiteren Reaktionen sind ausgehend von $[(W_6I_8)I_3(CH_3CN)_3]I_7 \cdot I_2$ die beiden Spezies $[(W_6I_8)I(CH_3CN)_5](I_3)_2(BF_4)$ und $[(W_6I_8)(CH_3CN)_6](I_3)(BF_4)_3 \cdot (H_2O)$, mit den in den Strukturen enthaltenen Clusterkationen $[(W_6I_8)I(CH_3CN)_5]^{3+}$ und $[(W_6I_8)(CH_3CN)_6]^{4+}$, hergestellt worden. Bedingt durch die enthaltenen I_3^- bzw. I_7^--Anionen weisen die kristallinen Pulver oder Einkristalle dunkle Farben auf und zeigen optisch keine Photolumineszenz.

Weitere Reaktionen lieferten $[W_6I_8(CH_3CN)_6](BF_4)_4 \cdot (CH_3CN)_2$ in Form gelber Plättchen bzw. eines gelben Pulvers. Diese Verbindung zeigt im Festkörper die typische Photolumineszenz oktaedrischer Metallhalogenidcluster mit den charakteristischen breiten Anregungs- und Emissionsbanden. Im Gegensatz zu Verbindungen mit elektronenziehenden Liganden sind die Lebenszeiten der Photolumineszenz allerdings sehr kurz und es findet kein Quenching in Gegenwart von molekularem Sauerstoff statt. In der berechneten ELF zeigt sich eine deutlich höhere d-Elektronendichte am Wolframatom für $[W_6I_8(CH_3CN)_6](BF_4)_4 \cdot (CH_3CN)_2$ und eine geringere Ionizität der W–N-Bindung im Vergleich zur stark quenchenden Spezies $(TBA)_2[W_6I_8(CO_2C_3F_7)_6]$. Daraus kann abgeleitet werden, dass die Ionizität der W–*L*-Bindung die Aufspaltung der emittierendenTriplettsublevel und dadurch die Lebenszeit beeinflusst.

Neben den kationischen konnte auch eine neutrale Clusterspezies synthetisiert und deren Eigenschaften untersucht werden. Die Verbindung $[W_6I_{12}(NCC_6H_5)_2]$ gehört mit zwei apikalen Benzonitril- und vier Iodidoliganden zu den heteroleptischen Clustern. Hierbei kann eine gute Hydrolysestabilität, sowie eine bemerkenswerte thermische Stabilität bis 400 °C beobachtet werden. Die Photolumineszenz im Festkörper ist im Hinblick auf ihre Intensität, Lebenszeit und Quantenausbeute nur schwach ausgeprägt. Ungeachtet dessen eignet sich die Verbindung durch ihre Hydrolyse- und Temperaturstabilität sowie einer optischen Bandlücke von 2,17 eV für photokatalytische Anwendungen. Dies konnte am Beispiel der photokatalytischen Zersetzung von Rhodamin B in wässriger Lösung gezeigt werden.

In weiteren durchgeführten Reaktionen konnten darüber hinaus die Verbindungen $[W_6I_8(CH_3CN)_6](ClO_4)_4 \cdot (CH_3CN)_2$ und $[W_6I_8(DMSO)_6](I_3)_4$ mit Clusterkationen in der Struktur hergestellt werden. Zusätzliche Reaktionen mit anderen Lösungsmitteln legen ein hohes Potential für die Herstellung anderer kationischer oder neutraler Wolframiodidcluster nahe.

Dadurch könnten zusätzlich neue Erkenntnisse über die photophysikalischen Eigenschaften der Cluster und weitere hochstabile Verbindungen mit Anwendungspotential möglich sein.

Des Weiteren konnten mit den Verbindungen $(^{n}Bu_4N)_2[M_6I_8(NCO)_6]$ (M = Mo, W) neue Metalliodidcluster publiziert werden. In deren Strukturen sind die NCO-Liganden über den Stickstoff an den $[M_6I_8]$-Kern gebunden. Im Festkörper zeigen sie die typische Photolumineszenz mit schwach ausgeprägtem Quenching in Gegenwart von molekularem Sauerstoff.

Für den Vergleich der photophysikalischen Eigenschaften mit den analogen Iodiden, wurden die Verbindungen $(PPN)_2[W_6Cl_{14}]\cdot(CH_2Cl_2)_2$ und $(PPh_4)_2[W_6Cl_{14}]\cdot(C_3H_6O)_2$ hergestellt. Die entsprechenden oktaedrischen Wolframiodide zeigen im Festkörper hohe Quantenausbeuten. Im Gegensatz dazu ist die Photolumineszenz der beiden erhaltenen Wolframchloridcluster nur schwach ausgeprägt mit sehr kurzen Lebenszeiten und nicht messbaren Quantenausbeuten.

Ein weiterer Teil der Arbeit war die Synthese von Verbindungen, die Wolframhalogenidcluster mit Metallionen, auf die ein Energietransfer möglich wäre, verbindet. Reaktionen mit *RE*-Chloriden (*RE* = Gd, Tb, Eu) lieferten die Spezies GdW_6Cl_{15}, TbW_6Cl_{15} und EuW_6Cl_{14}. Die Untersuchung mittels magnetischer Messungen offenbarte einen Paramagnetismus entsprechend den magnetischen Momenten der Seltenerd-Ionen. Photolumineszenzspektren der Clusterspezies im Festkörper zeigten keine Emission der Seltenerd-Ionen.

In Kooperation mit Dr. T. Maulbetsch wurde die Verbindung $[Fe(CTP)]_2[W_6I_{14}]$ hergestellt. Bei Raumtemperatur konnte mittels Photolumineszenzmessungen keine Emission festgestellt werden. Um die Frage eines Energietransfer von $[W_6I_{14}]^{2-}$ auf Fe^{3+} zu beantworten, wurden daher Messungen bei tiefen Temperaturen (zwischen 3 K und 100 K) vorgenommen, die ebenfalls keine Emission zeigten.

In zusätzlichen Versuchen zur Herstellung einer supramolekularen $[W_6I_{14}]$-Metallkomplex-Verbindung konnten Kristalle der Spezies $[Fe(CH_3CN)_6][W_6I_{14}]$ dargestellt werden. Diese zeigten optisch ebenfalls keine Photolumineszenz, offenbaren aber Potential für Herstellung weiterer Verbindungen bestehend aus Metallkomplex und $[W_6I_{14}]^{2-}$.

List of Publications

Publication 1:

The Heteroleptic Cluster Cation $[(W_6I_8)I_3(CH_3CN)_3]^+$

Florian Pachel, Jacqueline Händel, Markus Ströbele, Hans-Jürgen Meyer

Eur. J. Inorg. Chem. **2020**, *42*, 3987–3990.

Publication 2:

Preparation, Photoluminescence and Excited State Properties of the Homoleptic Cluster Cation $[(W_6I_8)(CH_3CN)_6]^{4+}$

Florian Pachel, Philipp Frech, Markus Ströbele, David Enseling, Carl P. Romao, Thomas Jüstel, Marcus Scheele, Hans-Jürgen Meyer

Dalton Trans. **2023**, *52*, 3777–3785.

Publication 3:

The Remarkable Robust, Photoactive Tungsten Iodide Cluster $[W_6I_{12}(NCC_6H_5)_2]$

Florian Pachel, Markus Ströbele, Carl P. Romao, David Enseling, Thomas Jüstel, Hans-Jürgen Meyer

Eur. J. Inorg. Chem. **2023**, *26*, e202300096.

Publication 4:

Synthesis, Crystal Structure, and Luminescence of Metal Iodide Cluster Compounds $(^nBu_4N)_2[M_6I_8(NCO)_6]$ with M = Mo, W

Arin-Daniel Fuhrmann, Florian Pachel, Markus Ströbele, David Enseling, Thomas Jüstel, Hans- Jürgen Meyer

Z. Anorg. Allg. Chem. **2020**, *646*, 1650–1654.

Publication 5:

Crystal structure, Magnetic and Photoluminescence Properties of GdW_6Cl_{15}, TbW_6Cl_{15}, and EuW_6Cl_{14}

Florian Pachel, Markus Ströbele, David Enseling, Thomas Jüstel, Hans-Jürgen Meyer

Z. Anorg. Allg. Chem. **2021**, *647*, 1392–1396.

Scientific Contribution

Publication 1:

The Heteroleptic Cluster Cation $[(W_6I_8)I_3(CH_3CN)_3]^+$

The manuscript was written in collaboration with Prof. H.-J. Meyer and Dr. M. Ströbele. I planned the synthesis and the experiments were carried out by J. Händel. The thermogravimetric analysis was performed together with J. Händel and interpreted by me. A single crystal of $[(W_6I_8)I_3(CH_3CN)_3]I_7 \cdot I_2$ was measured by me and the subsequent structure solution and refinement was done by Dr. M. Ströbele.

Publication 2:

Preparation, Photoluminescence and Excited State Properties of the Homoleptic Cluster Cation $[(W_6I_8)(CH_3CN)_6]^{4+}$

Dr. C. Romao wrote the part on the electron localization function (ELF) and P. Frech and I wrote the part on the excited state properties. The manuscript was written in collaboration with Prof. H.-J. Meyer. Dr. C. Romao, Prof. T. Jüstel and Prof. M. Scheele edited the manuscript. I carried out all of the reported reactions as well as the nuclear magnetic resonance (NMR) and infrared (IR) measurements and their interpretation. M. Ghani performed the elemental analysis (EA) and Dr. C. Romao the ELF calculations. Dr. D. Enseling recorded all of the photoluminescence spectra and lifetime measurements and I interpreted them. A single crystal of the compound $[(W_6I_8)I(CH_3CN)_5](I_3)_2(BF_4)$ was measured by Dr. M. Ströbele, who also performed the structure solution and refinement. The single crystals of $[(W_6I_8)(CH_3CN)_6](I_3)(BF_4)_3 \cdot (H_2O)$ and $[W_6I_8(CH_3CN)_6](BF_4)_4 \cdot (CH_3CN)_2$ were measured by me and the structure was solved and refined by me. The transient absorption measurements were performed, evaluated and interpreted by P. Frech.

Publication 3:

The Remarkable Robust, Photoactive Tungsten Iodide Cluster $[W_6I_{12}(NCC_6H_5)_2]$

The draft of the manuscript was written by me, completed by Prof. H.-J. Meyer and edited by Dr. C. Romao and Prof. T. Jüstel. All reactions as well as the photocatalysis experiments, thermogravimetric analysis and investigations into the hydrolytic stability were carried out by me. M. Ghani performed the EA and Dr. C. Romao the ELF and band structure calculations. The reflection measurements were recorded by P. Janoschek and evaluated by me. Dr. D. Enseling measured the photoluminescence spectra, lifetimes and quantum yields and I interpreted them. IR spectra were recorded by myself. A single crystal of $[W_6I_{12}(NCC_6H_5)_2]$ was measured and the structure solved and refined by myself. All powder x-ray diffraction (PXRD) patterns were

recorded by myself. E. Nadler recorded the scanning electron microscope (SEM) images and energy dispersive X-ray spectroscopy (EDX) data.

Publication 4:

Synthesis, Crystal Structure, and Luminescence of Metal Iodide Cluster Compounds $(^{n}Bu_4N)_2[M_6I_8(NCO)_6]$ *with M = Mo, W*

The manuscript was written in collaboration with Prof. H.-J. Meyer and edited by Prof. T. Jüstel. Reactions were carried out by A.-D. Fuhrmann. I recorded the IR spectra and interpreted them. Photoluminescence and lifetime measurements were done by Dr. D. Enseling and interpreted in cooperation with Prof. H.-J. Meyer. Single crystal measurements were performed by A.-D. Fuhrmann and the structure was solved and refined by Dr. M. Ströbele.

Publication 5:

Crystal structure, Magnetic and Photoluminescence Properties of GdW_6Cl_{15}, TbW_6Cl_{15}, *and* EuW_6Cl_{14}

The manuscript was written in collaboration with Prof. H.-J. Meyer and edited by Prof. T. Jüstel. All reactions were performed by me. Photoluminescence spectra were recorded by Dr. D. Enseling and interpreted together with Prof. T. Jüstel. The Rietveld refinement for the compound EuW_6Cl_{14} was performed by Dr. M. Ströbele and the refinements of GdW_6Cl_{15} and TbW_6Cl_{15} by myself together with Dr. M. Ströbele. Dr. J. Glaser conducted the magnetic measurements and supported me interpreting them.

1. Introduction

1.1 Binary tungsten halides

Binary tungsten halides show versatile molecular or three-dimensional structures related to the oxidation state of tungsten. In the W–Cl system, compounds with oxidation states ranging from W^{2+} to W^{6+} are known. Higher oxidation states of tungsten are usually associated with molecular structures, like the isolated WCl_6[1] octahedra in the structure of WCl_6 (W^{+6}) or the W_2Cl_{10}[2] dimers in WCl_5 (W^{+5}), which are build of two WCl_6 octahedra sharing one edge. For WCl_4[3] (W^{4+}) one-dimensional strings of edge sharing WCl_6 octahedra are observed. At lower oxidations states than W^{4+} octahedral tungsten chloride clusters are formed. In the structure of WCl_3 (W^{3+})[4], the cluster $[W_6Cl_{12}Cl_6]$ is present featuring 12 chlorido ligands above the edges of the W_6 octahedron and six ligands over the vertices. The most prominent member of the W–Cl-system is WCl_2 (W^{2+})[5] with $[W_6Cl_8Cl_6]$ clusters in the structure. Herein eight chlorido ligands are located above the faces of the octahedron and one above each vertex. Four of these ligands above the vertices are shared and connect adjacent tungsten clusters.

The W–Br-system strongly resembles the W–Cl-system, showing all mentioned compounds except for WBr_3 with $[W_6Br_{12}Br_6]$ clusters.[6] In addition, the octahedral cluster $[W_6Br_{14}]$[7] without connection between adjacent clusters via halide ligands is known. Further, the bromido ligands can form complex anions leading to the two species $[W_6Br_{16}]$[8] and $[W_6Br_{18}]$[9] featuring Br_4^{2-}-bridges connecting adjacent clusters. Aside from the octahedral clusters also the tetrahedral tungsten cluster $[W_4Br_{10}]$[10] is formed in the W–Br-system.

In the W–I-system, compounds featuring tungsten in higher oxidation states (+3, +4, +5, +6) are unknown. Nevertheless, the greatest variety of binary tungsten halide compounds is found in this system enabled by the willingness of iodine to form I_3^-- or I_2-bridges.[11] Allowing for various tungsten iodide clusters to form. Known are trigonal (W_3I_8,[12] W_3I_9,[13] W_3I_{12}),[13] tetrahedral (W_4I_{10},[14] W_4I_{13}),[15] square pyramidal (W_5I_{11},[16] W_5I_{12},[17] $W_5I_{13}{\cdot}nI_2$,[16] W_5I_{15},[16] W_5I_{16},[17] $W_{15}I_{47}$)[18] and octahedral tungsten clusters (W_6I_{12},[19] W_6I_{14},[20] W_6I_{16},[15] W_6I_{18},[15] W_6I_{22})[20] (Figure 1).

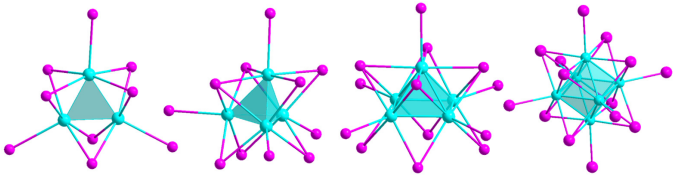

Figure 1. *Cluster fragments $[(W_3I_6^i)I_3^a]$, $[(W_4I_7)I_4^a]$, $[(W_5I_8^i)I_5^a]$ and $[(W_6I_8^i)I_6^a]$ (from left to right) of the structures featuring trigonal, tetrahedral, square pyramidal and octahedral tungsten cluster (W: turquoise, I: pink).*

1.2 Synthesis of binary tungsten iodides

The synthesis of binary tungsten iodides can be achieved by a variety of approaches and is well documented in the literature. The simplest reported method is the direct reaction between the elements at temperatures between 600 °C and 800 °C.[21] However, long reaction times are required, and yields are low. Additionally, the synthesis involves a high iodine pressure in closed ampoules.[21] Another approach utilizes WCl_6 and HI as reactants.[22] This reaction can only be carried out in small amounts and with the possibility of incomplete exchange of chloride for iodide.[22] Furthermore, the synthesis starting from $W(CO)_6$ and elemental iodine is reported.[15, 23] During the reaction, enormous amounts of CO gas are released, leading to a potential detonation of the closed reaction vessel.[15, 23] Moreover, the chlorido ligands of W_6Cl_{12} can be exchanged by heating the cluster in a ten-fold excess of a molten KI/LiI mixture (70 mol %/30 mol %).[24] Afterwards, the product has to be rinsed with water to remove the flux and is subsequently dissolved in ethanol.[24] This leads to the formation of an ethanol adduct which is thermally decomposed.[24]

The work group of Prof. Meyer developed a simple and safe method for synthesizing binary tungsten iodides starting from WCl_6.[13] In a Schlenk tube, WCl_6 is mixed with SiI_4 and kept at 120 °C for 16 h.[13] After the reaction, the excess of iodine and the formed silicon chlorides are removed in an argon flow affording pure W_3I_{12} as a black, crystalline powder.[13] W_3I_{12} can be employed as starting material for the synthesis of the complete family of binary tungsten iodides, for example, W_6I_{12} and W_6I_{22} or ternary compounds like $Cs_2W_6I_{14}$ (Figure 2).[19, 25]

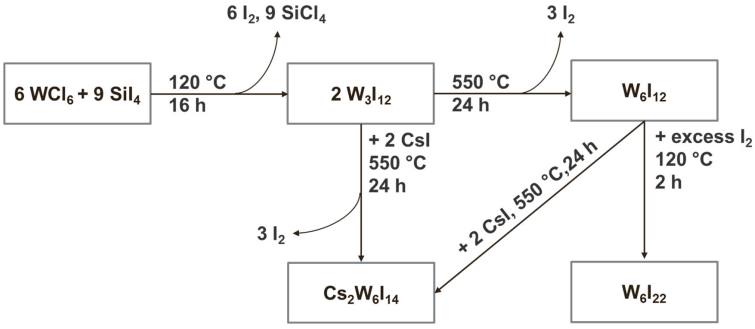

Figure 2. *Reaction scheme for the synthesis of the binary tungsten halides W_3I_{12}, W_6I_{12} und W_6I_{22} and the ternary $Cs_2W_6I_{14}$, starting from WCl_6 and SiI_4.*

1.3 Octahedral tungsten iodide clusters

The research investigating octahedral metal halides $[M_6X_{12}]$ (M = Mo, W; X = Cl, Br, I) has a long historical background. The first compounds with the formula $[W_6X_{12}]$ (X = Cl, Br, I) were reported as early as the 19th century.[21] The crystal structure of the binary tungsten iodide W_6I_{12} features the characteristic W_6 octahedron surrounded by eight inner μ_3-bridging iodido ligands (I^i) above the edges of the octahedron and six apical iodido ligands (I^a) located above the vertices (Figure 3).[26] The species W_6Cl_{12}, W_6Br_{12}, or analogous compounds with molybdenum are isotypic.[5]

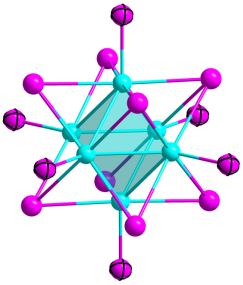

Figure 3. *Schematic illustration of the $[W_6I_{14}]^{2-}$-anion present in the structure of the binary tungsten iodide W_6I_{12} (W: turquoise, I^i: pink, I^a: pink with black lines).*

In the crystal structure of W_6I_{12}, adjacent clusters are interconnected by four of their terminal iodido ligands, resulting in a layered arrangement. Introducing additional iodine into the structure replaces the interconnecting iodido ligands with I_3^-, as observed for W_6I_{22} (Figure 4).[20]

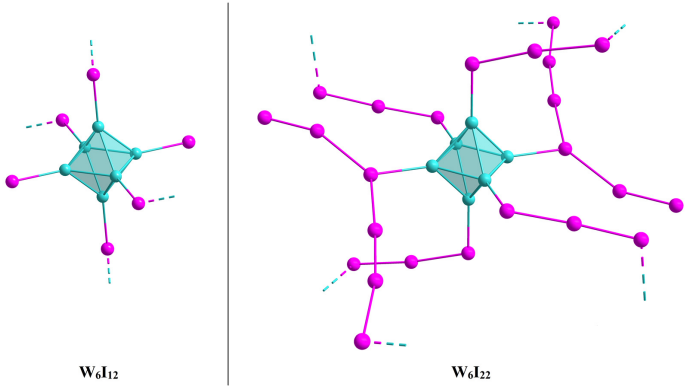

Figure 4. *Comparison of interconnections in binary tungsten halides on the basis of W_6I_{12} and the iodine-rich W_6I_{22}. Broken-off bonds illustrate connections to adjacent clusters. Inner iodido ligands have been omitted for clarity (W: turquoise, I: pink).*

These interconnections are mainly based on van der Waals forces and, therefore, weaker. This results in a binary tungsten iodide cluster species (W_6I_{22}) that is soluble in common organic solvents.[20] Another way to weaken the direct interconnections between adjacent clusters in the structure is dimensional reduction.[27] This method is based on the incorporation of inorganic salts into the structure, as has been shown by T. Hummel *et al.* for W_6I_{12} using *A*I as a salt(*A* = Li, Na, K, Rb, Cs).[25, 28] Ternary tungsten iodide clusters of the form $A_x[W_6I_{14}]$ were synthesized this way.[25, 28] In the crystal structure of these obtained species, adjacent clusters are connected through I–*A*–I bridges and not directly by the iodido ligands.[25, 28] Based on these ternary tungsten iodide clusters, further substitution reactions can be carried out in solution. Subsequent modifications may involve cation exchange reactions (1) by replacing the alkali cations like Cs for large organic cations, most commonly tetrabutylammonium (TBA).[29]

$$Cs_2[W_6I_{14}] + 2\,TBAI \rightarrow (TBA)_2[W_6I_{14}] + 2CsI \qquad (\mathbf{1})$$

Furthermore, the apical iodido ligands can be exchanged for neutral or anionic organic ligands using silver salts (2), as has been described for the compound $(TBA)_2[W_6I_8(CO_2CF_3)_6]$.[29]

$$(TBA)_2[W_6I_{14}] + 6\,Ag(CO_2CF_3) \rightarrow (TBA)_2[W_6I_8(CO_2CF_3)_6] + 6\,AgI \qquad (\mathbf{2})$$

Using this or similar reaction schemes, octahedral metal halide clusters with many different anionic or neutral ligands are achievable.[30]

1.4 Photoluminescence properties of octahedral metal halide clusters

Octahedral metal halide clusters are known for their remarkable photophysical properties and are being investigated for possible applications in various fields, such as medicine[31] (X-ray contrast agents,[32] photodynamic therapy[33]), hygiene/purification (surface,[34] wastewater[35] and air purification[36]), solar energy harvesting (solar cells, [37] photocatalysis,[38] luminescent solar concentrators[39]), luminescent nanoparticles,[40] gas sensors[41] or heavy crude oil upgrading.[42]

Among these properties are their yellow, orange, or red body color as crystalline powders and band gaps in the order of 2 eV.[35b, 35c, 43] However, their most prominent feature is a bright orange-to-red photoluminescence. First described in 1980 by Maverick *et al.* for $(TBA)_2[Mo_6Cl_{14}]$ in acetonitrile[44], their photoluminescence has been extensively studied since then. In particular, octahedral metal iodide clusters are at the centre of attention because of their superior quantum yields and lifetimes compared to the analogue bromides and chlorides.[45] The

photoluminescence originates from ground state excitation using UV/Vis light into excited singlet states (s_m), followed by intersystem crossing (ISC) into a triplet state (T_1) and subsequent relaxation into the ground state via phosphorescence (Figure 5).[44, 46] In 1990, Jackson *et al.* discovered the quenching of photoluminescence in the presence of molecular oxygen. Upon contact with oxygen, an energy transfer occurs to produce singlet oxygen.[47]

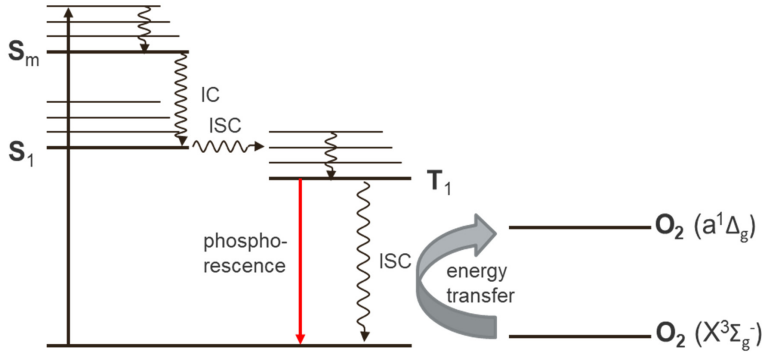

Figure 5. *Scheme of the involved electronic transitions in the photoluminescence of octahedral metal halide clusters $[M_6X_8L_6]^{2-}$ and the energy transfer towards molecular oxygen based on a modified Jablonski diagram.*[48]

A vast amount of studies dealt with influencing the photoluminescence properties of octahedral metal halide clusters. Their results showed that major improvements in the emission lifetime, quantum yields, or stronger oxygen quenching can be achieved by cation and ligand exchange, as can be seen from the example of ternary tungsten iodide clusters such as $Na[W_6I_{14}]$ or $Cs_2[W_6I_{14}]$, which exhibit strong thermal quenching of their photoluminescence in the solid state.[25b, 28] The emission can only be recorded properly upon cooling with liquid nitrogen.[25b, 28] In the work of T. Hummel *et al.*, an exchange of the alkali metal cations for large organic cations (TBA^+, PPh_4^+, or PPN^+) significantly increased the quantum yield of crystalline samples at room temperature up to 42 % for $(PPN)_2[W_6I_{14}]$.[28, 49] Photoluminescence lifetimes for these compounds are reported to be between 12 µs and 20 µs. Quenching of the luminescence in the presence of molecular oxygen has not been observed.[28, 49] Further enhancement of the photoluminescence properties can be achieved by exchanging the apical halide ligands for organic anions. Especially employing strong electron-withdrawing ligands like trifluoroacetate or p-toluene sulfonate (OTs) significantly increases lifetimes and oxygen quenching in the solid state.[29, 30d, 43a, 50] Additionally, a strong hypsochromic shift of the emission maximum is observed upon ligand exchange. These trends in the photoluminescence properties of metal halide

clusters, as described for tungsten clusters, are also observed for analogue molybdenum species.[30c, 30e, 51]

Some representative examples of the emission maxima, lifetimes, and quantum yields of crystalline octahedral metal iodide clusters are listed in Table 1.

Table 1. Values of emission maxima $\lambda_{em,max}$ [nm], lifetimes τ [µs] and quantum yields Φ_{em} of crystalline samples of some representative examples for tungsten and molybdenum iodide clusters.

Compound	$\lambda_{em,max}$ [nm]	Lifetime τ [µs]	Quantum yield Φ_{em}
$(TBA)_2[W_6I_{14}]$	680[49]; 685[52]; 730[43a]	12[52]; 14[43a]	0.16[49]; 0.29[52]
$(PPN)_2[W_6I_{14}]$	696[49]	19[49]	0.42[49]
$(PPh_4)_2[W_6I_{14}]$	690[49]	13[49]	0.16[49]
$(TBA)_2[W_6I_8(SO_3C_7H_7)_6]$	678[43a]; 640[52]	24[43a]; 35[52]	0.28[52]
$(TBA)_2[W_6I_8(CO_2CF_3)_6]$	660[29]	30[29]	0.23[29]
$(TBA)_2[W_6I_8(CO_2C_3F_7)_6]$	632[30d]	$\tau_1 = 55$ $\tau_2 = 27$[30d]	0.30[30d]
$(TBA)_2[Mo_6I_{14}]$	698[49]; 727[53]; 734[30c]; 735[52]	19[30c, 52]; 18[53]	0.1[52-53]
$(PPN)_2[Mo_6I_{14}]$	688[49]	70[49]	<0.05[49]
$(PPh_4)_2[Mo_6I_{14}]$	690[49]	109[49]	
$(TBA)_2[Mo_6I_8(SO_3C_7H_7)_6]$	675[43a]; 662[52]	147[43a]; $\tau_1 = 135$ $\tau_2 = 56$[52]	0.44[52]
$(TBA)_2[Mo_6I_8(CO_2CF_3)_6]$	675[29]; 670[30c]; 667[30e]	159[29]; 215[30c]; $\tau_1 = 52$ $\tau_2 = 29$[30e]	0.13[30e]
$(TBA)_2[Mo_6I_8(CO_2C_3F_7)_6]$	659[30e, 54]	$\tau_1 = 166$ $\tau_2 = 124$[30e]; 150[54]; 235[55]	0.36[30e, 54]

To further understand these photophysical properties, Kitamura *et al.* developed a model to explain the cluster emission.[55-56] Based on the work of Saito *et al.*,[57] they proposed a splitting of the emitting excited triplet level into five different sublevels (Figure 6).[56d] The emission can only be observed for four of these sublevels, since the fourth can couple with the ground state by an electronically allowed dipole transition.[56d] Thus, leading to an intense and short-lived emission. The other sublevels exhibit forbidden transitions, therefor, the emission is long-lived.[56d] In experiments, the strong temperature dependence of the emission lifetime for $(TBA)_2[Mo_6Cl_{14}]$ (210 µs at 80 K and 120 µs at 300 K)[44] and $(TEA)_2[Mo_6Cl_{14}]$ (370 µs at 1.4 K and 130 µs at 300 K)[57] has been observed. These results can satisfactorily be explained by a strong thermal population of the highest emitting sublevel, as suggested by the described model.

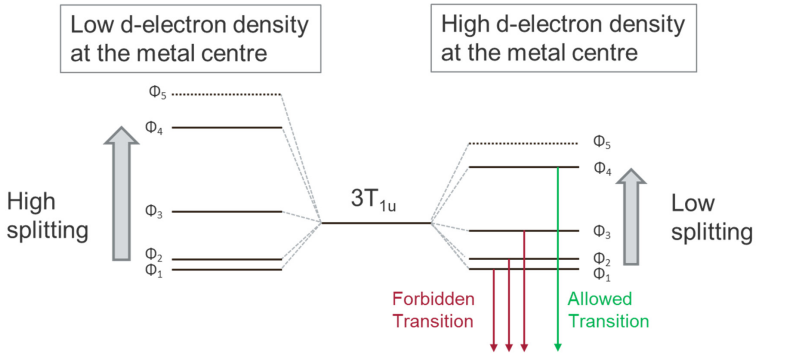

Figure 6. *Model to describe the photoluminescence of tungsten and molybdenum halide clusters by Kitamura et al..*[56d] *They propose a splitting of the emissive triplet level into five sublevels. The highest one is supposed to be invisible due to the fourth level possessing an allowed transition into the ground state Forbidden transitions are displayed as red, and allowed transitions as green arrows). Differences in the d-electron density at the metal centers are responsible for the variable splitting of the triplet sublevels.*

Further studies on different molybdenum halide clusters $(TBA)_2[Mo_6X_8Y_6]$ (X, Y = Cl, Br, I) revealed a correlation between the d-electron density at the metal centre and the energetic splitting of these triplet sublevels.[56b] Whereas a low density led to a high splitting and a high density to a low splitting.[56b] In addition, they also studied the temperature dependence on the molybdenum halide clusters $(TBA)_2[Mo_6X_8(CO_2C_3F_7)_6]$ (X = Cl, Br, I) featuring strong electron-withdrawing ligands.[55] These experiments showed smaller full width half maximum values (FWHM) and less change in the emission lifetime in the temperature range between 3 K and 300 K when switching the inner ligand from Cl to I.[55] They attributed this to a growing energetic splitting of the excited triplet state sublevels.[55]

In contrast to photoluminescence, studies regarding the excited state properties of metal halide clusters are scarce. Pico- and nanosecond photoluminescence spectroscopy on crystalline samples were reported by Strauss *et al.* and showed lifetimes for the singlet states between 600 ps and 1100 ps.[58] Later studies used transient absorption spectroscopy to investigate the excited states as has been described for molybdenum halide clusters in acetonitrile solution.[45a] The results obtained revealed significant differences between the work of Strauss *et al.* with lifetimes ranging from 120 fs to 1.7 ps for the singlet states.[45a] They explained these discrepancies with strongly deviating experimental conditions (photoluminescence on crystalline samples and transient absorption in solution).[45a] In addition, they discovered another short-lived excited state which they assigned to a hot triplet state with a lifetime between 2.16 ps and 5.35 ps.[45a]

1.5 Cationic and neutral metal halide clusters

Research into the photophysical properties of octahedral metal halide clusters has usually focused on compounds featuring anionic clusters $[M_6X_8L_6]^{2-}$ (M = Mo, W; X = Cl, Br, I; L = Cl, Br, I, organic anions). Even though cationic and neutral species have been reported as early as 1962, investigations into their photophysical properties are scarce. The first examples feature pyridine, dimethyl sulfoxide (DMSO), and dimethylformamide (DMF) as ligands with the compositions $[Mo_6I_8X_4L_2]$ (X = Cl, Br; L = pyridine)[59], $[Mo_6Cl_8X_4L_2]$ (X = Cl, SO_3CH_3; L = DMSO, DMF)[30a] and $[Mo_6Cl_8L_6]^{4+}$ (L = DMSO, DMF).[30a] In the following various compounds involving different neutral ligands and even the first species of neutral tungsten clusters were mentioned,[24, 60] but none of these cluster species has been structurally characterized. The structural characterization by single-crystal X-ray diffraction was later achieved for $[Mo_6Cl_8(CH_3CN)_6]^{+4}$ with $SbCl_6^-$ as counterion, without any comment regarding the photoluminescence properties (Table 2).[61]

Table 2. A list of reported neutral and cationic tungsten and molybdenum halide clusters and the status of their crystal structure and photoluminescence data.

Compound	X	L	Anion	Crystal structure	Luminescence
$[Mo_6Cl_8X_4L_2]$[30a]	Cl, SO_3CH_3	DMSO, DMF		-	-
$[Mo_6Cl_8L_6]$[30a]		DMSO, DMF	ClO_4	-	-
$[Mo_6I_8X_4L_2]$[59]	Cl, Br	Pyridine		-	-
$[Mo_6Cl_8X_4L_2]$[60]	Cl	CH_3CN, C_2H_5CN, C_3H_7CN, $N(CH_3)_3$, Pyridine, Pyrazine, Chinoline, γ-Picoline		-	-
$[W_6I_8X_4L_2]$[24]	I	EtOH		-	-
$[W_6Cl_8X_4L_2]$[24]	Cl	CH_3CN		-	-
$[Mo_6Cl_8L_6]$[61]		CH_3CN	$SbCl_6$	+	-
$[Mo_6I_8(L)_6]$[62]		DMSO	NO_3	+	+
$[W_6I_8(L)_6]$[62]		DMSO	NO_3	-	+
$[Mo_6I_8X_4L_2]$[43b]	I	Pyridine		+	+
$[Mo_6I_8X_2L_4]$[63]	OH	H_2O	NO_3, OTs	+	+
$[Mo_6I_8X_4L_2]$[63]	OH	H_2O		+	+

+ known, - unknown

Photoluminescence data for cationic and neutral metal halide clusters are only given for a limited list of compounds, namely $[Mo_6I_8(DMSO)_6](NO_3)_4$, $[W_6I_8(DMSO)_6](NO_3)_4$,[62] $[Mo_6I_8I_4(pyridine)_2]$,[43b] $[Mo_6I_8OH_4(H_2O)_2]$, $[Mo_6I_8OH_2(H_2O)_4](NO_3)_2$ and $[Mo_6I_8OH_2(H_2O)_4](OTs)_2$.[63] Due to the limited number of known species, the influence of neutral ligands on the photoluminescence properties of the resulting cationic or neutral tungsten and molybdenum halide clusters is not yet understood.

2. Objective

The structure of binary tungsten and molybdenum halides was described decades ago. The Photoluminescence properties of the corresponding compounds $(A)_2[M_6X_8L_6]$ (M = Mo, W; A = Na, Cs, TBA, PPN, PPh_4; X = Cl, Br, I; L = Cl, Br, I, organic anions) have been of great interest for research in many different fields since the discovery of their optical properties in the 1980s and 1990s. Since then, it has been determined, that large organic cations and electron-withdrawing organic ligands strongly enhance the photoluminescence in the solid state in terms of lifetime, quantum yield, and quenching in the presence of molecular oxygen. Nevertheless, many aspects of cluster photoluminescence remain to be investigated. For example, almost all reported compounds and studies regarding the photoluminescence or optical properties are based on species containing anionic clusters $[M_6X_8L_6]^{2-}$. Cationic and neutral tungsten or molybdenum halide clusters were reported as early as 1965. However, characterization in terms of the crystal structure or photoluminescence properties is limited to a few examples. Thus, the aim of this work is to synthesize new cationic and neutral tungsten iodide clusters, elucidate their structures and characterize their photoluminescence.

Further experiments are focused on generally expanding the field of known tungsten halide clusters and the knowledge about their photophysical properties.

Besides the production of singlet oxygen, energy transfer from excited clusters onto other ions or molecules is also possible. This has been described for supramolecular [Crypt-*RE*]-$[W_6I_{14}]$ solids with *RE* = Yb, Nd.[64] Based on this, another aim of this thesis was to combine tungsten halide clusters with *RE* ions or d-metal ions and study their photoluminescence in regard to an energy transfer.

3. Summary of the main results

Single-crystal X-ray diffraction

The crystal structures of the compounds $[(W_6I_8)(CH_3CN)_6](ClO_4)_4 \cdot (CH_3CN)_2$ (CCDC: 2065518),[65] $[W_6I_8(DMSO)_6](I_3)_4$ (CCDC: 2111522),[66] $(PPN)_2[W_6Cl_{14}] \cdot (CH_2Cl_2)_2$ (CCDC: 2121320),[67] $(PPh_4)_2[W_6Cl_{14}] \cdot (C_3H_6O)_2$ (CCDC: 2121373),[68] $[Fe(CTP)]_2[W_6I_{14}]$ and $[Fe(CH_3CN)_6][W_6I_{14}]$ (CCDC: 2087031)[69] were obtained by single-crystal X-ray diffraction (XRD). The XRD studies were performed on a Rigaku XtaLab Synergy-S diffractometer with Mo-K_α radiation (λ = 0.71073 Å) and a mirror monochromator. Measurements of single-crystals were carried out under N_2 cooling at 100 K or 200 K. Corrections for absorption effects were applied with CrysAlisPro 1.171.41.65a (Rigaku Oxford Diffraction, 2020). The structures were solved by direct methods SHELXT,[70] and full-matrix least-squares structure refinements were performed with SHELXL-2014[71] implemented in Olex2 1.3-ac4 or with SHELXL-97 in ShelXLe.

Photoluminescence studies

The excitation and emission spectrum of crystalline $[W_6I_8(CH_3CN)_6](ClO_4) \cdot (CH_3CN)_2$ were collected with a Horiba Fluorolog-3 DF spectrofluorometer equipped with a 450 W Xenon lamp for steady-state measurements. Emission was detected in 15° angle using a Hamamatsu R2658P PMT (UV/Vis/NIR, 200 nm < λ_{em} < 1000 nm). A double grating monochromator 320DFX (1200 grooves per nm, blazed at 330 nm) was used for spectral selection in the excitation path, while in the emission path the single grating monochromator iHR550 (950 grooves per nm, blazed at 900 nm) was used. To avoid higher order excitation light, long pass filter glass plates were used when needed.

Excitation and emission spectra of powder samples of $(TBA)_2[W_6Cl_{14}]$, $(PPN)_2[W_6Cl_{14}]$, $(PPh_4)_2[W_6Cl_{14}]$ and $[Fe(CTP)]_2[W_6I_{14}]$ were collected by using a fluorescence spectrometer *FLS920* (*Edinburgh Instruments*) equipped with a 450 W Xenon discharge lamp (*OSRAM*) and a cryostat "*MicrostatN*" or Optistat AC-V 12 (He cryostat) from *Oxford Instruments* as the sample chamber for adjusting the atmosphere during the measurements and to adjust the temperature. Additionally, a mirror optic for powder samples was applied. For detection, an *R2658P* single-photon-counting photomultiplier tube (*Hamamatsu*) was used. All photoluminescence spectra were recorded with a spectral resolution of 1 nm, a dwell time of 0.5 s in 1 nm steps and 2 or 5 repeats. Quantum yields were measured according to Yuichiro Kawamura.[72] For recording the emission lifetimes a picosecond pulsed laser Laser Hamamatsu EPL 440 or a Xe µ-flash lamp µF920 were used as excitation source.

Powder X-ray diffraction

Powdered samples of $(TBA)_2[W_6Cl_{14}]$, $(PPN)_2[W_6Cl_{14}]$ and $(PPh_4)_2[W_6Cl_{14}]$ were verified using a Stoe STADI-P powder diffractometer equipped with a Ge-monochromator and a Mythen-1K detector using Cu-$K_{\alpha 1}$ (λ = 1.540598 Å) radiation in the range of $5° < 2\theta < 70°$ (step width 0.02°). The powder samples were fixated between two layers of mylar foil using lithelen grease.

3.1 The Heteroleptic Cluster Cation $[(W_6I_8)I_3(CH_3CN)_3]^+$ (Publication 1)[73]

The aim of this thesis was to synthesize cationic and neutral tungsten iodide clusters and to characterize their photophysical properties. First, a starting material with good solubility had to be selected and then suitable reaction conditions had to be found. Preliminary work by this group in the field of tungsten halide clusters and binary tungsten halides led to the identification of W_6I_{22} as the perfect starting material. It shows superior solubility in organic solvents compared to the commonly used compounds W_6I_{12} and $Cs_2W_6I_{14}$, which is a consequence of weaker bonding between adjacent cluster units in the structure in contrast to W_6I_{12}, resulting from fragile $I_3^{(a\text{-}a)}$-bridges.[20]

Initial experiments involved dissolving W_6I_{22} in acetonitrile and gave a single crystal of the compound $[(W_6I_8)I_3(CH_3CN)_3]I_7{\cdot}I_2$ featuring the first heteroleptic tungsten iodide cluster cation $[(W_6I_8)I_3(CH_3CN)_3]^+$. Subsequent reactions using solvothermal conditions in acetonitrile afforded the species as black, crystalline powder in quantitative amounts.

The crystal structure of $[(W_6I_8)I_3(CH_3CN)_3]I_7{\cdot}I_2$ was solved and refined on the basis of XRD and shows the cluster cation $[(W_6I_8)I_3(CH_3CN)_3]^+$, an heptaiodide anion ($I_7^-$) and I_2 in the structure (Figure 7). The cation resembles the typical octahedral tungsten clusters with eight inner

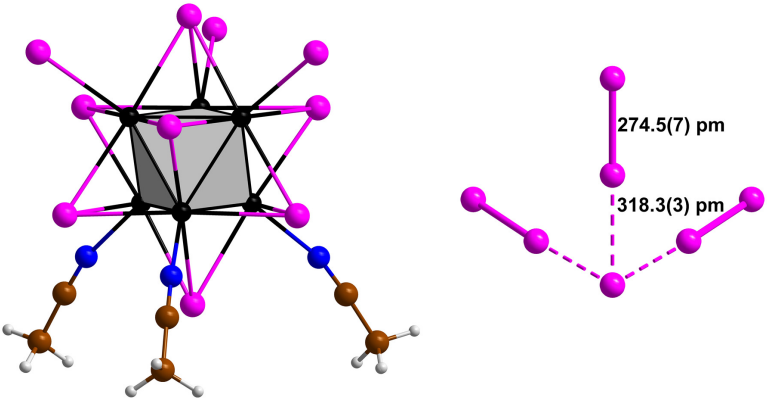

Figure 7. *Structure of the cluster cation $[(W_6I_8)I_3(CH_3CN)_3]^+$ (left side) and the I_7^- anion with interatomic I–I distances (right side, W: black, I: pink, N: blue, C: brown, H: white).*

iodido ligands and six apical ligands, three of which are iodide and the other three are acetonitrile. Averaged W–W distances of 266.4(1) pm appear similar to other compounds with the $[(W_6I_8)I_6]^{2-}$ core (267.2 ± 1.9 pm),[25a] which can be expected due to the same number of

electrons in W–W bonding states (24 electrons). Interestingly, the W–W distances associated with the acetonitrile ligands (264.3(1) pm) are shorter then the respective distances associated with the iodido ligands (267.8(1) pm) resulting in two opposing triangles and an almost trigonal-antiprismatic tungsten cluster. The six distances connecting these two triangles are 266.8(1) pm.

Averaged W–I^i [279.1(2) pm] and W–I^a [282.3(2) pm] distances also appear similar to reported values for $[(W_6I_8)I_6]^{2-}$ compounds (W–I^i 279.4 ± 1.1 pm and W–I^a 282.3 ± 3.9 pm).[25a] The triangular heptaiodide anion features distances of $d_{I\cdots I-I}$ = 318 pm and 275 pm, which are in good agreement with other compounds in the literature.[74] Additionally, an I_2 unit is present with a bond length [271.8(9) pm] comparable to elemental iodine [272.1(1) pm].[75]

The crystal structure of $[(W_6I_8)I_3(CH_3CN)_3]I_7 \cdot I_2$ is represented by a layered arrangement in the a,b-plane, where $[(W_6I_8)I_3(CH_3CN)_3]^+$ and I_7^- are interconnected by I_2 units via Van der Waals and Coulomb forces (Figure 8). These I_2 units are centered on a threefold rotation axes and thus disordered. Adjacent layers are also connected with each other via Van der Waals forces.

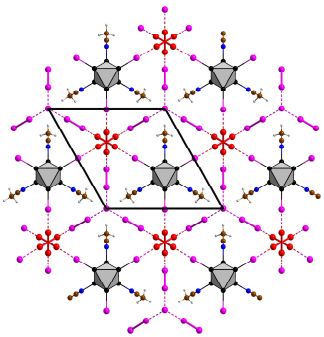

Figure 8. *Projection of the layered structure of $[(W_6I_8)I_3(CH_3CN)_3](I_7)\cdot I_2$ in the ab plane. Inner iodido ligands of the cluster are omitted for clarity.*

The thermal stability of $[(W_6I_8)I_3(CH_3CN)_3]I_7 \cdot I_2$ was studied using differential thermal analysis (DTA) showing a decomposition between 150 °C and 250 °C without pronounced steps. Subsequently, a continuous mass loss occurs between 300 °C and 600 °C, which is typical for tungsten iodides and leads to the formation of W_6I_{12}.[11b]

Among the family of $[M_6X_8]$ clusters the heteroleptic cation $[(W_6I_8)I_3(CH_3CN)_3]^+$ is extraordinary and a comparison of the photoluminescence properties with $[W_6I_8I_6]^{2-}$ and $[W_6I_8L_6]^{2-}$ clusters is of great interest. Unfortunately, $[(W_6I_8)I_3(CH_3CN)_3]I_7 \cdot I_2$ displays a dark color due to the high iodine content excluding any photoluminescence.

3.2 Preparation, photoluminescence and excited state properties of the homoleptic cluster cation $[(W_6I_8)(CH_3CN)_6]^{4+}$ (Publication 2)[76]

In order to investigate the photophysical properties of cationic tungsten iodide clusters the previously obtained species $[(W_6I_8)I_3(CH_3CN)_3]I_7 \cdot I_2$ was not suitable due to the dark color of the powder.[73] Logically, subsequent experiments dealt with the exchange of the iodido ligands and the removal of the iodine. This was done analogously to previous ligand exchanges on anionic tungsten clusters[77] by a reaction of $[(W_6I_8)I_3(CH_3CN)_3]I_7 \cdot I_2$ with a silver salt, namely $AgBF_4$. From these experiments the heteroleptic $[(W_6I_8)I(CH_3CN)_5](I_3)_2(BF_4)$ and the homoleptic $[(W_6I_8)(CH_3CN)_6](I_3)(BF_4)_3 \cdot (H_2O)$ acetonitrile-rich species are obtained as deep-red crystals. Unfortunately, due to their dark color they appear unattractive for optical studies. Nevertheless, a reaction of $[(W_6I_8)I_3(CH_3CN)_3]I_7 \cdot I_2$ with four equivalents of $AgBF_4$ gave the compound $[W_6I_8(CH_3CN)_6](BF_4)_4 \cdot (CH_3CN)_2$ as yellow crystals or powder with a bright orange luminescence.

The crystal structures of $[(W_6I_8)I(CH_3CN)_5](I_3)_2(BF_4)$, $[(W_6I_8)(CH_3CN)_6](I_3)(BF_4)_3 \cdot (H_2O)$ and $[W_6I_8(CH_3CN)_6](BF_4)_4 \cdot (CH_3CN)_2$ were solved and refined on the basis of XRD and feature the heteroleptic cluster cation $[(W_6I_8)I(CH_3CN)_5]^{3+}$ or the homoleptic $[W_6I_8(CH_3CN)_6]^{4+}$ (Figure 9).

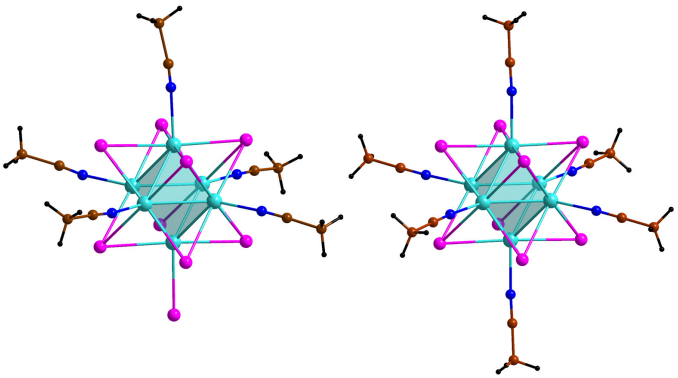

Figure 9. *Structure of the two cluster cations $[W_6I_8I(CH_3CN)_5]^{3+}$ (left) and $[(W_6I_8)(CH_3CN)_6]^{4+}$ (right; W: turquoise, I: violet, N: blue, C: brown, H: black).*

In all three structures a layered arrangement can be observed. For the compounds featuring I_3^- units this is exemplified in Figure 10 (left side) on the basis of the structure of

$[(W_6I_8)(CH_3CN)_6](I_3)(BF_4)_3 \cdot (H_2O)$. Alternating layers of cluster cations with I_3^- units and BF_4^- ions with H_2O are found. In the case of $[W_6I_8(CH_3CN)_6](BF_4)_4 \cdot (CH_3CN)_2$, the cluster cations adopt a layered arrangement along the b axis with BF_4^- ions and free acetonitrile filling the voids (Figure 10, right side).

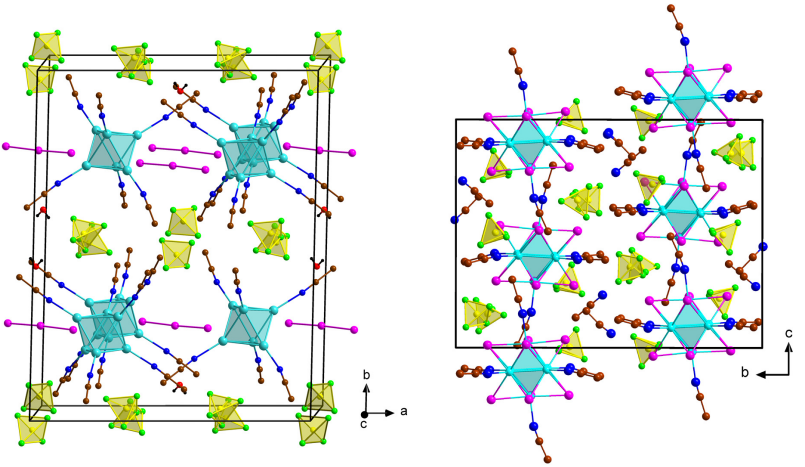

Figure 10. *Projection of the crystal structure of $[(W_6I_8)(CH_3CN)_6](I_3)(BF_4)_3 \cdot (H_2O)$ in the ab plane (left side). Inner iodide ligands of the cluster and hydrogen atoms of acetonitrile are omitted for clarity. Projection of the crystal structure of $[W_6I_8(CH_3CN)_6](BF_4)_4 \cdot (CH_3CN)_2$ in the bc plane (right side). Hydrogen atoms are omitted for clarity (W: turquoise, I: violet, N: blue, C: brown, B: yellow, F: green, O: red, H: black).*

Further research efforts were focused on investigating the properties of the compound $[W_6I_8(CH_3CN)_6](BF_4)_4 \cdot (CH_3CN)_2$, since it was the only one displaying photoluminescence.

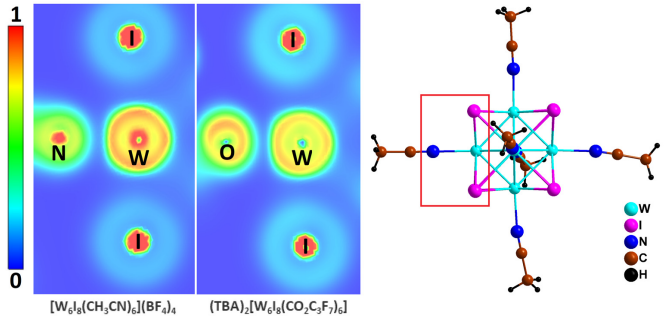

Figure 11. *Electron localization function (ELF) of the investigated compounds $[W_6I_8(CH_3CN)_6](BF_4)_4 \cdot (CH_3CN)_2$ and $(TBA)_2[W_6I_8(CO_2C_3F_7)_6]$ (left side). The view onto the clusters depicted in the ELF is shown on the right side with the cut-out marked with a red box.*

In order to investigate the nature of the W–N bond the electron localization function (ELF) of $[W_6I_8(CH_3CN)_6](BF_4)_4 \cdot (CH_3CN)_2$ was calculated and compared with that of the anionic tungsten iodide cluster species $[(TBA)_2[W_6I_8(CO_2C_3F_7)_6]$ bearing strong electron-withdrawing ligands (Figure 11). These calculations revealed a significantly higher d-electron density at the metal center for $[W_6I_8(CH_3CN)_6](BF_4)_4 \cdot (CH_3CN)_2$ compared to the anionic species $[(TBA)_2[W_6I_8(CO_2C_3F_7)_6]$. This indicates a reduced ionicity of the W–N bond. Nevertheless, both *M–L* investigated are primarily ionic as can be deduced from the presence of nodal planes at the bond centers.

Photoluminescence spectra recorded of crystalline $[W_6I_8(CH_3CN)_6](BF_4)_4 \cdot (CH_3CN)_2$ are shown in Figure 12 and display the typical broad excitation and emission bands of tungsten iodide clusters ($[W_6I_8L_6]^{2-}$).[29, 43a, 50] Interestingly, the emission is centered at 630 nm and thus not very different from that of $[(TBA)_2[W_6I_8(CO_2C_3F_7)_6]$ ($\lambda_{em,max} \approx 630$ nm) bearing strong electron-withdrawing ligands.[30d] In contrast the emission lifetimes differ significantly with $\tau = 11$ µs for $[W_6I_8(CH_3CN)_6](BF_4)_4 \cdot (CH_3CN)_2$ and $\tau = 36$ µs for $[(TBA)_2[W_6I_8(CO_2C_3F_7)_6]$ (the original work included a bi-exponential decay with $\tau = 27$ and 55 µs).[30d] The quenching of the photoluminescence in the presence of molecular oxygen shows similar results, with almost no atmosphere dependent difference in the emission for the cationic and a strong one for the anionic species. This supports the fact that the quenching is related to the lifetime of the emission process in tungsten iodide clusters.

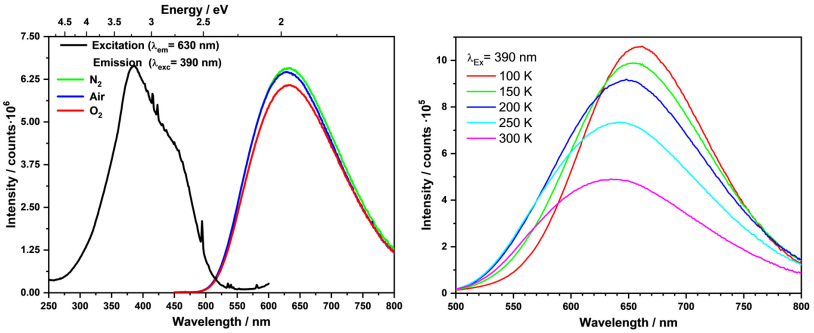

Figure 12. *Recorded excitation (black) and emission (red, blue, green) spectra (left side) and temperature-dependent emission spectra between 100 K and 300 K (right side) of crystalline $[W_6I_8(CH_3CN)_6](BF_4)_4 \cdot (CH_3CN)_2$ powder.*

To understand the significant differences in the emission behavior of the two compounds compared, the model developed by Kitamura has to be considered. [56b, 56d] They describe the cluster emission originating from four different triplet sublevels, the highest of which features an allowed transition to the ground state.[56d] Additionally, the splitting of these sublevels is strongly

altered by the electron density at the metal centres. Increasing splitting is observed with decreasing electron density and vice versa.[56b]

This theory can also be applied to the conducted photoluminescence studies, as we observed a significantly higher d-electron density at the metal centers for the compound $[W_6I_8(CH_3CN)_6](BF_4)_4{\cdot}(CH_3CN)_2$ compared to $[(TBA)_2[W_6I_8(CO_2C_3F_7)_6]$ (Figure 11).Thus, the energetic splitting of the sublevels is lower and therefore a short emission lifetime can be expected for $[W_6I_8(CH_3CN)_6](BF_4)_4{\cdot}(CH_3CN)_2$.

Temperature-dependent photoluminescence spectra were recorded in the temperature range between 100 K and 300 K and show a hypsochromic shift of the emission band of $[W_6I_8(CH_3CN)_6](BF_4)_4{\cdot}(CH_3CN)_2$ (Figure 12). The determined full width at half maximum (FWHM) values are ~3100 cm^{-1} at 100 K and ~4100 cm^{-1} at 300 K. These observations are in contrast to the results obtained for $[(TBA)_2[W_6I_8(CO_2C_3F_7)_6]$, which show almost no shift and FWHM values of ~2800 cm^{-1} at 100 K and ~3600 cm^{-1} at 300 K. Thus, adding to the conclusion that emission from more triplet sublevels takes place for $[W_6I_8(CH_3CN)_6](BF_4)_4{\cdot}(CH_3CN)_2$ due to a lower energetic splitting.

The results obtained for the discussed tungsten iodide clusters suggest a strong influence of the W–L bond polarity on the photoluminescence properties of this class of compounds.

In addition to photoluminescence studies the excited state properties were also investigated. Measurements were conducted based on femtosecond and nanosecond transient absorption of $[W_6I_8(CH_3CN)_6](BF_4)_4{\cdot}(CH_3CN)_2$ in acetonitrile solution (Figure 13). The experiments showed

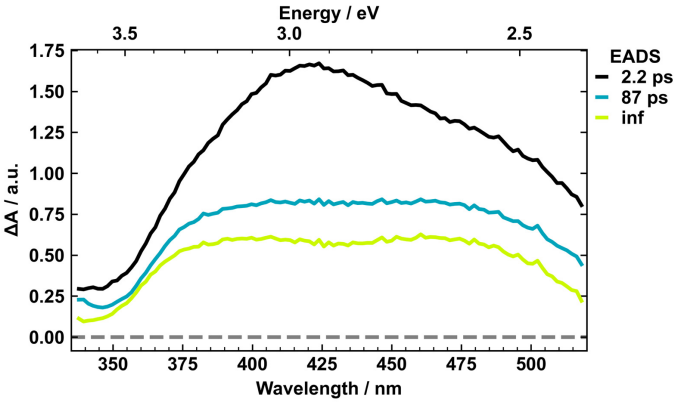

Figure 13. *Evolution-associated difference spectra (EADS) resulting from the global analysis of $[W_6I_8(CH_3CN)_6](BF_4)_4{\cdot}(CH_3CN)_2$ in acetonitrile after excitation at 300 nm. The black spectrum forms instantaneously at time zero and evolves in 2.2 ps into the blue component which decays in 87 ps into the yellow component with a lifetime longer than the measurement window.*

dynamics that could be attributed to three different components by sequential global fitting analysis, with lifetimes of 2.2 ps (component 1), 87 ps (component 2) and a decay longer than the limit of 7.5 ns (component 3). Component 2 and 3 were attributed to the excited triplet states of the cluster since the obtained spectra are in accordance with spectra obtained on the microsecond timescale. For molybdenum clusters, the second component was described as a hot triplet state, which can be also be applied in our case.[55] The spectra of component 1 exhibit an entirely different shape and are probably related to an exited singlet state. In total these results were in good agreement with previously reported data for $(TBA)_2[Mo_6X_8Y_6]$ (X = Cl, Br, I; Y = Cl, Br, I, CO_2CF_3).[55]

3.3 The Remarkable Robust, Photoactive Tungsten Iodide Cluster $[W_6I_{12}(NCC_6H_5)_2]$ (Publication 3)[78]

Previous reactions involving W_6I_{22} yielded different cluster compounds featuring cationic tungsten iodide clusters with acetonitrile ligands.[73, 76] Subsequently, the photoluminescence properties of one of these cationic species were then investigated.[76] Further understanding of the photophysical properties of tungsten iodide clusters can be gained by using other solvents to produce different species. Therefore, the following experiments involved different organic solvents, including benzonitrile. Treatment of W_6I_{22} with benzonitrile under solvothermal conditions resulted in the formation of $[W_6I_{12}(NCC_6H_5)_2]$ as black, cube-shaped crystals (Figure 14). We attributed the black color to the excess of iodine during in the reaction mixture. Attempts to remove the excess by dissolving the compound were futile due to the insolubility of the compound in common organic solvents. Thus, follow-up experiments included $Cs_2W_6I_{14}$ as a starting material paired with ZnI_2 to capture CsI during the reaction and gave the desired $[W_6I_{12}(NCC_6H_5)_2]$ as red cube-shaped crystals with orange photoluminescence (Figure 14).

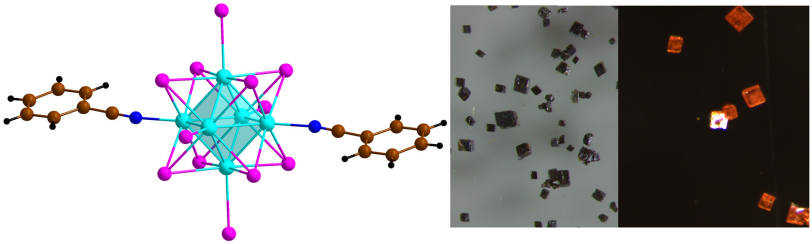

Figure 14. *Structure of the neutral tungsten iodide cluster $[W_6I_{12}(NCC_6H_5)_2]$ (left side; W: turquoise, I: pink, N: blue, C: brown, H: black). Cube-shaped single crystals of $[W_6I_{12}(NCC_6H_5)_2]$ were obtained starting from $[W_6I_{22}]$ (middle) or $Cs_2W_6I_{14}$ with addition of ZnI_2 (right side).*

The crystal structure of $[W_6I_{12}(NCC_6H_5)_2]$ was solved and refined on the basis of XRD and shows a heteroleptic cluster, with four of the apical ligands being iodide and two benzonitrile. In the bc plane the clusters adopt a layered arrangement and are alternately tilted to the left or right to allow a dense packing (Figure 15). Interestingly, H···I contacts between adjacent clusters in the structure are with 301.83 pm and 306.56 pm below the sum of the VdW radii (3.35 Å)[79] and imply H···I-bridges.

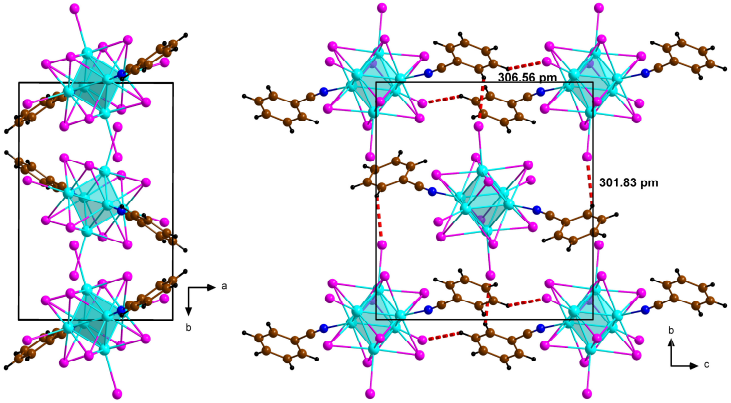

Figure 15. *Projections of the crystal structure of $[W_6I_{12}(NCC_6H_5)_2]$ in the ab (left side) and bc plane (right side) with red dashed bonds emphasizing short distances between hydrogen and iodine (W: turquoise, I: pink, C: brown, N: blue, H: black).*

To gain further insight into the nature of the bonding towards apical ligands and compare W–N, W–I and W–O bonds the ELF was calculated for $[W_6I_{12}(NCC_6H_5)_2]$, $(TBA)_2[W_6I_{14}]$ and $[(TBA)_2[W_6I_8(CO_2C_3F_7)_6]$. High electron densities at the metal centers are observed for $[W_6I_{12}(NCC_6H_5)_2]$ and $(TBA)_2[W_6I_{14}]$, while they are considerably lower for $[(TBA)_2[W_6I_8(CO_2C_3F_7)_6]$ (Figure 16). This implies reduced ionicity of the W–N and W–I bonds compared to the W–O bond. Nevertheless, the presence of nodal planes in the centers of the W–N/O/I bonds confirms the primary ionicity.

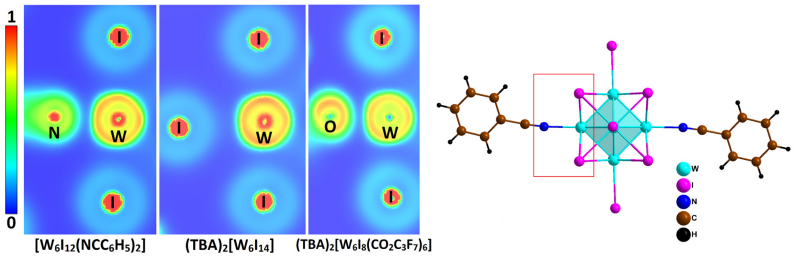

Figure 16. *Electron localization functions of $[W_6I_{12}(NCC_6H_5)_2]$, $(TBA)_2[W_6I_{14}]$ and $(TBA)_2[W_6I_8(CO_2C_3F_7)_6]$ (from left to right) and an illustration of the observed area marked with a red box (right side).*

The calculated band structure with a band gap of 1.9 eV is characteristic for a semiconductor and is in good agreement with the determined optical band gap of 2.17 eV.

The employment of a given material, such as octahedral metal halide clusters in fields like oxygen sensing,[41a, 41b] photocatalysis[35a, 35b, 38, 80] or solar cells[37] requires long-term stability. Therefore, we investigated the thermal and hydrolytic stability of $[W_6I_{12}(NCC_6H_5)_2]$.

Surprisingly, the conducted thermogravimetric analysis revealed a first decomposition step above 400 °C, which is unusually high for tungsten iodide clusters bearing organic ligands. The decomposition leads to the evaporation of benzonitrile and the formation of W_6I_{12} until the complete disintegration into the elements above 650 ° (Figure 17).

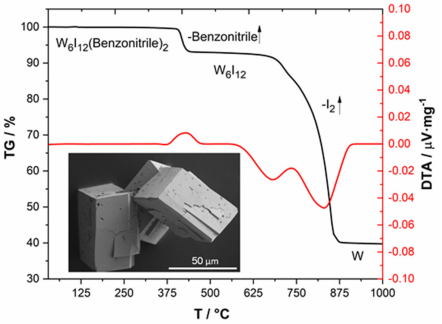

Figure 17. *Thermal analysis of $[W_6I_{12}(NCC_6H_5)_2]$ performed under argon flow with the thermogravimetric (TG) curve displayed in black and the differential thermal analysis (DTA) curve in red. The inset shows a SEM micrograph of the crystalline cluster compound.*

In addition to the thermal stability, we also investigated the hydrolytic stability of $[W_6I_{12}(NCC_6H_5)_2]$. Normally, when exposed to water, tungsten- or molybdenum halide clusters tend to partially exchange the apical ligands with hydroxyl groups.[62, 81] However, after being dispersed in water for over a month, the powder pattern of $[W_6I_{12}(NCC_6H_5)_2]$ was still phase pure and the color of the powder was unchanged, suggesting hydrolytic stability.

The recorded photoluminescence spectra of $[W_6I_{12}(NCC_6H_5)_2]$ show the broad excitation (250 nm to 550 nm) and emission bands (550 nm to 750 nm, $\lambda_{em,max}$ = 630 nm, Figure 18) characteristic for octahedral metal halide clusters.[29, 30c-e, 43a, 45a, 50] However, the emission is pronounced rather weak and the lifetimes of τ_1 = 0.48 µs (29 %) and τ_2 = 1.57 µs (71 %) and the quantum yield of 0.4 % are very low. The short lifetimes can be attributed to a low energetic splitting between the emitting triplet sublevels leading to a thermal population of the highest emitting sublevel with allowed transition to the ground state. The low energetic splitting is explained as a consequence of high d-electron density on the metal atoms,[56b] which has been observed in the calculated ELF. Additionally, close contacts to adjacent clusters can promote non-radiative energy transfer.[56d, 63, 82]

Despite the negligible photoluminescence, good hydrolytic and thermal stability as well as an optical band gap of 2.17 eV make $[W_6I_{12}(NCC_6H_5)_2]$ interesting for an application as a

photocatalyst. The potential in this field has already been demonstrated for other octahedral metal halide clusters, e.g. the photocatalytic decomposition of rhodamine B (RhB) in water us-

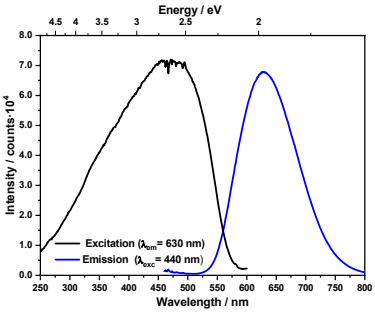

Figure 18. *Recorded excitation (black) and emission (blue) spectra of crystalline $[W_6I_{12}(NCC_6H_5)_2]$ at room temperature.*

ing $Na_2[Mo_6Br_8(N_3)_6]$.[35b] In the following we conducted experiments trying to photocatalytically decompose RhB. For this purpose, the cluster was dispersed in a RhB solution in water and the reaction was monitored over a period of 180 min using a UV/Vis spectrometer (Figure 19). In the plot displaying the change of concentration over time, the adsorption and desorption equilibrium is visible at 0 min and reveals 22 % adsorption. In the following 150 min of irradiation, more than 40 % of the dye have been degraded. The control experiment without photo-

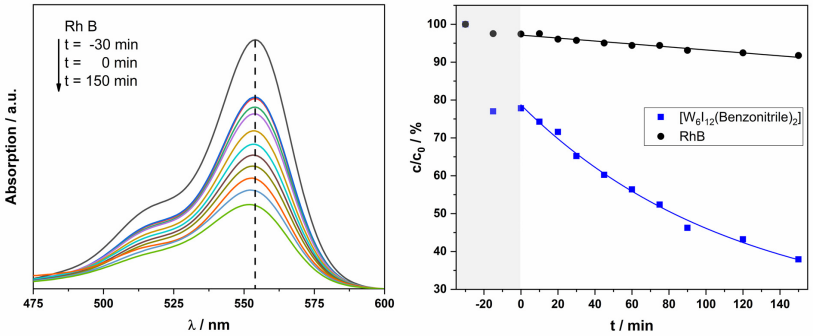

Figure 19. *UV/Vis absorption spectra of RhB during the photocatalytic decomposition experiments with $[W_6I_{12}(NCC_6H_5)_2]$ as a photocatalyst. Spectra were recorded starting from -30 min to 150 min irradiation time (left side). Time-dependent change of the RhB concentration in solution during the photocatalysis experiment with and without the photocatalyst.*

catalyst showed less than 10 % degradation after 150 min of UV irradiation. Complementary experiments used daylight as a radiation source to decompose RhB. The dispersions were

handled in small screwcap vials and placed in front of the window. In a cycle of three days, the reaction mixtures were colorless and the old solution was replaced with fresh RhB solution. The decomposition pace remained constant throughout the three conducted cycles.

In spite of weakly pronounced photoluminescence properties $[W_6I_{12}(NCC_6H_5)_2]$ shows great promise as a photocatalyst for the degradation of persistent organic pollutants in water. Accompanied by good thermal and hydrolytic stability this compound is a perfect example of a photocatalyst.

3.4 Other cationic tungsten iodide clusters

The process of synthesizing the photoluminescent $[W_6I_8(CH_3CN)_6](BF_4)_4 \cdot (CH_3CN)_2$ involved the reaction of $[(W_6I_8)I_3(CH_3CN)_3]I_7 \cdot I_2$ with four equivalents of $AgBF_4$ to remove iodide anions.[76] This reaction scheme was also applied using other silver salts, for example with four equivalents of $AgClO_4$, which gave yellow, stick-shaped crystals with orange photoluminescence (Figure 20).

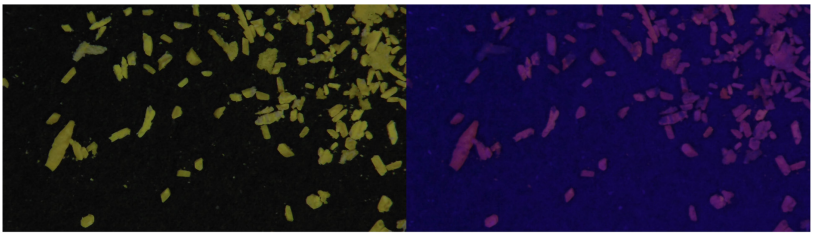

Figure 20. *Stick-shaped crystals from the reaction of $[(W_6I_8)I_3(CH_3CN)_3]I_7 \cdot I_2$ with four equivalents of $AgClO_4$ under visible light (left side) and UV light (365 nm, right side).*

The crystal structure of the identified compound $[W_6I_8(CH_3CN)_6](ClO_4)_4 \cdot (CH_3CN)_2$ was solved and refined on the basis of XRD. Crystal data are presented in Table **A 1**. In the crystal structure, the cluster cations $[W_6I_8(CH_3CN)_6]^{4+}$ adopt a layered arrangement in the *ac* plane with ClO_4^- anions and uncoordinated acetonitrile filling the voids (Figure 21). The obtained W–W (265.90(3)–266.83(2) pm), W–I (276.78(3)–278.56(3) pm) and W–N distances (215.6(4)–217.2(4) pm) are similar to the values obtained for the other described cationic cluster species with acetonitrile ligands.[73, 76]

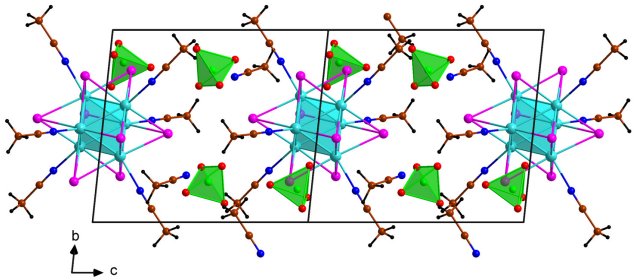

Figure 21. *Projection of the crystal structure of $[W_6I_8(CH_3CN)_6](ClO_4)_4 \cdot (CH_3CN)_2$ in the bc plane (W: turquois, I: pink, N: blue, C: brown, O: red, Cl: green, H: black).*

Photoluminescence spectra of $[W_6I_8(CH_3CN)_6](ClO_4)_4 \cdot (CH_3CN)_2$ were recorded by Dr. W. Leis and show broad absorption bands between 250 nm and 500 nm as well as an emission centered around 650 nm, characteristic for octahedral metal halide clusters (Figure 22).[29, 30c-e, 43a, 45a, 50] The location of the emission maximum is similar to that of $[W_6I_8(CH_3CN)_6](BF_4)_4$ or octahedral metal halide clusters bearing strong electron-withdrawing ligands.[29, 30c-e, 43a, 50, 76] Further investigation of the photophysical properties of $[W_6I_8(CH_3CN)_6](ClO_4)_4 \cdot (CH_3CN)_2$ was omitted, due to the explosive nature of the compound.

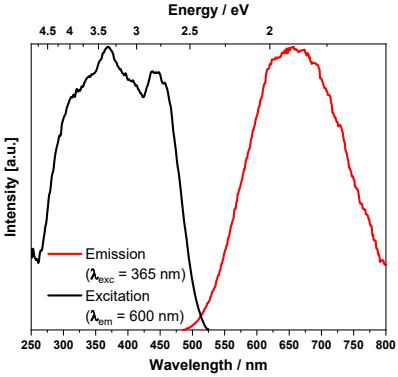

Figure 22. *Recorded excitation (black) and emission spectra (red) of a crystalline sample of the compound* $[W_6I_8(CH_3CN)_6](ClO_4)_4 \cdot (CH_3CN)_2$.

The reactions carried out to synthesize cationic or neutral tungsten iodide clusters starting from W_6I_{22} were not limited to acetonitrile and benzonitrile as organic solvents. Instead, experiments with DMSO lead to the formation of $[W_6I_8(DMSO)_6](I_3)_4$ as dark brown crystals, featuring the cationic clusters $[W_6I_8(DMSO)_6]^{4+}$. A similar compound has been reported and structurally characterized for molybdenum iodide clusters as $[Mo_6I_8(DMSO)_6](NO_3)_4$, and the analogous tungsten compound is believed to be isotypic, but no crystal data are available.[62] The crystal structure of $[W_6I_8(DMSO)_6](I_3)_4$ has been solved and refined on the basis of XRD. A layered arrangement with alternating layers of I_3^- anions and $[W_6I_8(DMSO)_6]^{4+}$ cations mixed with I_3^- anions is observed in the structure (Figure 23). Crystal data are given in Table A 1.

Averaged W–W [265.2(1) pm], W–I [280.7(1) pm] and W–O [214.6(1) pm] distances appear similar to other $[W_6I_8L_6]^{2-}$ clusters (W–W 265.4 ± 0.8 pm, W–I 278.8 ± 3.4 pm and W–O 213.7 ± 2.6 pm).[29, 43a, 50] The I_3^- anions show bond distances in the range of 286.9(1) pm and 299.6(1) pm and are asymmetric as previously reported for binary tungsten iodides or other compounds containing triiodides.[11a, 20, 74b]

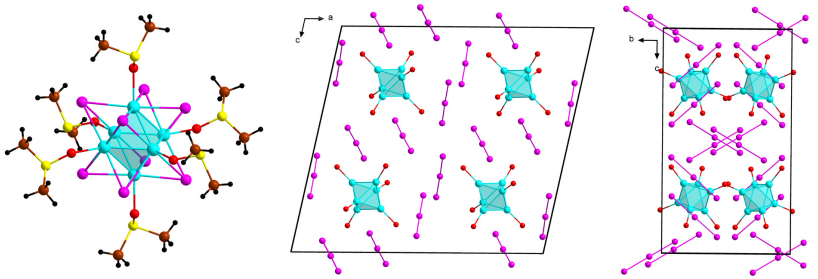

Figure 23. *Structure of the cluster cation $[W_6I_8(DMSO)_6]^{4+}$ (left side) and projections of the structure of $[W_6I_8(DMSO)_6](I_3)_4$ in the ac (middle) and bc plane. Inner iodido ligands and $S(CH_3)_2$ are omitted for clarity in the projections (W: turquoise, I: pink, O: red, S: yellow, C: brown, H: black).*

The compound $[W_6I_8(DMSO)_6](I_3)_4$ has a high iodine content in the structure and therefore the crystals appear with a dark color, as previously observed for $[(W_6I_8)I_3(CH_3CN)_3]I_7 \cdot I_2$.[73] Subsequent reactions with silver salts ($AgBF_4$, $AgClO_4$) to exchange the iodide anions yielded orange to yellow powders with a strongly pronounced photoluminescence, but failed to produce single crystals suitable for structure determination by XRD.

Further reactions of W_6I_{22} with different organic solvents (DMF, ethanol, THF) did not produce any single crystals or crystalline material suitable for structure determination, but yielded yellow to orange powders with red photoluminescence. Thus, these reactions, as well as the number of reports for this type of compounds in the literature,[24, 30a, 60-61] indicate a vast amount of possible cationic and neutral tungsten iodide clusters with solvent molecules as ligands. Additional obtained compounds could be the basis for further understanding of the photoluminescence of octahedral metal halide clusters.

3.4.1 Experimental

Synthesis of $[W_6I_8(CH_3CN)_6](ClO_4)_4 \cdot (CH_3CN)_2$

The synthesis was carried out according to the reported synthesis of $[W_6I_8(CH_3CN)_6](BF_4)_4 \cdot (CH_3CN)_2$.[76] In the beginning a thimble was filled with 150 mg (39.9 mmol) $[W_6I_{11}(CH_3CN)_3](I_7) \cdot I_2$ and 33 mg (159.4 mmol) $AgClO_4$ and placed in a Soxhlet extractor. Connected to the extractor was a round flask with 120 ml of acetonitrile. The flask with acetonitrile was heated under reflux for 16 h and then cooled to room temperature. After the extraction the solvent showed a yellow color, while white and yellow precipitate had formed at the bottom of the flask. The yellow solution was collected and the acetonitrile evaporated to give a yellow crystalline powder and small stick-shaped crystals (estimated yield > 50 %). Both the powder and the crystals showed orange luminescence when irradiated with UV light. Upon scratching or contact with a flame the yellow powder detonates.

Synthesis of $[W_6I_8(DMSO)_6](I_3)_4$

A homemade quartz ampoule with 10.6 ml volume was filled with 150 mg W_6I_{22} (38.5 µmol) and 2 ml DMSO. Subsequently the ampoule was sealed under vacuum and kept at 85 °C for two days. After cooling to room temperature, the black solution was removed and the remaining brown crystals rinsed with diethyl ether. (yield: 100 mg, 24.4 µmol, 64 %).

3.5 Synthesis, Crystal Structure, and Luminescence of Metal Iodide Cluster Compounds (^{n}Bu$_4$N)$_2$[M$_6$I$_8$(NCO)$_6$] with M = Mo, W (Publication 4)[83]

Octahedral metal halide clusters are known for their remarkable photophysical properties, including a bright red phosphorescence, long emission lifetimes, high emission quantum yields and a strong quenching of the emission in the presence of molecular oxygen. Especially long lifetimes and strong oxygen quenching are usually associated with cluster species featuring strong electron-withdrawing organic ligands.[29, 30c-e, 43a, 45a, 50]

Herein we introduce the cluster compounds (^{n}Bu$_4$N)$_2$[*M*$_6$I$_8$(NCO)$_6$] (M = Mo, W) with purely inorganic NCO ligands. Corresponding compounds of the form (^{n}Bu$_4$N)$_2$[Mo$_6$Cl$_8$(NCO)$_6$], (^{n}Bu$_4$N)$_2$[Mo$_6$Br$_8$(NCO)$_6$] and (^{n}Bu$_4$N)$_2$[W$_6$Cl$_8$(NCO)$_6$] have been previously published and their spectroscopic properties have been analyzed.[84]

The preparation of the title compounds was carried out in a ligand exchange reaction removing the six apical iodido ligands of (^{n}Bu$_4$N)$_2$[*M*$_6$I$_{14}$] (*M* = Mo, W) and exchanging them for NCO$^-$. After the synthesis, the resulting products (^{n}Bu$_4$N)$_2$[*M*$_6$I$_8$(NCO)$_6$] (*M* = Mo, W) were isolated as orange or red, crystalline powders.

The crystal structures of (^{n}Bu$_4$N)$_2$[*M*$_6$I$_8$(NCO)$_6$] (*M* = Mo, W) were solved and refined on the basis of XRD and feature the cluster anions [*M*$_6$I$_8$(NCO)$_6$]$^{2-}$ (Figure 24) and ^{n}Bu$_4$N$^+$. Both structures are isotypic to the known compounds (^{n}Bu$_4$N)$_2$[Mo$_6$*X*$_8$(NCO)$_6$] (*X* = Cl, Br) and (^{n}Bu$_4$N)$_2$[W$_6$Cl$_8$(NCO)$_6$][84] and show a strongly distorted tetrahedral environment of the ^{n}Bu$_4$N$^+$ cations with [*M*$_6$I$_8$(NCO)$_6$]$^{2-}$ anions. The anions are located at the edges of the unit cell (Figure 24).

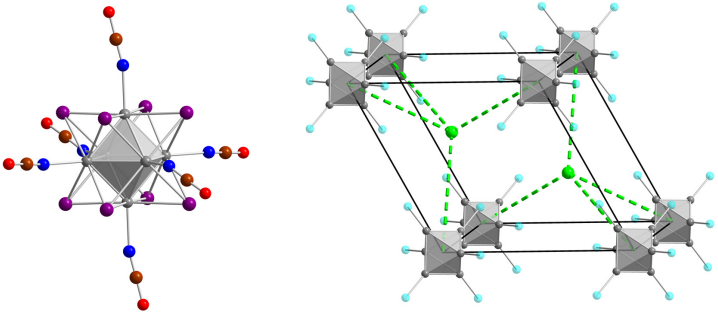

Figure 24. *The cluster ion [M$_6$I$_8$(NCO)$_6$]$^{2-}$ from the crystal structure of (^{n}Bu$_4$N)$_2$[M$_6$I$_8$(NCO)$_6$] (right side; Color code M: grey, N: blue, C: brown, O: red, I: violet). Illustration of the tetrahedral environment of ^{n}Bu$_4$N cations in the unit cell of (^{n}Bu$_4$N)$_2$[Mo$_6$I$_8$(NCO)$_6$] (left side; M: grey, NCO$^-$-ligands: light blue, centres of gravity of ^{n}Bu$_4$N cations: green). The inner iodido ligands of the cluster core are omitted for clarity.*

In contrast to the vast majority of $[M_6I_8L_6]^{2-}$ clusters the apical cyanato ligands are connected to the $[M_6I_8]$ core via the nitrogen atom. This observation is confirmed by the *M*–N bond distances with averaged values of 2.131(3) Å (Mo–N) and 2.17(1) Å (W–N), which are in good agreement with obtained literature distances between 2.044 Å and 2.177 Å (Mo–N).[84] In addition, the IR spectra show intrinsic vibrations of cyanato ligands in the expected regions for N–C (W 2210 cm^{-1} and Mo 2200 cm^{-1}) and C–O (W 1344 cm^{-1} and Mo 1379 cm^{-1}) valence vibrations. The photoluminescence properties of the two cluster compounds $(^nBu_4N)_2[M_6I_8(NCO)_6]$ (*M* = Mo, W) were also investigated. Recorded spectra reveal broad excitation bands between 250 nm and 600 nm and an emission centered around 700 nm, which are characteristic observations for this type of cluster (Figure 25).[29, 30c-e, 43a, 45a, 50] Measurements under different atmospheres show a quenching of the photoluminescence in the presence of molecular oxygen of only 3 % for $(^nBu_4N)_2[W_6I_8(NCO)_6]$ and 10 % for $(^nBu_4N)_2[Mo_6I_8(NCO)_6]$. The recorded emission lifetimes lead to the same conclusion with values of 187 µs (N_2) and 180 µs (O_2) obtained for $(^nBu_4N)_2[Mo_6I_8(NCO)_6]$. Differences in the lifetimes for the compound $(^nBu_4N)_2[W_6I_8(NCO)_6]$ were even smaller.

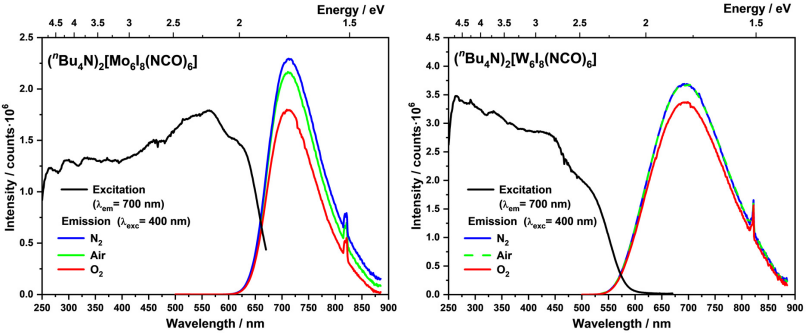

Figure 25. *Recorded excitation (black) and emission spectra of $[(^nBu)_4N)_2[M_6I_8(NCO)_6]$ with M = Mo, W. Emission spectra were recorded under nitrogen (blue), air (green) and oxygen (red) atmosphere.*

3.6 The Photoluminescence of $A_2[W_6Cl_{14}]$ with A = TBA, PPN or PPh_4

The photoluminescence of tungsten and molybdenum halide clusters $[M_6X_8Y_6]^{2-}$ (M = Mo, W; X = Cl, Br, I; Y = Cl, Br, I) in solution has been studied extensively in the past. In terms of emission lifetimes, quantum yields and quenching in the presence of molecular oxygen, the octahedral metal iodides show the best results.[45b, 47] More recently, new results in solution indicate longer lifetimes, higher quantum yields and stronger oxygen quenching for the chloride compounds in the series of molybdenum halide clusters $(TBA)_2[Mo_6X_{14}]$ (X = Cl, Br, I).[45a] Therefore, in this work, the photoluminescence properties of tungsten chloride clusters in the solid state were revisited. The studies were focused on the compounds $(TBA)_2[W_6Cl_{14}]$, $(PPN)_2[W_6Cl_{14}]$ and $(PPh_4)_2[W_6Cl_{14}]$, to compare them to the analogous tungsten iodide clusters. A strong influence of large organic cations on the emission quantum yields of octahedral metal halide clusters was observed in preliminary work by Dr. T. Hummel *et al.*[28, 49]

The synthesis of the compounds described in the following was carried out by K. Röseler during an internship in this group. All reactions used W_6Cl_{12} and ACl (A = PPN, PPh_4, TBA) as starting materials for solid-state reactions. The growth of single-crystals suitable for XRD was achieved by crystallization from acetone or DCM for the compounds $(PPN)_2[W_6Cl_{14}]\cdot(CH_2Cl_2)_2$ and $(PPh_4)_2[W_6Cl_{14}]\cdot(C_3H_6O)_2$. Crystal data are given in Table A 1. The crystal structures feature $[W_6Cl_{14}]^{2-}$ anions and the organic cations PPN^+ and PPh_4^+ (Figure 26). Furthermore, the synthesis of $(TBA)_2[W_6Cl_{14}]$ was verified by PXRD since the crystal structure is known.[85]

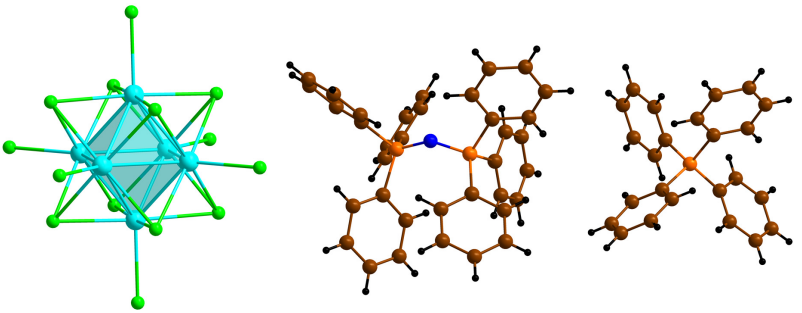

Figure 26. *Structure of the $[W_6Cl_{14}]^{2-}$ anion and the two cations PPN^+ and PPh_4^+ (from left to right; W: turquoise, Cl: green, N: blue, P: orange, C: brown, H: black).*

In the structure of $(PPN)_2[W_6Cl_{14}]\cdot(CH_2Cl_2)_2$ the $[W_6Cl_{14}]^{2-}$ anions are coordinated by ten PPN^+ cations to form an elongated triangular bipyramid (Johnson solid No. 15)[86] (Figure 27), while the cations are coordinated by five anions in a square pyramidal manner.

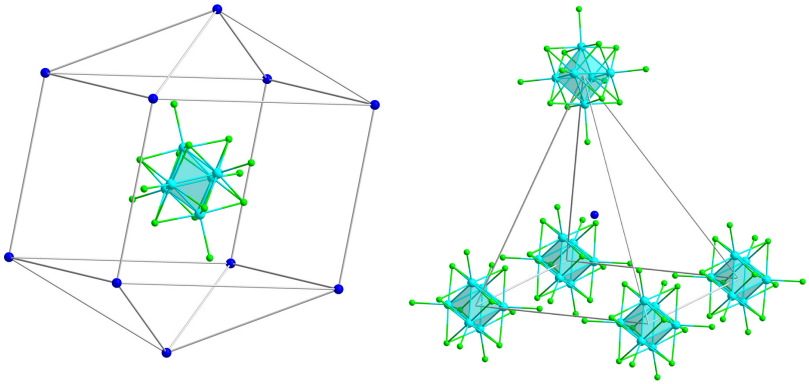

Figure 27. *Coordination environment of $[W_6Cl_{14}]^{2-}$ anions (left side) and PPN^+ cations (right side) in the crystal structure of $(PPN)_2[W_6Cl_{14}]\cdot(CH_2Cl_2)_2$. Cations are represented by the central nitrogen atom, while the carbon, phosphorous and hydrogen atoms as well as the DCM molecules are omitted for clarity (W: turquoise, Cl: green, N: blue).*

The crystal structure of $(PPh_4)_2[W_6Cl_{14}]\cdot(C_3H_6O)_2$ shows the $[W_6Cl_{14}]^{2-}$ anions in trigonal prismatic surrounding by six PPh_4^+ cations (Figure 28) and the cations are surrounded trigonal planar by three anions.

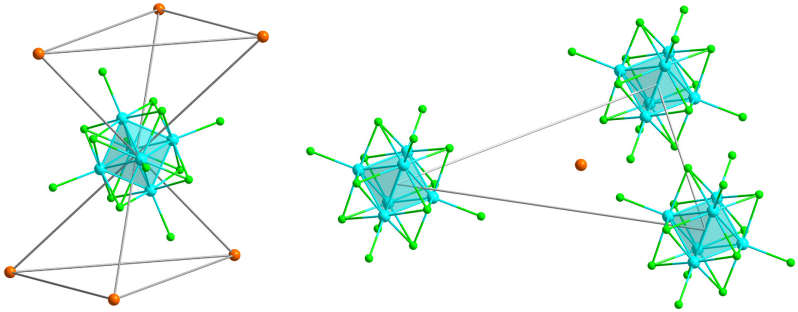

Figure 28. *Coordination environment of $[W_6Cl_{14}]^{2-}$ anions (left side) and PPh_4^+ cations (right side) in the crystal structure of $(PPh_4)_2[W_6Cl_{14}]\cdot(C_3H_6O)_2$. Cations are represented by the central phosphorous atom, while the carbon, and hydrogen atoms as well as the acetone molecules are omitted for clarity (W: turquoise, Cl: green, P: orange).*

Averaged W–W distances of 261.4(1), W–Cl^i of 249.7(1) pm and W–Cl^a of 243.0(1) pm are in agreement with values previously reported for $[W_6Cl_{14}]^{2-}$ clusters (W–W 261.0 ± 1.2 pm, W–Cl^i 247.9 ± 2.9 pm, W–Cl^a 246.8 ± 5.3 pm).[85, 87]

All photoluminescence spectra, emission lifetimes and quantum yields were recorded by Dr. D. Enseling. Investigations of the photoluminescence properties of $(TBA)_2[W_6Cl_{14}]$, $(PPN)_2[W_6Cl_{14}]$ and $(PPh_4)_2[W_6Cl_{14}]$ reveal a weakly pronounced emission (Figure 29, Figure

A 1, Figure A 2), short emission lifetimes between 4.99 µs and 2.13 µs, undetectable quantum yields and no oxygen quenching. Determined values for the emission lifetimes are well below the known values for the analogue tungsten iodide clusters.[28, 49, 52] The observed short lifetimes could be a consequence of a low splitting of the emitting triplet sublevels and thus a thermal population of the energetically highest sublevel featuring an allowed transition into the ground state.[56b, 76]

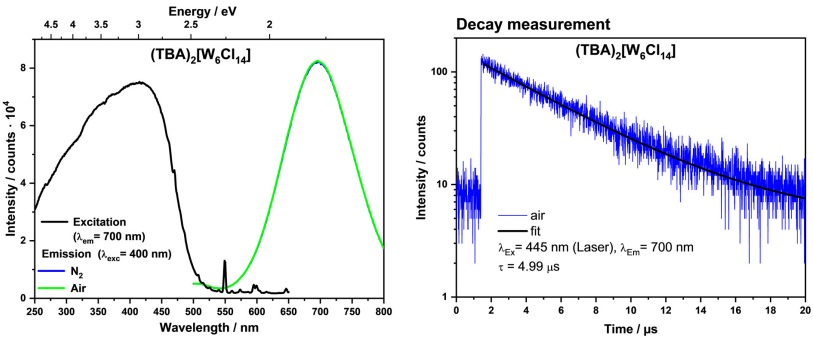

Figure 29. *Recorded excitation (black) and emission spectra (green N_2, blue air, left side) and decay measurement (right side) of crystalline $(TBA)_2[W_6Cl_{14}]$.*

Overall, tungsten halide clusters show emission lifetimes with a maximum of 55 µs (biexponential decay τ = 27 and 55 µs)[30d] in the solid state. Usually the longer lifetimes are associated with compounds featuring strong electron-withdrawing ligands such as trifluoroacetate, OTs or heptafluorobutyrate.[29, 30d, 43a, 76] Logically, these species showing long lifetimes also exhibit strong oxygen quenching of the emission. However, in terms of oxygen quenching analogous molybdenum iodide clusters are superior compared to their tungsten counterparts.[29, 43a, 50] This is likely related to their higher emission lifetimes, with up to 235 µs for strong quenching species.[55]

3.6.1 Experimental

Synthesis of $(A)_2[W_6Cl_{14}]$ (A = TBA, PPN, PPh_4)

300 mg W_6Cl_{12} (196 µmol, 1 equivalent) and 109 mg TBACl (392 µmol, 2 equivalents) or 225 mg PPNCl (392 µmol, 2 equivalents) or 147 mg PPh_4 (392 µmol, 2 equivalents) were thoroughly mixed with an agate mortar in a glove box. Subsequently, the mixtures were transferred into quartz ampoules with 2.7 ml volume (l = 7 cm, d = 0.7 cm), which were sealed under vacuum. Afterwards the ampoules were placed in a furnace and heated with 2 °C/min to 200 °C

(*A* = TBA) or 300 °C (*A* = PPN, PPh_4) and kept at the temperature for 24 . The resulting powders showed bright yellow color. Plate-shaped crystals of $PPN_2[W_6Cl_{14}]$ were grown by dissolving the powder in DCM and subsequent evaporation of the solvent. Single-crystals of $(PPh_4)_2[W_6Cl_{14}]$ were achieved using the same method with acetone.

3.7 Crystal structure, Magnetic and Photoluminescence Properties of GdW_6Cl_{15}, TbW_6Cl_{15}, and EuW_6Cl_{14} (Publication 5)[88]

The energy transfer from excited triplet states of octahedral metal halide clusters onto molecular oxygen to produce singlet oxygen is one of the most prominent properties of this class of compounds. Interestingly, an energy transfer onto other photoluminescent ions or species is also possible, as has been reported by this group.[28, 64] In preliminary work, a supramolecular compound based on an octahedral metal halide cluster and a cryptate-*RE* complex, namely [Crypt-*RE*]-[W_6I_{14}] (*RE* = Nd, Yb) has been synthesized.[28, 64] This cluster species exhibits an energy transfer from the cluster to the *RE* ions.[28, 64]

Using a solid-state route, we produced the compounds GdW_6Cl_{15}, TbW_6Cl_{15} and EuW_6Cl_{14} starting from W_6Cl_{12} and an excess of $RECl_3$ (*RE* = Gd, Tb) or $EuCl_2$. Their crystal structures were refined isotypic to BiW_6Cl_{15}[87] or $PbMo_6Cl_{14}$[89] on the basis of PXRD, using Rietveld refinement.

The crystal structures of GdW_6Cl_{15} and TbW_6Cl_{15} show *RE* ions surrounded by seven chloride ions, while six of them are apical chloride ligands of $[W_6Cl_{14}]^{2-}$ clusters one is terminally bound to the *RE* cation (Figure 30). These chlorido ligands show a bond length to the *RE* ions between

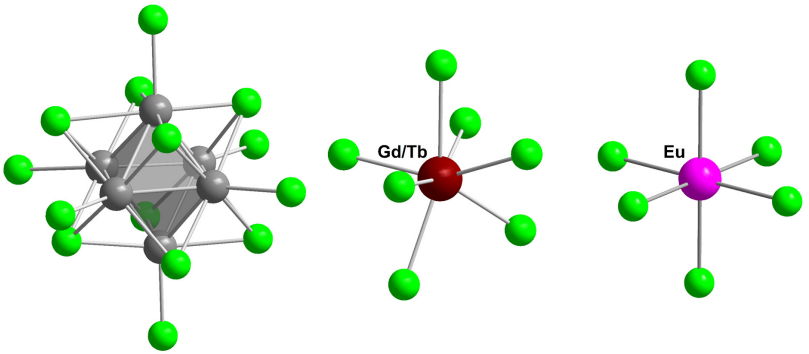

Figure 30. *Structure of the $[W_6Cl_{14}]^{2-}$ cluster ion (left side) and coordination environments of Gd^{3+} and Tb^{3+}-ions in GdW_6Cl_{15} and TbW_6Cl_{15} (center) and of Eu^{2+}-ions in EuW_6Cl_{14} (right side; W: grey, Gd/Tb: red, Cl: green Eu: pink).*

2.665(2)–2.936(2) Å (Gd) or 2.621(2)–2.915(1) Å (Tb), while the terminally bound ligand features the shortest distance. Similar results were obtained for Bi–Cl distances in BiW_6Cl_{15} and $BiMo_6Cl_{15}$.[87] The general arrangement of $[W_6Cl_{14}]^{2-}$ clusters and $(RECl)^{2+}$ cations can be regarded as a distorted rock-salt super-structure (Figure 31), where the mass centres of cluster anions and RE^{3+} cations occupy positions similar to those of Na^+ and Cl^- in the NaCl structure.

In the crystal structure of EuW_6Cl_{14}, Eu^{2+} ions are surrounded by six apical chloride ligands of $[W_6Cl_{14}]^{2-}$ clusters. The general arrangement also follows the rock-salt structure motif.

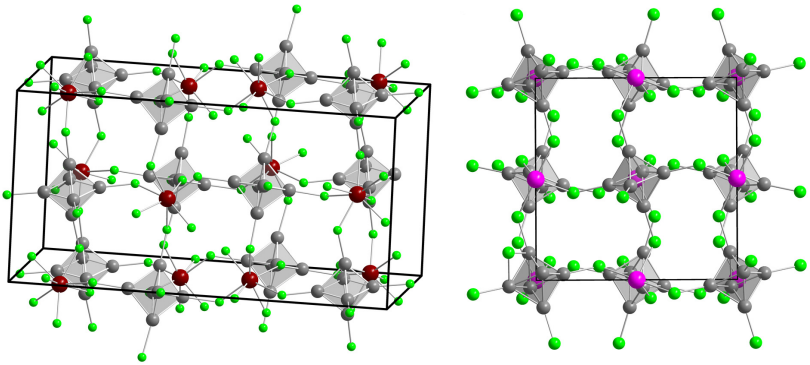

Figure 31. *Unit cells of GdW_6Cl_{15}, TbW_6Cl_{15} (left side) and EuW_6Cl_{14} (right side) with inner Cl ligands of the clusters (Cl') omitted for clarity (W: grey, Gd/Tb: red, Eu: pink, Cl: green).*

Magnetic measurements recorded for the compounds GdW_6Cl_{15}, TbW_6Cl_{15} and EuW_6Cl_{14} indicate paramagnetic behavior (Figure 32). However, the calculated magnetic moments (TbW_6Cl_{15} 10.49 μ_B, GdW_6Cl_{15} 9.27 μ_B and EuW_6Cl_{14} 10.07 μ_B) are higher than the expected values (≈ 9.7 μ_B for Tb^{3+} and ≈ 7.9 μ_B for Gd^{3+} and Eu^{2+})[90] due to residual *RE* chlorides in the product powders after rinsing with acetonitrile. The results show no coupling between the magnetic moments of the *RE* ions as would be expected from isolated Gd^{3+}, Tb^{3+} and Eu^{2+}ions in the respective structures.

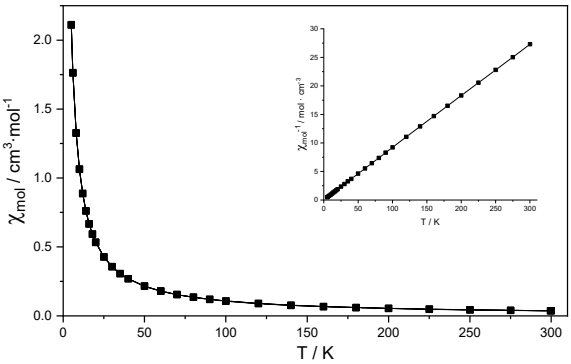

Figure 32. *Plot of magnetic susceptibility against temperature for GdW_6Cl_{15} and a plot of the inverse susceptibility against temperature in the inset (top right side).*

Photoluminescence spectra recorded for crystalline TbW_6Cl_{15} and EuW_6Cl_{14} at room temperature show the characteristic broad excitation bands of tungsten halide clusters between 250 nm and 450 nm and only weak emission bands between 550 nm and 800 nm (**Figure 33**).[25b, 28, 49, 87, 91] The weak emission intensity is probably related to thermal quenching, as has been reported for ternary octahedral tungsten iodide clusters like $Cs_2W_6I_{14}$.[25b] Furthermore, no emission of the *RE* ions is observed because the energy level of the excited triplet states is rather low compared to the emitting states of Eu^{2+} or Tb^{3+}, making an energy transfer unlikely.[92]

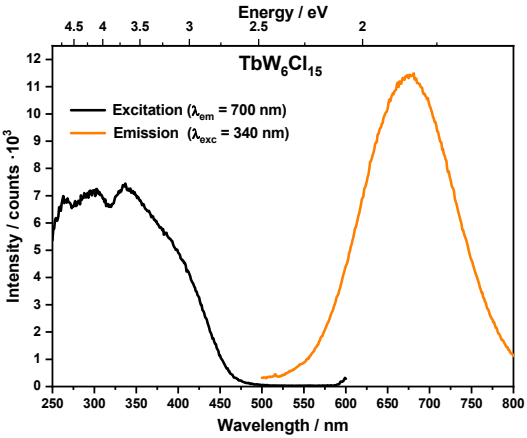

Figure 33. *Recorded excitation (black) and emission (orange) spectra of crystalline TbW_6Cl_{15} at room temperature.*

3.8 The $[W_6I_{14}]^{2-}$ anion combined with cationic metal complexes

Further research regarding an energy transfer from tungsten iodide clusters towards metal centers were conducted in cooperation with Dr. T. Maulbetsch from workgroup of Prof. Kunz.[93] Their research focuses on carbenaporphyrins, which, are like their natural occurring counterparts (porphyrins) combinable with various different metal centers.[94] Thus, possibly allowing a combination of $[W_6I_{14}]^{2-}$ with different metal centers. First approaches carried out by Dr. T. Maulbetsch involved the reaction of $TBA_2[W_6I_{14}]$ with $[Fe(CTP)](BF_4)$ and gave $[Fe(CTP)]_2[W_6I_{14}]$ as a product.[93]

The crystal structure of $[Fe(CTP)]_2[W_6I_{14}]$ has been solved and refined on the basis of XRD and reveals a molecular structure with isolated $[Fe(CTP)]_2[W_6I_{14}]$ units.[93] Herein two $[Fe(CTP)]^+$ cations coordinate one $[W_6I_{14}]^{2-}$ anion via opposing apical iodido ligands (Figure 34). Crystal data are included in Table A 1.

Averaged W–W distances of 266.1(1) pm, W–I^i of 279.8(1) pm and W–I^a of 282.2(1) pm are in good agreement with reported values for the $[(W_6I_8)I_6]^{2-}$ core (W–W 267.2 ± 1.9 pm, W–I^i 279.4 ± 1.1 pm and W–I^a 282.3 ± 3.9 pm).[25a] The two W–I^a distances related to the Fe are slightly longer (284.0(1) pm and 289.0(1) pm).

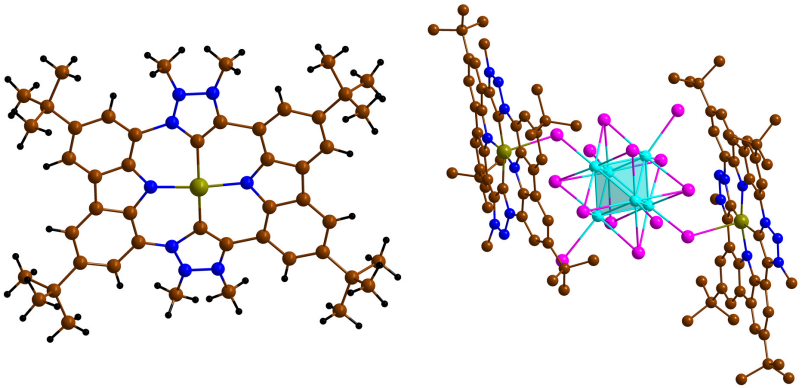

Figure 34. *Structure of the $[Fe(CTP)]^+$ cation (left side) and the molecular complex $[Fe(CTP)]_2[W_6I_{14}]$ (right side). In the depiction of the complex hydrogen atoms are omitted for clarity. Disorders of the cation and anion are omitted (W: turquoise, I: pink, Fe: green, C: brown, N: blue, H: black).*

Investigations into the photoluminescence of crystalline $[Fe(CTP)]_2[W_6I_{14}]$ conducted by Dr. D. Enseling revealed no emission in contrast to pure carbenaporphyrins[94] or $(TBA)_2[W_6I_{14}]$[47, 49, 52] (Figure A 3). Additional spectra recorded under cooling with liquid nitrogen or helium also showed no photoluminescence emission. Hence, the emission of the tungsten iodide clusters is completely quenched, which could be due to an energy transfer onto the Fe^{3+} complex.

Further investigations to clarify whether an energy transfer occurs should include different $[M(CTP)]^+$ complexes containing luminescent and non-luminescent ions. This way either the photoluminescence emission of the tungsten iodide clusters, carbenaporphyrins or an emitting ion should be observed.

Photoelectron spectroscopy performed by K. Greulich from the workgroup Chassé showed that the HOMO is composed purely of $[W_6I_{14}]^{2-}$ states.

Further experiments to combine the octahedral tungsten iodide cluster $[W_6I_{14}]^{2-}$ with a metal complex were attempted by the reaction of $(TBA)_2[W_6I_{14}]$ with $[Fe(C_5H_5)_2](BF_4)$. Surprisingly, the expected compound $[Fe(C_5H_5)_2]_2[W_6I_{14}]$ didn't form, however a small amount of green crystals formed in the reaction vessel and were identified as $[Fe(CH_3CN)_6][W_6I_{14}]$. A contamination of the reactant with $FeCl_2$ is likely, since the starting material $[Fe(C_5H_5)_2](BF_4)$ is produced by oxidation of $[Fe(C_5H_5)_2]$ using $FeCl_3$ (Fe^{3+}) as the oxidant.[95]

In the structure, Fe^{2+} ions appear in an octahedral coordination environment with six acetonitrile molecules, resulting in a $[Fe(CH_3CN)_6]^{2+}$ cation next to the $[W_6I_{14}]^{2-}$ anions (Figure 35). Anions and cations surround each other in a distorted cubic fashion (Figure 36). Crystal data are included in Table A 1.

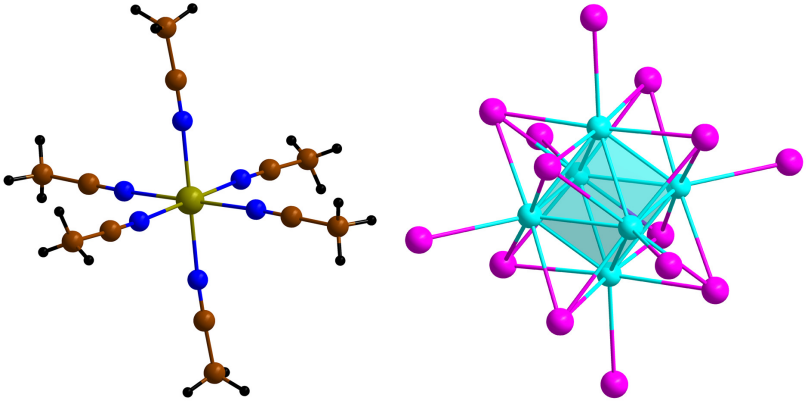

Figure 35. *Structure of the $[Fe(CH_3CN)_6]^{2+}$ cation (left side) and $[W_6I_{14}]^{2-}$ anion (right side) in the crystal structure of $[Fe(CH_3CN)_6]W_6I_{14}$ (W: turquoise, I: pink, Fe: green, N: blue, C: brown, H: black).*

Averaged W–W distances of 266.8(1) pm, W–I^i of 280.5(1) pm and W–I^a of 283.5(1) pm are in good agreement with reported values for the $[(W_6I_8)I_6]^{2-}$ core (W–W 267.2 ± 1.9 pm, W–I^i 279.4 ± 1.1 pm and W–I^a 282.3 ± 3.9 pm).[25a]

The obtained crystals did not show any photoluminescence emission. Nevertheless, the reaction reveals potential for the synthesis of new tungsten iodide cluster species based on cationic metal-solvent complexes and the $[W_6I_{14}]^{2-}$ anion.

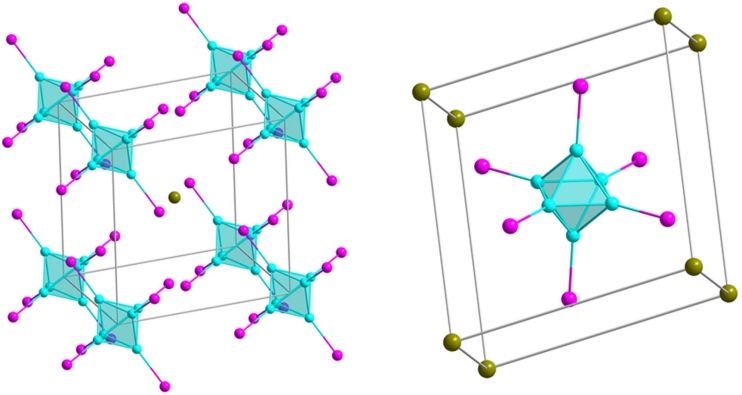

Figure 36. *Coordination environment of the $[Fe(CH_3CN)_6]^{2+}$ cations and the $[W_6I_{14}]^{2-}$ anions in the structure of $[Fe(CH_3CN)_6][W_6I_{14}]$. Acetonitrile ligands are omitted for clarity (W: turquoise, I: pink Fe: green).*

3.8.1 Experimental

Synthesis of $[Fe(CTP)]_2[W_6I_{14}]$

The synthesis of the compound $[Fe(CTP)]_2[W_6I_{14}]$ is described in the thesis of Dr. T Maulbetsch.[93]

Synthesis of $[Fe(CH_3CN)_6][W_6I_{14}]$

50.0 mg $(TBA)_2[W_6I_{14}]$ (14.9 µmol) were dissolved in 10 ml acetonitrile. Subsequently the solution was cooled with liquid nitrogen until solidification. 8,1 mg $[Fe(C_5H_5]_2](BF_4)$ (29.8 µmol) were dissolved in 10 ml DCM and slowly layered onto the solid $(TBA)_2[W_6I_{14}]$ in acetonitrile while simultaneously cooling with liquid nitrogen. In the following 7 d the Schlenk tube with the mixture was kept at -30 °C in a fridge. Afterwards small hexagonal-shaped crystals had formed on the wall of the tube.

4. References

[1] J. A. A. Ketelaar, G. W. van Oosterhout, *Recueil des Travaux Chimiques des Pays-Bas* **1943**, *62*, 197–200.
[2] F. A. Cotton, C. E. Rice, *Acta Crystallogr. B* **1978**, *34*, 2833–2834.
[3] V. Kolesnichenko, D. C. Swenson, L. Messerle, *Inorg. Chem.* **1998**, *37*, 3257–3262.
[4] a) R. Siepmann, H.-G. v. Schnering, H. Schäfer, *Angew. Chem., Int. Ed. Engl.* **1967**, *6*, 637–637; b) A. Nägele, J. Glaser, H.-J. Meyer, *Z. Anorg. Allg. Chem.* **2001**, *627*, 244–249.
[5] H. Schäfer, H. G. von Schnering, J. Tillack, F. Kuhnen, H. Wöhrle, H. Baumann, *Z. Anorg. Allg. Chem.* **1967**, *353*, 281–310.
[6] a) M. Ströbele, H.-J. Meyer, *Russ. J. Coord. Chem.* **2012**, *38*, 178–182; b) W. Willing, U. Muller, *Acta Crystallogr. C* **1987**, *43*, 1425–1426; c) Y.-Q. Zheng, K. Peters, W. Hönle, Y. Grin, H. G. Schnering, *Z. Kristallogr. Cryst. Mater.* **1997**, *212*, 453–457.
[7] J. Saßmannshausen, H.-G. von Schnering, *Z. Anorg. Allg. Chem.* **1994**, *620*, 1312–1320.
[8] a) R. Siepmann, H. G. von Schnering, *Z. Anorg. Allg. Chem.* **1968**, *357*, 289–298; b) H. Schäfer, H. G. von Schnering, A. Simon, D. Giegling, D. Bauer, R. Siepmann, B. Spreckel, *Journal of the Less-Common Metals* **1966**, *10*, 154–155.
[9] H. Schäfer, R. Siepmann, *Z. Anorg. Allg. Chem.* **1968**, *357*, 273–288.
[10] M. Ströbele, H.-J. Meyer, *Z. Anorg. Allg. Chem.* **2012**, *638*, 945–949.
[11] a) P. H. Svensson, L. Kloo, *Chem. Rev.* **2003**, *103*, 1649–1684; b) M. Ströbele, H.-J. Meyer, *Dalton Trans.* **2019**, *48*, 1547–1561.
[12] M. Ströbele, H.-J. Meyer, *Z. Anorg. Allg. Chem.* **2016**, *642*, 631–634.
[13] M. Ströbele, C. Castro, R. F. Fink, H.-J. Meyer, *Angew. Chem., Int. Ed.* **2016**, *55*, 4814–4817.
[14] M. Ströbele, H.-J. Meyer, *Z. Anorg. Allg. Chem.* **2016**, *642*, 1409–1411.
[15] J. D. Franolic, J. R. Long, R. H. Holm, *J. Am. Chem. Soc.* **1995**, *117*, 8139–8153.
[16] M. Ströbele, H.-J. Meyer, *Inorg. Chem.* **2017**, *56*, 14300–14305.
[17] M. Ströbele, H.-J. Meyer, *Z. Anorg. Allg. Chem.* **2016**, *642*, 677–680.
[18] M. Ströbele, H.-J. Meyer, *Z. Anorg. Allg. Chem.* **2010**, *636*, 62–66.
[19] M. Ströbele, H.-J. Meyer, *Inorg. Chem.* **2017**, *56*, 5880–5884.
[20] M. Ströbele, H.-J. Meyer, *Inorg. Chem.* **2019**, *58*, 12867–12872.
[21] A. Riche, *Annales de chimie et de physique* **1857**, *3*, 5–80.
[22] a) E. Defacqz, *Comptes rendus de l'Académie des sciences* **1898**, *127*, 510–512; b) E. Defacqz, *Comptes rendus de l'Académie des sciences* **1898**, *126*, 962–694.
[23] A. D. Westland, N. Muriithi, *Inorg. Chem.* **1973**, *12*, 2356–2361.
[24] R. D. Hogue, R. E. McCarley, *Inorg. Chem.* **1970**, *9*, 1354–1360.
[25] a) T. Hummel, A. Mos-Hummel, A. Merkulova, M. Ströbele, A. Krishnamurthy, S. Kroeker, H.-J. Meyer, *Inorg. Chem.* **2018**, *57*, 2570–2576; b) T. Hummel, M. Ströbele, D. Schmid, D. Enseling, T. Jüstel, H.-J. Meyer, *Eur. J. Inorg. Chem.* **2016**, *2016*, 5063–5067.
[26] H. Schäfer, H. G. Schulz, *Z. Anorg. Allg. Chem.* **1984**, *516*, 196–200.
[27] E. G. Tulsky, J. R. Long, *Chem. Mater.* **2001**, *13*, 1149–1166.
[28] T. Hummel, Dissertation, Universität Tübingen **2020**.
[29] L. Riehl, A. Seyboldt, M. Ströbele, D. Enseling, T. Jüstel, M. Westberg, P. R. Ogilby, H.-J. Meyer, *Dalton Trans.* **2016**, *45*, 15500–15506.

[30] a) F. A. Cotton, N. F. Curtis, *Inorg. Chem.* **1965**, *4*, 241–244; b) W. Preetz, P. Braack, K. Harder, G. Peters, *Z. Anorg. Allg. Chem.* **1992**, *612*, 7–13; c) K. Kirakci, P. Kubat, M. Dusek, K. Fejfarova, V. Sicha, J. Mosinger, K. Lang, *Eur. J. Inorg. Chem.* **2012**, 3107–3111; d) M. N. Sokolov, K. A. Brylev, P. A. Abramov, M. R. Gallyamov, I. N. Novozhilov, N. Kitamura, M. A. Mikhaylov, *Eur. J. Inorg. Chem.* **2017**, *2017*, 4131–4137; e) M. A. Mikhailov, K. A. Brylev, P. A. Abramov, E. Sakuda, S. Akagi, A. Ito, N. Kitamura, M. N. Sokolov, *Inorg. Chem.* **2016**, *55*, 8437–8445.

[31] K. Kirakci, M. A. Shestopalov, K. Lang, *Coordin Chem Rev* **2023**, *481*, 215048.

[32] A. A. Krasilnikova, M. A. Shestopalov, K. A. Brylev, I. A. Kirilova, O. P. Khripko, K. E. Zubareva, Y. I. Khripko, V. T. Podorognaya, L. V. Shestopalova, V. E. Fedorov, Y. V. Mironov, *J. Inorg. Biochem.* **2015**, *144*, 13–17.

[33] a) K. Kirakci, J. Zelenka, M. Rumlova, J. Cvacka, T. Ruml, K. Lang, *Biomater. Sci.* **2019**, *7*, 1386–1392; b) A. Verger, G. Dollo, S. Martinais, Y. Molard, S. Cordier, M. Amela-Cortes, N. Brandhonneur, *J. Pharm. Sci.* **2022**, *111*, 3377–3383; c) K. Kirakci, M. Kubáňová, T. Přibyl, M. Rumlová, J. Zelenka, T. Ruml, K. Lang, *Inorg. Chem.* **2022**, *61*, 5076–5083; d) M. R. Tavares, K. Kirakci, N. Kotov, M. Pechar, K. Lang, R. Pola, T. Etrych, *Nanomaterials* **2022**, *12*, 3350; e) H. C. D. Medeiros, C. Yang, C. K. Herrera, D. Broadwater, E. Ensink, M. Bates, R. R. Lunt, S. Y. Lunt, *Chem. Eur. J.* **2023**, *29*, e202202881; f) V. A. Bardin, Y. A. Vorotnikov, D. V. Stass, N. A. Vorotnikova, M. A. Shestopalov, *Nanomaterials* **2022**, *12*, 3580; g) C. de la Torre, R. Gavara, A. García-Fernández, M. Mikhaylov, M. N. Sokolov, J. F. Miravet, F. Sancenón, R. Martínez-Máñez, F. Galindo, *Biomater. Adv.* **2022**, *140*, 213057.

[34] T. Hummel, D. Dutczak, A. Y. Alekseev, L. S. Adamenko, A. M. Shestopalov, Y. V. Mironov, D. Enseling, T. Jüstel, H.-J. Meyer, *RSC Adv.* **2020**, *10*, 22257–22263.

[35] a) A. Barras, M. R. Das, R. R. Devarapalli, M. V. Shelke, S. Cordier, S. Szunerits, R. Boukherroub, *Appl. Catal., B* **2013**, *130–131*, 270–276; b) A. Barras, S. Cordier, R. Boukherroub, *Appl. Catal., B* **2012**, *123*, 1–8; c) M. N. Ivanova, Y. A. Vorotnikov, E. E. Plotnikova, M. V. Marchuk, A. A. Ivanov, I. P. Asanov, A. R. Tsygankova, E. D. Grayfer, V. E. Fedorov, M. A. Shestopalov, *Inorg. Chem.* **2020**, *59*, 6439–6448.

[36] M. O. Sunday, H. Sakugawa, *Sci. Total Environ.* **2020**, *746*, 141186.

[37] a) A. Renaud, P.-Y. Jouan, N. Dumait, S. Ababou-Girard, N. Barreau, T. Uchikoshi, F. Grasset, S. Jobic, S. Cordier, *ACS Appl. Mater. Interfaces* **2022**, *14*, 1347–1354; b) A. Renaud, F. Grasset, B. Dierre, T. Uchikoshi, N. Ohashi, T. Takei, A. Planchat, L. Cario, S. Jobic, F. Odobel, S. Cordier, *ChemistrySelect* **2016**, *1*, 2284–2289.

[38] a) M. Feliz, M. Puche, P. Atienzar, P. Concepcion, S. Cordier, Y. Molard, *ChemSusChem* **2016**, *9*, 1963–1971; b) P. Kumar, S. Kumar, S. Cordier, S. Paofai, R. Boukherroub, S. L. Jain, *RSC Adv.* **2014**, *4*, 10420–10423; c) M. Feliz, P. Atienzar, M. Amela-Cortés, N. Dumait, P. Lemoine, Y. Molard, S. Cordier, *Inorg. Chem.* **2019**, *58*, 15443–15454.

[39] a) J. Choi, D. Nguyen, E. Gi, K. A. Brylev, J. W. Yu, D. Kim, W. B. Lee, D. H. Kim, I. Chung, K. K. Kim, S.-J. Kim, *J. Mater. Chem. C* **2022**, *10*, 4402–4410; b) Y. Zhao, R. R. Lunt, *Adv. Energy Mater.* **2013**, *3*, 1143–1148; c) S. Khlifi, J. Bigeon, M. Amela-Cortes, N. Dumait, G. h. Loas, S. Cordier, Y. Molard, *ACS Appl. Mater. Interfaces* **2020**, *12*, 14400–14407.

[40] T. Aubert, F. Cabello-Hurtado, M. A. Esnault, C. Neaime, D. Lebret-Chauvel, S. Jeanne, P. Pellen, C. Roiland, L. Le Polles, N. Saito, K. Kimoto, H. Haneda, N. Ohashi, F. Grasset, S. Cordier, *J. Phys. Chem. C* **2013**, *117*, 20154–20163.

[41] a) R. N. Ghosh, G. L. Baker, C. Ruud, D. G. Nocera, *Appl. Phys. Lett.* **1999**, *75*, 2885–2887; b) P. Zhang, D. J. Osborn, G. L. Baker, R. N. Ghosh, *IEEE Sens. 2005, 4th* **2005**, *1–2*, 628–631; c) D. J. Osborn, G. L. Baker, R. N. Ghosh, *J. Sol-Gel Sci. Techn.* **2005**, *36*, 5–10; d) R. N. Ghosh, P. A. Askeland, S. Kramer, R. Loloee, *Appl.*

Phys. Lett. **2011**, *98*, 221103–221103; e) M. Zhang, F. Grasset, Y. Masubuchi, T. Shimada, T. K. N. Nguyen, N. Dumait, A. Renaud, S. Cordier, D. Berthebaud, J.-F. Halet, T. Uchikoshi, *Nanomaterials* **2023**, *13*, 478; f) J. Casanova-Chafer, R. Garcia-Aboal, P. Atienzar, M. Feliz, E. Llobet, *ACS Appl. Mater. Interfaces* **2022**, *14*, 57122–57132.

[42] O. F. Al-Mishaal, M. A. Suwaid, A. A. Al-Muntaser, M. A. Khelkhal, M. A. Varfolomeev, R. Djimasbe, R. R. Zairov, S. A. Saeed, N. A. Vorotnikova, M. A. Shestopalov, C. Yuan, M. H. Hakimi, *Catalysts* **2022**, *12*, 1125.

[43] a) A. Seyboldt, D. Enseling, T. Jüstel, M. Ivanovic, H. Peisert, T. Chassé, H.-J. Meyer, *Eur. J. Inorg. Chem.* **2017**, *2017*, 5387–5394; b) M. V. Marchuk, Y. A. Vorotnikov, A. A. Ivanov, I. V. Eltsov, N. V. Kuratieva, M. A. Shestopalov, *Symmetry* **2022**, *14*, 2117.

[44] A. W. Maverick, H. B. Gray, *J. Am. Chem. Soc.* **1981**, *103*, 1298–1300.

[45] a) K. Kirakci, P. Kubat, J. Langmaier, T. Polivka, M. Fuciman, K. Fejfarova, K. Lang, *Dalton Trans.* **2013**, *42*, 7224–7232; b) T. C. Zietlow, D. G. Nocera, H. B. Gray, *Inorg. Chem.* **1986**, *25*, 1351–1353.

[46] T. C. Zietlow, M. D. Hopkins, H. B. Gray, *J. Solid. State. Chem.* **1985**, *57*, 112–119.

[47] J. A. Jackson, C. Turro, M. D. Newsham, D. G. Nocera, *J. Phys. Chem.* **1990**, *94*, 4500–4507.

[48] P. R. Ogilby, *Chem. Soc. Rev.* **2010**, *39*, 3181–3209.

[49] T. Hummel, M. Ströbele, A. D. Fuhrmann, D. Enseling, T. Jüstel, H.-J. Meyer, *Eur. J. Inorg. Chem.* **2019**, *2019*, 4014–4019.

[50] A.-D. Fuhrmann, A. Seyboldt, A. Schank, G. Zitzer, B. Speiser, D. Enseling, T. Jüstel, H.-J. Meyer, *Eur. J. Inorg. Chem.* **2017**, *2017*, 4259–4266.

[51] O. A. Efremova, Y. A. Vorotnikov, K. A. Brylev, N. A. Vorotnikova, I. N. Novozhilov, N. V. Kuratieva, M. V. Edeleva, D. M. Benoit, N. Kitamura, Y. V. Mironov, M. A. Shestopalov, A. J. Sutherland, *Dalton Trans.* **2016**, *45*, 15427–15435.

[52] D. V. Evtushok, A. R. Melnikov, N. A. Vorotnikova, Y. A. Vorotnikov, A. A. Ryadun, N. V. Kuratieva, K. V. Kozyr, N. R. Obedinskaya, E. I. Kretov, I. N. Novozhilov, Y. V. Mironov, D. V. Stass, O. A. Efremova, M. A. Shestopalov, *Dalton Trans.* **2017**, *46*, 11738–11747.

[53] M. N. Sokolov, M. A. Mikhailov, K. A. Brylev, A. V. Virovets, C. Vicent, N. B. Kompankov, N. Kitamura, V. P. Fedin, *Inorg. Chem.* **2013**, *52*, 12477–12481.

[54] M. N. Sokolov, M. A. Mihailov, E. V. Peresypkina, K. A. Brylev, N. Kitamura, V. P. Fedin, *Dalton Trans.* **2011**, *40*, 6375–6377.

[55] S. Akagi, E. Sakuda, A. Ito, N. Kitamura, *J. Phys. Chem. A* **2017**, *121*, 7148–7156.

[56] a) S. Akagi, T. Horiguchi, S. Fujii, N. Kitamura, *Inorg. Chem.* **2019**, *58*, 703–714; b) S. Akagi, S. Fujii, N. Kitamura, *J. Phys. Chem. A* **2018**, *122*, 9014–9024; c) S. Akagi, S. Fujii, T. Horiguchi, N. Kitamura, *J. Cluster Sci.* **2017**, *28*, 757–772; d) N. Kitamura, Y. Kuwahara, Y. Ueda, Y. Ito, S. Ishizaka, Y. Sasaki, K. Tsuge, S. Akagi, *Bull. Chem. Soc. Jpn.* **2017**, *90*, 1164–1173.

[57] Y. Saito, H. K. Tanaka, Y. Sasaki, T. Azumi, *J. Phys. Chem.* **1985**, *89*, 4413–4415.

[58] U. Strauss, N. Perchenek, W. W. Rühle, H. J. Queisser, A. Simon, *Chem. Phys. Lett.* **1993**, *202*, 415–418.

[59] J. C. Sheldon, *J. Chem. Soc* **1962**, 410–415.

[60] W. M. Carmichael, D. A. Edwards, *J. Inorg. Nucl. Chem.* **1967**, *29*, 1535–1538.

[61] G. M. Ehrlich, C. J. Warren, R. C. Haushalter, F. J. DiSalvo, *Inorg. Chem.* **1995**, *34*, 4284–4286.

[62] E. V. Svezhentseva, Y. A. Vorotnikov, A. O. Solovieva, T. N. Pozmogova, I. V. Eltsov, A. A. Ivanov, D. V. Evtushok, S. M. Miroshnichenko, V. V. Yanshole, C. J. Eling, A. M. Adawi, J. S. G. Bouillard, N. V. Kuratieva, M. S. Fufaeva, L. V.

Shestopalova, Y. V. Mironov, O. A. Efremova, M. A. Shestopalov, *Chem. Eur. J.* **2018**, *24*, 17915–17920.
[63] M. V. Marchuk, N. A. Vorotnikova, Y. A. Vorotnikov, N. V. Kuratieva, D. V. Stass, M. A. Shestopalov, *Dalton Trans.* **2021**, *50*, 8794–8802.
[64] T. Hummel, W. Leis, A. Eckhardt, M. Ströbele, D. Enseling, T. Jüstel, H.-J. Meyer, *Dalton Trans.* **2020**, *49*, 9795–9803.
[65] Florian Pachel, Phillip Frech, Markus Ströbele, David Enseling, Carl Romao, Thomas Jüstel, Marcus Scheele, H.-J. Meyer, *CSD Communication* **2023**.
[66] F. Pachel, M. Ströbele, H.-J. Meyer, *CSD Communication* **2022**.
[67] Florian Pachel, Kai Röseler, Markus Ströbele, H.-J. Meyer, *CSD Communication* **2023**.
[68] Florian Pachel, Kai Röseler, Markus Ströbele, H.-J. Meyer, *CSD Communication* **2023**.
[69] F. Pachel, M. Ströbele, H.-J. Meyer, *CSD Communication* **2023**.
[70] G. Sheldrick, *Acta Crystallogr. A* **2015**, *71*, 3–8.
[71] C. B. Huebschle, G. M. Sheldrick, B. Dittrich, *J. Appl. Crystallogr.* **2011**, *44*, 1281–1284.
[72] Y. Kawamura, H. Sasabe, C. Adachi, *Jpn. J. Appl. Phys.* **2004**, *43*, 7729–7730.
[73] F. Pachel, J. Händel, M. Ströbele, H.-J. Meyer, *Eur. J. Inorg. Chem.* **2020**, *2020*, 3987–3990.
[74] a) A. Starkholm, L. Kloo, P. H. Svensson, *ACS Appl. Energy Mater.* **2019**, *2*, 477–485; b) P. H. Svensson, L. Bengtsson-Kloo, P. Persson, *J. Chem. Soc. Dalton* **1998**, 1425–1430.
[75] O. M. R. M. Ibberson, C. Petrillo, *Mol. Phys.* **1992**, *76*, 395–403.
[76] F. Pachel, P. Frech, M. Ströbele, D. Enseling, C. P. Romao, T. Jüstel, M. Scheele, H.-J. Meyer, *Dalton Trans.* **2023**, *52*, 3777–3785.
[77] M. K. Simsek, D. Bublitz, W. Preetz, *Z. Anorg. Allg. Chem.* **1997**, *623*, 1885–1891.
[78] F. Pachel, M. Ströbele, C. P. Romao, D. Enseling, T. Jüstel, H.-J. Meyer, submitted to *Eur. J. Inorg. Chem.* **2023**.
[79] a) C. L. D. Gibb, E. D. Stevens, B. C. Gibb, *J. Am. Chem. Soc.* **2001**, *123*, 5849–5850; b) L. Garzón-Tovar, Á. Duarte-Ruiz, K. Wurst, *Inorg. Chem. Commun.* **2013**, *32*, 64–67.
[80] a) M. Puche, R. García-Aboal, M. A. Mikhaylov, M. N. Sokolov, P. Atienzar, M. Feliz, *Nanomaterials* **2020**, *10*, 1259; b) M. Feliz, M. Puche, P. Atienzar, P. Concepción, S. Cordier, Y. Molard, *ChemSusChem* **2016**, *9*, 1963–1971.
[81] a) A. M. Cheplakova, A. O. Solovieva, T. N. Pozmogova, Y. A. Vorotnikov, K. A. Brylev, N. A. Vorotnikova, E. V. Vorontsova, Y. V. Mironov, A. F. Poveshchenko, K. A. Kovalenko, M. A. Shestopalov, *J. Inorg. Biochem.* **2017**, *166*, 100–107; b) K. Kirakci, P. Kubat, M. Kucerakova, V. Sicha, H. Gbelcova, P. Lovecka, P. Grznarova, T. Ruml, K. Lang, *Inorg. Chim. Acta.* **2016**, *441*, 42–49; c) Y. A. Vorotnikov, O. A. Efremova, I. N. Novozhilov, V. V. Yanshole, N. V. Kuratieva, K. A. Brylev, N. Kitamura, Y. V. Mironov, M. A. Shestopalov, *J. Mol. Struct.* **2017**, *1134*, 237–243.
[82] K. Costuas, A. Garreau, A. Bulou, B. Fontaine, J. Cuny, R. Gautier, M. Mortier, Y. Molard, J. L. Duvail, E. Faulques, S. Cordier, *Phys. Chem. Chem. Phys.* **2015**, *17*, 28574–28585.
[83] A.-D. Fuhrmann, F. Pachel, M. Ströbele, D. Enseling, T. Jüstel, H.-J. Meyer, *Z. Anorg. Allg. Chem.* **2020**, *646*, 1650–1654.
[84] a) M. K. Simsek, W. Preetz, *Z. Allg. Anorg. Chem* **1997**, *623*, 515–523; b) C. S. Weinert, C. L. Stern, D. F. Shriver, *Inorg. Chim. Acta* **2000**, *307*, 139–143.
[85] T. C. Zietlow, W. P. Schaefer, B. Sadeghi, N. Hua, H. B. Gray, *Inorg. Chem.* **1986**, *25*, 2195–2198.

[86] N. W. Johnson, *Can. J. Math.* **1966**, *18*, 169–200.
[87] M. Ströbele, T. Jüstel, H. Bettentrup, H.-J. Meyer, *Z. Anorg. Allg. Chem.* **2009**, *635*, 822–827.
[88] F. Pachel, M. Ströbele, D. Enseling, T. Jüstel, H.-J. Meyer, *Z. Anorg. Allg. Chem.* **2021**, *647*, 1392–1396.
[89] S. Böschen, H. L. Keller, *Z. Kristallogr.* **1992**, *200*, 305–315.
[90] a) S. Arajs, R. Colvin, *Journal of Applied Physics* **1961**, *32*, 336–337; b) W. Klemm, H. Bommer, *Z. Anorg. Allg. Chem.* **1937**, *231*, 138–171; c) F. Spedding, S. Legvold, A. Daane, L. Jennings, in *Progress in low temperature physics, Vol. 2*, Elsevier, **1957**, pp. 368–394.
[91] T. Hummel, A. Mos-Hummel, M. Ströbele, H.-J. Meyer, *Z. Anorg. Allg. Chem.* **2019**, *645*, 831–834.
[92] a) M. J. Freiser, S. Methfessel, F. Holtzberg, *Journal of Applied Physics* **1968**, *39*, 900–902; b) G. Blasse, B. C. Grabmaier, in *Luminescent materials*, 1 ed., Springer, Heidelberg-Berlin, **1994**, pp. 25–27.
[93] T. Maulbetsch, Dissertation, Universität Tübingen **2021**.
[94] T. Maulbetsch, D. Kunz, *Angew. Chem., Int. Ed.* **2021**, *60*, 2007–2012.
[95] M. J. Carney, J. S. Lesniak, M. D. Likar, J. R. Pladziewicz, *J. Am. Chem. Soc.* **1984**, *106*, 2565–2569.

5. Appendix

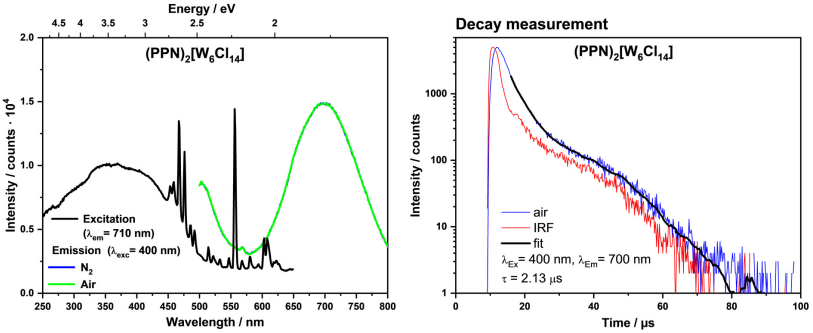

Figure A 1. *Recorded excitation (black) and emissions spectra (green N_2, blue air, left) and lifetime measurement (right) of crystalline $(PPN)_2[W_6Cl_{14}]$ in air.*

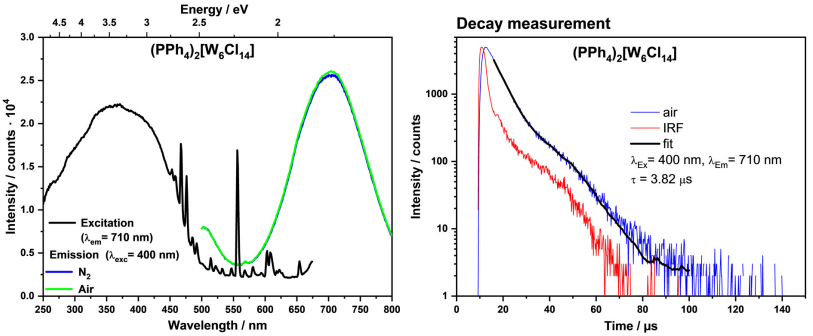

Figure A 2. *Recorded excitation (black) and emissions spectra (green N_2, blue air, left) and lifetime measurement (right) of crystalline $(PPh_4)_2[W_6Cl_{14}]$ in air.*

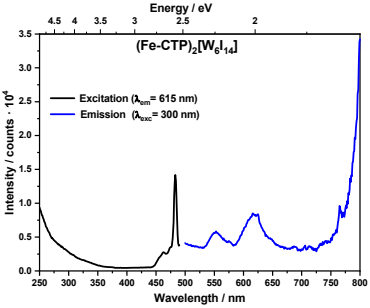

Figure A 3. *Recorded excitation (black) and emission (blue) spectra of crystalline* $[Fe(CTP)]_2[W_6I_{14}]$.

Figures from publications were used as shown in the published articles except those declared below:

Figure 7: The cluster cation and the I_7^- anion are depicted in two separate images in the article. In the article the iodine atoms are numbered.

Figure 12: The two spectra are shown in two independent figures in the article.

Figure 15: The projection of the crystal structure and the projection with added H···I distances are two separate images in the article. The projection without distances was excluded.

Figure 24: The cluster anion and the unit cell are displayed in two different images in the article.

Figure 25: In the article one graph is above the other, herein the graphs are next to each other.

Figure 31: Depicted unit cells are shown in two separate images.

Table A 1. Crystal data and structure refinement for $[W_6I_8(CH_3CN)_6](ClO_4)_4\cdot(CH_3CN)_2$,[65] $[W_6I_8(DMSO)_6](I_3)_4$,[66] $(PPN)_2[W_6Cl_{14}]\cdot(CH_2Cl_2)_2$,[67] $(PPh_4)_2[W_6Cl_{14}]\cdot(C_3H_6O)_2$,[68] $[Fe(CTP)]_2[W_6I_{14}]$[93] and $[Fe(CH_3CN)_6][W_6I_{14}]$.[69]

Compound		$[W_6I_8(CH_3CN)_6](ClO_4)_4\cdot(CH_3CN)_2$	$[W_6I_8(DMSO)_6](I_3)_4$	$(PPN)_2[W_6Cl_{14}]\cdot(CH_2Cl_2)_2$	$(PPh_4)_2[W_6Cl_{14}]\cdot(C_3H_6O)_2$	$[Fe(CTP)]_2[W_6I_{14}]$[93]	$[Fe(CH_3CN)_6][W_6I_{14}]$
CCDC code		2065518	2111522	2121320	2121373		2087031
Formula weight (g/mol)		2844.53	4109.87	2846.34	2394.3	4421.27	3181.87
Temperature (K)		100.0(1)	100.0(1)	200.0(1)	100.0(1)	100(2)	100.0(1)
Wavelength (pm)		71.073	71.073	71.073	71.073	71.073	71,073
Space group		*P*-1	*I*2/*a*	$P2_1/n$	*P*-1	*P*-1	*R*-3
Unit cell dimensions (pm, degree)	*a*	1106.09(3)	2407.17(2)	1040.43(1)	1129.97(1)	1379.45(2)	1603.53(1)
	b	1133.45(3)	1235.14(1)	2903.73(3)	1226.76(1)	1758.08(2)	1603.53(1)
	c	1141.04(3)	2199.62(2)	1413.24(1)	1261.04(1)	2674.56(3)	1622.67(2)
	α	79.049(2)	90	90	72.447(1)	89.985(1)	90
	β	77.880(3)	102.378(1)	93.436(1)	77.794(1)	89.972(1)	90
	γ	61.677(3)	90	90	83.089(1)	67.710(1)	120
Volume (nm^3)		1.22440(7)	6.3879(1)	4.2619(1)	1.62598(3)	6.0016(2)	3.6134(1)
Z		1	4	4	2	2	3
Density (calc.; g/cm^3)		3.858	4.273	2.218	2.445	2.447	4.387
Absorption coefficient (mm^{-1})		19.359	20.648	8.746	11.232	9.605	23.544
Goodness-of-fit on F^2		1.072	1.146	1.117	1.084	1.025	1.184
Final R indices ($I > 2\sigma(I)$)		$R1 = 0.0206$;	$R1 = 0.0227$;	$R1 = 0.0188$;	$R1 = 0.0125$;	$R1 = 0.0415$;	$R1 = 0.0173$;
		$wR2 = 0.0472$	$wR2 = 0.0594$	$wR2 = 0.0374$	$wR2 = 0.0275$	$wR2 = 0.0765$	$wR2 = 0.0431$
R indices (all data)		$R1 = 0.0240$;	$R1 = 0.0227$;	$R1 = 0.0229$;	$R1 = 0.0138$;	$R1 = 0.0664$;	$R1 = 0.0205$;
		$wR2 = 0.0482$	$wR2 = 0.0594$	$wR2 = 0.0385$	$wR2 = 0.0278$	$wR2 = 0.0834$	$wR2 = 0.0448$

6. Publications

Publication 1

The Heteroleptic Cluster Cation $[(W_6I_8)I_3(CH_3CN)_3]^+$

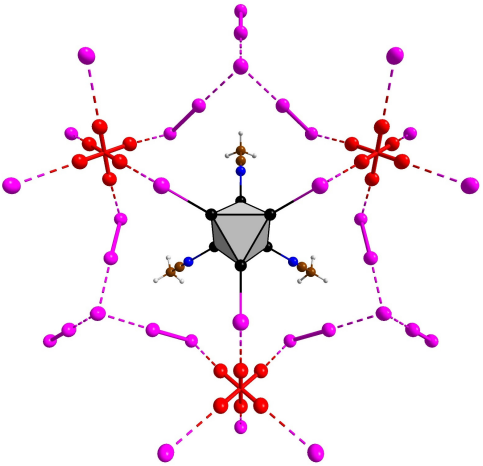

https://doi.org/10.1002/ejic.202000694

Reprinted with permission from

Eur. J. Inorg. Chem. **2020**, *42*, 3987–3990

EurJIC
European Journal of Inorganic Chemistry

Full Paper
doi.org/10.1002/ejic.202000694

Chemistry Europe
European Chemical Societies Publishing

Tungsten Iodide Cluster | *Very Important Paper* |

The Heteroleptic Cluster Cation $[(W_6I_8)I_3(CH_3CN)_3]^+$

Florian Pachel,[a] Jacqueline Händel,[a] Markus Ströbele,[a] and Hans-Jürgen Meyer*[a]

Abstract: The iodide-rich compound $[(W_6I_8)I_3(CH_3CN)_3]I_9$ was synthesized solvothermally from W_6I_{22} and I_2 in acetonitrile. The refined crystal structure reveals the presence of the novel heteroleptic cluster cation $[(W_6I_8)I_3(CH_3CN)_3]^+$ containing the $[W_6I_8]^{4+}$ cluster with an octahedral tungsten cluster core, coordinated by three apical iodido and three acetonitrile ligands via cluster vertices. The iodide-rich starting material W_6I_{22} with the addition of I_2, produces the heptaiodide ion $(I_7)^-$ that is present in the structure of $[(W_6I_8)I_3(CH_3CN)_3](I_7)\cdot I_2$. The novelty of this compound is based on the cationic nature of the $[(W_6I_8)I_3(CH_3CN)_3]^+$ cluster after anionic $[(W_6I_8)I_6]^{2-}$ clusters and their ligand (L) substituted derivatives $[(W_6I_8)L_6]^{2-}$ have been widely reported for their versatile photophysical properties.

Introduction

Research on binary tungsten iodide clusters containing the $[W_6I_8]^{4+}$ cluster core has a long lasting tradition due to a versatile chemistry,[1] unusual electronic properties including metal–metal bonding[2] and remarkable photophysical properties.

Recently, we have summarized compounds appearing in the binary tungsten iodide system of which the vast majority is based on the $[W_6I_8]^{4+}$ core.[3] Most prominent is the remarkably stable compound W_6I_{12}. Its crystal structure is commonly described as $[(W_6I_8^i)I_2^aI_{4/2}^{a-a}]$[4] implying a bridging connectivity of four apical $I^{(a-a)}$ iodide ligands forming a nearly planar, rectangular network structure of $[W_6I_8]^{4+}$ clusters. This network is highly robust, allowing phase transitions, the incorporation of I_2 molecules[5] and resists solvent extractions. Consequently, $A_2[W_6I_{14}]$ compounds with A = Li, Na, K, Cs have been developed by solid-state reactions,[6] which were then complimented with organic cations (such as tetrabutylammonium = TBA) in order to generate convenient soluble species such as $(TBA)_2[W_6I_{14}]$.[7] The substitution of six terminal ligands of the $[W_6I_8]^{4+}$ cluster has led to the development of $(TBA)_2[W_6I_8L_6]$ compounds of which several (predominantly organic) examples reveal remarkably enhanced photophysical properties, such as intense phosphorescence[8] and/or phosphorescence-quenching in the presence of molecular oxygen with the production of singlet oxygen, $O_2(a^1\Delta_g)$.[9]

With the development of iodine-rich tungsten iodide cluster compounds we aimed to break down the robust (I^{a-a}) connectivity obtained in structures like W_6I_{12}. Indeed, such an alternative has been established with the iodine-rich cluster compound W_6I_{22},[10] whose structure can be described as $[(W_6I_8^i)I_2^a(I_3)^{a-a}{}_{4/2}]\cdot 2I_2\cdot(I_2)_{2/2}$ and thus to contain more labile $I_3^{(a-a)}$ bridges between clusters. Fortunately, this compound can be easily prepared by iodination of W_6I_{12} under mild conditions, in large volume.[11] After initial dissolution experiments appeared promising but failed to produce a uniform crystalline product, we herein describe the preparation of a novel $[W_6I_8]$ cluster species by solvothermal synthesis. The air-stable complex with the $[(W_6I_8)I_3(CH_3CN)_3]^+$ cluster cation compliments the well-known $[(W_6I_8)I_6]^{2-}$ anion that has been the source of compounds or systems that are showing interesting photophysical properties.

Results and Discussion

The preparation of the new compound $[(W_6I_8)I_3(CH_3CN)_3]I_9$ was successfully performed by solvothermal synthesis departing from the binary compound W_6I_{22}, iodine and acetonitrile. The reaction of W_6I_{22} with common polar solvents appears slow under ambient conditions. However, it can be assumed that the iodine-rich W_6I_{22} is a convenient compound for cluster excision due to the presence of $(I_3)^{a-a}$ bridges between clusters in $[(W_6I_8^i)I_2^a(I_3)^{a-a}{}_{4/2}]\cdot 2I_2\cdot(I_2)_{2/2}$ which are believed to behave more fragile than I^{a-a} bridges in the structure of W_6I_{12}.

In course of the reaction of W_6I_{22} with acetonitrile, the number of outer iodide ligands of the cluster changes from two in $[(W_6I_8^i)I_2^a(I_3)^{a-a}{}_{4/2}]$ to three in $[(W_6I_8)I_3^a(CH_3CN)_3^a]^+$ which can be envisioned by the disassembly of $(I_3)^-$ into I^- and I_2, whereat acetonitrile molecules substitute for three $(I_3)^-$ ions. It is likely to assume that more reactions of this type are possible to occur with other solvents or ions. Nevertheless, the precise understanding of reactivity pathways between molecules and extended solids remains challenging.

[a] F. Pachel, J. Händel, Dr. M. Ströbele, Dr. H.-J. Meyer
Section for Solid State and Theoretical Inorganic Chemistry, Institute of Inorganic Chemistry, University of Tübingen
Auf der Morgenstelle 18, D-72076 Tübingen, Germany
E-mail: juergen.meyer@uni-tuebingen.de
Supporting information and ORCID(s) from the author(s) for this article are available on the WWW under https://doi.org/10.1002/ejic.202000694.

The crystalline product of the reaction appeared phase-pure according to the X-ray powder diffraction (XRPD) pattern, which was subsequently fitted and refined with the data obtained from the crystal structure refinement (Figure S1). The crystal structure of $[(W_6I_8)I_3(CH_3CN)_3](I_7)\cdot I_2$ was solved and refined on basis of single-crystal X-ray diffraction data with the hexagonal space group $P6_3mc$ (No. 186). Some crystallographic data are presented in Table 1. The most important feature in the structure is the presence of the $[(W_6I_8)I_3(CH_3CN)_3]^+$ cluster cation displayed in Figure 1.

Table 1. Crystal data and structure refinement for $[W_6I_{11}(CH_3CN)_3](I_7)\cdot I_2$.

Compound	$[W_6I_{11}(NCCH_3)_3](I_7)\cdot I_2$
CCDC code	2011697
Formula weight	3764.26 g/mol
Temperature	100.0(2) K
Wavelength	71.073 pm
Space group	$P6_3mc$ (No. 186)
Unit cell dimensions	a = 1293.74(4) pm
	b = 1293.74(4) pm
	c = 1608.27(6) pm
Volume	2.33123(16) nm^3
Z	2
Density (calculated)	5.363 g/cm^3
Absorption coefficient	27.997 mm^{-1}
Goodness-of-fit on F^2	1.056
Final R indices [$I > 2\sigma(I)$][a]	R_1 = 0.0262, wR_2 = 0.0676
R indices (all data)	R_1 = 0.0285, wR_2 = 0.0692
Absolute structure parameter	−0.01(2)

[a] $R_1 = \Sigma||F_o| - |F_c||/\Sigma|F_o|$, and $wR_2 = \{\Sigma w[(F_o)^2 - (F_c)^2]^2/\Sigma w[(F_o)^2]^2\}^{1/2}$.

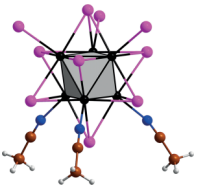

Figure 1. Structure of the cluster cation $[(W_6I_8)I_3(CH_3CN)_3]^+$. (W: black, I: violet, N: blue, C: brown, H: light gray).

The $[(W_6I_8)I_3(CH_3CN)_3]^+$ cluster cation is based on the octahedral tungsten cluster bearing eight (inner) iodide ligands and six (outer) ligands, represented by three iodido ligands and three acetonitrile molecules. Averaged W–W distances of the octahedral cluster core of $[(W_6I_8)I_3(CH_3CN)_3]^+$ are at 266.4(1) pm and appear similar to other compounds with the $[(W_6I_8)I_6]^{2-}$ cluster containing 24 electrons in W–W bonding states. However, due to the presence of two distinct outer ligands there are three shorter [264.3(1) pm, related to CH_3CN], and three longer [267.8(1) pm, related to the I ligands] W–W distances within triangles of the nearly trigonal-antiprismatic tungsten cluster, and six distances of 266.8(1) pm connecting the triangles.

Averaged W–I^i [279.1(2) pm] and W–I^a distances [282.3(2) pm] are also similar to the distances in $[(W_6I_8)I_6]^{2-}$ clusters.[1b]

Iodine atoms in the structure of $[(W_6I_8)I_3(CH_3CN)_3](I_7)\cdot I_2$ are represented by the triangular heptaiodide ion (I_7^-) with $d_{I\cdots I}$ = 318 pm and 275 pm (Figure 2), as has been described in several compounds in the literature.[12] The bond length of the I_2 unit [271.8(9) pm] in the structure appears similar to the corresponding distance in solid I_2 [272.1(1) pm].[13]

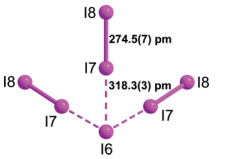

Figure 2. Structure and interatomic distances of the $(I_7)^-$ ion in the structure of $[(W_6I_8)I_3(CH_3CN)_3](I_7)\cdot I_2$.

The crystal structure of $[(W_6I_8)I_3(CH_3CN)_3](I_7)\cdot I_2$ is represented by layers in which the arrangement of cluster centers follows the motif of a closest packing. $[(W_6I_8)I_3(CH_3CN)_3]^+$ clusters and the I_2 units are centered on threefold rotation axes in the structure, and I_7^- ions on 6_3 axes, as may be imagined from Figure 3. Outer iodido ligands point above, and acetonitrile ligands point below the plane of projection of the layer in Figure 3. The I_2 units are disordered over three positions as a result of the threefold rotation axis. These units interconnect clusters and I_7^- ions within the two-dimensional plane via Van der Waals and Coulomb forces, as shown in Figure 3.

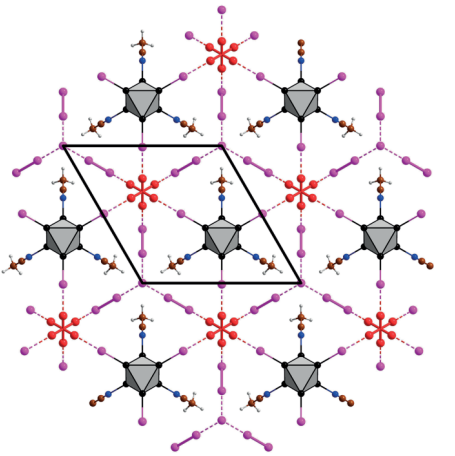

Figure 3. One layer of the crystal structure of $[(W_6I_8)I_3(CH_3CN)_3](I_7)\cdot I_2$ projected onto the a,b-plane. Inner iodido ligands of the $[W_6I_8]^{4+}$ cluster (I^i) are omitted from the structure drawing for clarity.

The arrangement of adjacent layers in the structure follows the motif of a hexagonal closest packing. Adjacent layers interact via Van der Waals forces of outer iodides of one layer and

acetonitrile ligands in the parent layer, respectively by hydrogen atoms of methyl groups (Figure 4).

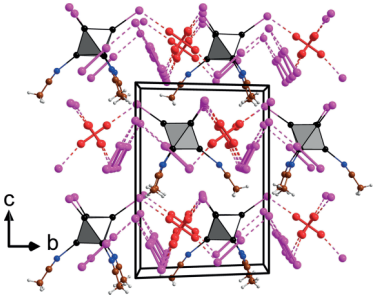

Figure 4. Layer sequence in the crystal structure of $[(W_6I_8)I_3(CH_3CN)_3](I_7)\cdot I_2$. Inner iodido ligands of the $[W_6I_8]^{4+}$ cluster (I^i) are omitted from the structure drawing for clarity.

The heteroleptic tungsten iodide cluster $[(W_6I_8)I_3(CH_3CN)_3]^+$ appears exceptional. Only a few number of examples of heteroleptic $[M_6X_8]$ type clusters have come to our attention. For example the compound $[(Mo_6Cl_8)Cl_4(PR_3)_2]$ which has been established from a reaction of Mo_6Cl_{12} in THF with tributylphosphine;[14] and the series of cluster hydrates $[Mo_6I_8(OH)_4(H_2O)_2]\cdot nH_2O$ (n = 2, 12, 14)[15] which have been reported as the result of a controlled hydrolysis of Mo_6I_{12} in alkaline media. The cluster phosphorescence was reported to be preserved in these compounds.

The characteristic photophysical properties of $[(W_6I_8)I_6]^{2-}$ and ligand (L) substituted $[(W_6I_8)L_6]^{2-}$ clusters have been studied in some detail. On photoexcitation they emit red luminescence (phosphorescence) from excited triplet states. Singlet oxygen is formed in the presence of oxygen, as a result of an energy transfer between triplet states of the cluster and oxygen, with quantum yields that are very much dependent on the nature of the apical ligand.[6b,7,8b,9,11,16] Crystalline powders of these compounds appear with yellow to orange body colors. The dark brown body color of crystalline $[(W_6I_8)I_3(CH_3CN)_3]I_9$ is attributed to the high iodine content in the structure and excludes any noteworthy phosphorescence. Nevertheless, the $[(W_6I_8)I_3(CH_3CN)_3]^+$ cluster is expected to inflate its luminescence properties when combined with a different anion. Moreover, energy transfer reactions will be possible when the cluster cation is combined with an appropriate metal center as has been demonstrated for supramolecular rare earth-cryptate-$[W_6I_{14}]$.[17]

The thermal stability of the compound, as studied by differential thermal analysis (DTA) revealed the decomposition of $[(W_6I_8)I_3(CH_3CN)_3](I_7)\cdot I_2$ between 150 °C and 250 °C without a pronounced transformation step, followed by a continuous mass loss between 300 °C and 600 °C, as has been obtained for other iodine-rich tungsten iodide cluster compounds.[3] In this temperature range W_6I_{12} is formed. If the temperature reaches 650 °C, a complete decomposition into elemental tungsten and iodine is observed (Figure S2).

Conclusions

With the solvothermal cluster excision departing from W_6I_{22} with acetonitrile we present a simple and efficient pathway for the preparation of a heteroleptic cluster cation. W_6I_{22} appears as an easy to make material and has led to the novel tungsten cluster compound $[(W_6I_8)I_3(CH_3CN)_3](I_7)\cdot I_2$ in high yields. The heteroleptic $[(W_6I_8)I_3(CH_3CN)_3]^+$ cluster cation contains three solvent molecules and three iodides as apical ligands. It is likely to assume that more reactions of this type are possible to occur in a similar way with other solvents or ions. The same solvothermal chemistry has been successfully developed by M. Köckerling and co-workers for niobium ($[Nb_6X_{12}]$-type) clusters bearing various outer ligands.[18]

Cluster cations like $[(W_6I_8)I_3(CH_3CN)_3]^+$ may be combined with complex anions carrying rare earth or transition metals to form double salts and allow electron transfer reactions between metal centers as has been recently demonstrated for supramolecular rare earth-cryptate-$[W_6I_{14}]$ assemblies with $[W_6I_{14}]^{2-}$ clusters.[17]

Experimental Section

Synthesis of $[(W_6I_8)I_3(CH_3CN)_3](I_7)\cdot I_2$: The preparation of the starting material W_6I_{22} was previously reported by us.[10]

Single-crystals identified as $[(W_6I_8)I_3(CH_3CN)_3]I_9$ were initially obtained from a mixture of W_6I_{22} in acetonitrile after solvent evaporation in air after approximately six weeks. Subsequent reactions were performed to accomplish a high yield synthesis.

A reaction mixture of 0.1 g of W_6I_{22} (0.0257 mmol), 3 mL of anhydrous acetonitrile (57.442 mmol) and 25 mg of iodine (0.098 mmol) were filled into a silica ampule under argon (glovebox) and afterwards fused therein under cooling with liquid nitrogen. The ampule was placed horizontally in an oven and heated for three days at 140 °C. After allowing to cool with the natural cooling rate of the oven, the ampule was opened in air. After removal of the solvent, the dark crystalline material was inspected by X-ray powder diffraction.

Thermoanalytic Studies: A differential thermal analysis (DTA) was performed with a STA 449F3 Jupiter apparatus (Netzsch, Selb, Germany). Samples were filled into homemade silica containers and analysed between room temperature and 500 °C with a heating and cooling rate of 2 K min^{-1}.

X-ray Powder Diffraction: X-ray powder diffraction (XRPD) experiments were carried out with a powder diffractometer (STOE Darmstadt, STADI-P, Ge-monochromator) using Cu-$K_{\alpha1}$ (λ = 1.540598 Å) radiation in the range of $3 < 2\theta < 120°$. The purity of $[(W_6I_8)I_3(CH_3CN)_3](I_7)\cdot I_2$ was checked and confirmed as single-phase, according to the XRPD pattern (Figure S1). A structure refinement of $[(W_6I_8)I_3(CH_3CN)_3](I_7)\cdot I_2$ based on the recorded powder pattern was performed using the Fullprof Suite.[19]

Single-Crystal X-ray Diffraction: The single-crystal X-ray diffraction (XRD) study on $[(W_6I_8)I_3(CH_3CN)_3](I_7)\cdot I_2$ was performed using a Rigaku XtaLab Synergy-S diffractometer with Mo-K_α radiation (λ = 0.71073 Å) and a mirror monochromator. A black needle-shaped single-crystal was used for the measurement under N_2 cooling at 100 K. Corrections for absorption effects were applied with CrysAlisPro 1.171.41.65a (Rigaku Oxford Diffraction, 2020). The structure was solved by direct methods (SHELXS),[20] and full-matrix

least-squares structure refinements were performed with SHELXL-2014[21] implemented in Olex2 1.3-ac4.

Supporting Information (see footnote on the first page of this article): Structure refinement data from powder X-ray diffraction and differential thermal analysis.

Deposition Number 2011697 contains the supplementary crystallographic data for this paper. These data are provided free of charge by the joint Cambridge Crystallographic Data Centre and Fachinformationszentrum Karlsruhe Access Structures service www.ccdc.cam.ac.uk/structures.

Author Information

The authors declare no competing financial interest.

Acknowledgment

Funding by the Deutsche Forschungsgemeinschaft (Bonn) via grant ME 914/31-1 is gratefully acknowledged. Open access funding enabled and organized by Projekt DEAL.

Keywords: Tungsten iodide · Cluster · Solvothermal synthesis · Structure elucidation · Thermal analysis

[1] J. D. Franolic, J. R. Long, R. H. Holm, *J. Am. Chem. Soc.* **1995**, *117*, 8139–8153.
[2] T. G. Gray, *Chem. Eur. J.* **2009**, *15*, 2581–2593.
[3] M. Ströbele, H.-J. Meyer, *Dalton Trans.* **2019**, *48*, 1547–1561.
[4] H. Schäfer, H. G. Schnering, *Angew. Chem.* **1964**, *76*, 833–849.
[5] M. Ströbele, H.-J. Meyer, *Inorg. Chem.* **2017**, *56*, 5880–5884.
[6] a) T. Hummel, A. Mos-Hummel, A. Merkulova, M. Ströbele, A. Krishnamurthy, S. Kroeker, H.-J. Meyer, *Inorg. Chem.* **2018**, *57*, 2570–2576; b) T. Hummel, M. Ströbele, D. Schmid, D. Enseling, T. Jüstel, H.-J. Meyer, *Eur. J. Inorg. Chem.* **2016**, *2016*, 5063–5067.
[7] L. Riehl, A. Seyboldt, M. Ströbele, D. Enseling, T. Jüstel, M. Westberg, P. R. Ogilby, H.-J. Meyer, *Dalton Trans.* **2016**, *45*, 15500–15506.
[8] a) M. A. Mikhaylov, M. A. Sokolov, *Eur. J. Inorg. Chem.* **2019**, *2019*, 4181–4197; b) M. N. Sokolov, K. A. Brylev, P. A. Abramov, M. R. Gallyamov, I. N. Novozhilov, N. Kitamura, M. A. Mikhaylov, *Eur. J. Inorg. Chem.* **2017**, *2017*, 4131–4137; c) N. A. Vorotnikova, M. V. Edeleva, O. G. Kurskaya, K. A. Brylev, A. M. Shestopalov, Y. V. Mironov, A. J. Sutherland, O. A. Efremova, M. A. Shestopalov, *Polym. Int.* **2017**, *66*, 1906–1912; d) B. Dierre, K. Costuas, N. Dumait, S. Paofai, M. Amela-Cortes, Y. Molard, F. Grasset, Y. Cho, K. Takahashi, N. Ohashi, T. Uchikoshi, S. Cordier, *Sci. Technol. Adv. Mater.* **2017**, *18*, 458–466; e) K. Kirakci, P. Kubat, J. Langmaier, T. Polivka, M. Fuciman, K. Fejfarova, K. Lang, *Dalton Trans.* **2013**, *42*, 7224–7232; f) M. N. Sokolov, M. A. Mihailov, E. V. Peresypkina, K. A. Brylev, N. Kitamura, V. P. Fedin, *Dalton Trans.* **2011**, *40*, 6375–6377.
[9] M. Bregnhoj, K. Strunge, R. J. Sorensen, M. Ströbele, T. Hummel, H.-J. Meyer, F. Jensen, P. R. Ogilby, *J. Phys. Chem. A* **2019**, *123*, 1730–1739.
[10] M. Ströbele, H.-J. Meyer, *Inorg. Chem.* **2019**, *58*, 12867–12872.
[11] T. Hummel, D. Dutczak, A. Y. Alekseev, L. S. Adamenko, A. M. Shestopalov, Y. V. Mironov, D. Enseling, T. Jüstel, H.-J. Meyer, *RSC Adv.* **2020**, *10*, 22257–22263.
[12] a) A. Starkholm, L. Kloo, P. H. Svensson, *Acs Appl. Energy Mater.* **2019**, *2*, 477–485; b) P. H. Svensson, L. Bengtsson-Kloo, P. Persson, *J. Chem. Soc., Dalton Trans.* **1998**, 1425–1430.
[13] O. M. R. M. Ibberson, C. Petrillo, *Mol. Phys.* **1992**, *76*, 395–403.
[14] T. Saito, H. Manabe, T. Yamagata, H. Imoto, *Inorg. Chem.* **1987**, *26*, 1362–1365.
[15] a) M. A. Mikhaylov, P. A. Abramov, V. Y. Komarov, M. N. Sokolov, *Polyhedron* **2017**, *122*, 241–246; b) Y. A. Vorotnikov, O. A. Efremova, N. A. Vorotnikova, K. A. Brylev, M. V. Edeleva, A. R. Tsygankova, A. I. Smolentsev, N. Kitamura, Y. V. Mironov, M. A. Shestopalov, *RSC Adv.* **2016**, *6*, 43367–43375.
[16] a) D. V. Evtushok, A. R. Melnikov, N. A. Vorotnikova, Y. A. Vorotnikov, A. A. Ryadun, N. V. Kuratieva, K. V. Kozyr, N. R. Obedinskaya, E. I. Kretov, I. N. Novozhilov, Y. V. Mironov, D. V. Stass, O. A. Efremova, M. A. Shestopalov, *Dalton Trans.* **2017**, *46*, 11738–11747; b) D. V. Evtushok, N. A. Vorotnikova, V. A. Logvinenko, A. I. Smolentsev, K. A. Brylev, P. E. Plyusnin, D. P. Pishchur, N. Kitamura, Y. V. Mironov, A. O. Solovieva, O. A. Efremova, M. A. Shestopalov, *New J. Chem.* **2017**, *41*, 14855–14861; c) T. Hummel, M. Ströbele, A. D. Fuhrmann, D. Enseling, T. Jüstel, H.-J. Meyer, *Eur. J. Inorg. Chem.* **2019**, *2019*, 4014–4019; d) M. Ströbele, D. Enseling, T. Jüstel, H.-J. Meyer, *Z. Anorg. Allg. Chem.* **2016**, *642*, 1435–1438; e) A. Seyboldt, D. Enseling, T. Jüstel, M. Ivanovic, H. Peisert, T. Chassé, H.-J. Meyer, *Eur. J. Inorg. Chem.* **2017**, *2017*, 5387–5394; f) M. A. Mikhailov, A. L. Gushchin, M. R. Gallyamov, A. V. Virovets, M. N. Sokolov, D. G. Sheven, V. V. Pervukhin, *Russ. J. Coord. Chem.* **2017**, *43*, 172–180.
[17] T. Hummel, W. Leis, A. Eckhardt, M. Ströbele, D. Enseling, T. Jüstel, H.-J. Meyer, *Dalton Trans.* **2020**, 9795–9803.
[18] a) A. Flemming, M. Köckerling, *Z. Anorg. Allg. Chem.* **2008**, *634*, 2309–2315; b) A. Flemming, J. König, M. Köckerling, *Z. Anorg. Allg. Chem.* **2013**, *639*, 2527–2531; c) E. Sperlich, M. Köckerling, *Z. Naturforsch. B* **2020**, *75*, 173; d) A. Flemming, M. Köckerling, *Angew. Chem. Int. Ed.* **2009**, *48*, 2605–2608; *Angew. Chem.* **2009**, *121*, 2643; e) I. Dartsch, J. König, M. Köckerling, *J. Cluster Sci.* **2018**, *29*, 319–323; f) J. König, M. Köckerling, *Z. Anorg. Allg. Chem.* **2020**, *646*, 1–7; g) D. H. Weiß, F. Schröder, M. Köckerling, *Z. Anorg. Allg. Chem.* **2017**, *643*, 345–351; h) D. H. Weiß, M. Köckerling, *Chem. Eur. J.* **2018**, *24*, 18613–18617.
[19] T. Roisnel, J. Rodríquez-Carvajal, *Mater. Sci. Forum* **2001**, *378*, 118–123.
[20] G. Sheldrick, University of Göttingen, Germany **1997**.
[21] G. Sheldrick, *Acta Crystallogr., Sect. C* **2015**, *71*, 3–8.

Received: July 22, 2020

European Journal of Inorganic Chemistry

Supporting Information

The Heteroleptic Cluster Cation $[(W_6I_8)I_3(CH_3CN)_3]^+$

Florian Pachel, Jacqueline Händel, Markus Ströbele, Hans-Jürgen Meyer*

Index

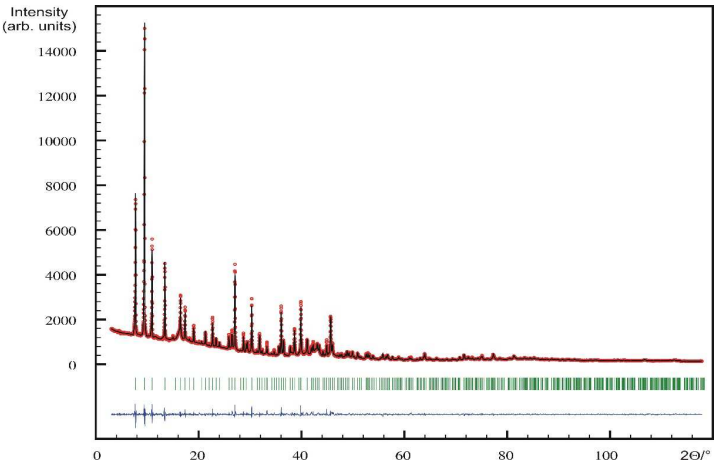

Figure S3. Fitted powder XRD pattern of $[(W_6I_8)I_3(CH_3CN)_3]I_9$ with space group *P6₃mc*. Red circles represent measured data points which are superimposed with the calculated powder pattern (black line). Green lines represent the Bragg positions; the difference curve is shown as a blue line.

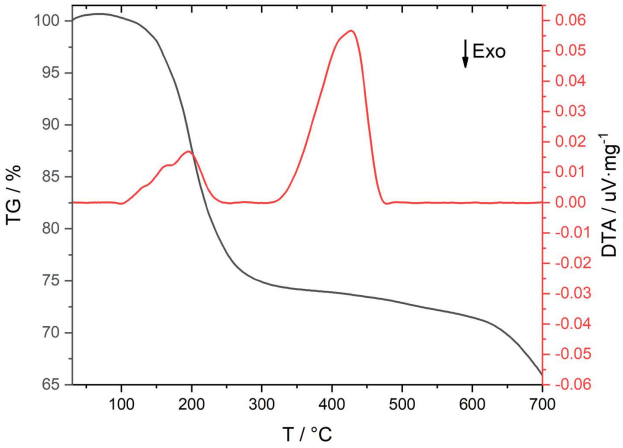

Figure S4. DTA/TG measurement of $[(W_6I_8)I_3(CH_3CN)_3]I_9$ in an open Al_2O_3 container up to 700 °C (DTA: red line, TG: black line).

Publication 2

Preparation, Photoluminescence and Excited State Properties of the Homoleptic Cluster Cation $[(W_6I_8)(CH_3CN)_6]^{4+}$

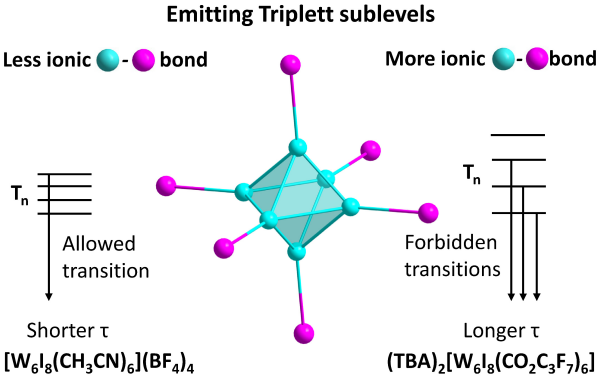

https://doi.org/10.1039/d2dt04063h

Reprinted with permission from

Dalton Trans. **2023**, *52*, 3777–3785

Dalton Transactions

ROYAL SOCIETY OF CHEMISTRY

PAPER

View Article Online
View Journal | View Issue

Cite this: *Dalton Trans.*, 2023, **52**, 3777

Preparation, photoluminescence and excited state properties of the homoleptic cluster cation $[(W_6I_8)(CH_3CN)_6]^{4+}$†

Florian Pachel, [a] Philipp Frech, [b] Markus Ströbele, [a] David Enseling, [c] Carl P. Romao, [d] Thomas Jüstel, [c] Marcus Scheele [b] and Hans-Jürgen Meyer *[a]

Received 19th December 2022,
Accepted 21st February 2023

DOI: 10.1039/d2dt04063h

rsc.li/dalton

Solvated tungsten iodide cluster compounds are presented with the homoleptic cluster cation $[(W_6I_8)(CH_3CN)_6]^{4+}$ and the heteroleptic $[(W_6I_8)I(CH_3CN)_5]^{3+}$, synthesized from W_6I_{22} in acetonitrile. Crystal structures were solved and refined on deep red single-crystals of $[(W_6I_8)(CH_3CN)_6](I_3)(BF_4)_3{\cdot}H_2O$, $[(W_6I_8)I(CH_3CN)_5](I_3)_2(BF_4)$, and on a yellow single-crystal of $[W_6I_8(CH_3CN)_6](BF_4)_4{\cdot}2(CH_3CN)$ on the basis of X-ray diffraction data. The structure of the homoleptic $[(W_6I_8)(CH_3CN)_6]^{4+}$ cluster is based on the octahedral $[W_6I_8]^{4+}$ tungsten iodide cluster core, coordinated by six apical acetonitrile ligands. The electron localisation function of $[(W_6I_8)(CH_3CN)_6]^{4+}$ is calculated and solid-state photoluminescence and its temperature depedence are reported. Additionally, photoluminescence and transient absorption measurements in acetonitrile are shown. Results of the obtained data are compared to compounds containing $[(M_6I_8)I_6]^{2-}$ and $[(M_6I_8)L_6]^{2-}$ (M = Mo or W; L = ligand) clusters.

Introduction

Octahedral metal halide clusters $[M_6X_{14}]^{2-}$ with M = Mo, W and X = Cl, Br, I are known for their photophysical properties, in particular their bright red luminescence, high quantum yields, long life times, and oxygen quenching.[1] The luminescence is based on ground state photoexcitation (S_0) leading to excited states (S_n) and intersystem crossing (ISC) into triplet states (T_n).[2] Luminescence from these triplet states may be quenched in the presence of molecular oxygen to form singlet oxygen $O_2(a^1\Delta_g)$.[3]

Some cluster compounds derived from $[M_6X_{14}]^{2-}$ have been optimized to obtain remarkable properties with regard to oxygen sensing,[4] photoreduction of CO_2,[5] photocatalysis[6] and medical applications (as photodynamic therapeutic agents,[7] X-ray contrast agents,[8] and bactericide[9]).

The clusters of interest are based on an octahedral metal core, surrounded by eight inner (i) and six outer (a) ligands as $[M_6X^i{}_8X^a{}_6]^{2-}$.[10] Apical halide ligands are bound more weakly to the cluster and can be exchanged by organic ligands, usually starting from the soluble cluster species $(TBA)_2[M_6X^i{}_8X^a{}_6]$ (TBA = tetrabutylammonium) to react with inorganic/organic silver salts.[11]

Ligand substituted compounds of the type $(TBA)_2[M_6X^i{}_8L^a{}_6]$ with L being an apical ligand have shown remarkably enhanced photophysical properties depending on the nature of L, when compared to the all-halide cluster counterpart. Ligands with strong electron withdrawing effects have shown to provide the highest luminescence (phosphorescence) quantum yields and the strongest luminescence quenching in the presence of molecular oxygen.[11b,c,12] One of the most remarkable compounds, $(TBA)_2[Mo_6I_8(CO_2CF_3)_6]$ is reported with a luminescence quantum yield of 1 in (oxygen-free) acetonitrile solution.[11c] The solid state phosphorescence of $(TBA)_2[Mo_6I_8(CO_2CF_3)_6]$ is expectedly, lower. However, with a remarkable luminescence quenching of 95% under pure oxygen.[11b]

To simulate the cluster luminescence, a model with four different emitting triplet sublevels has been developed describing the observations very accurately.[13] The energetically highest one of these emitting triplet sublevels possesses an allowed transition to the ground state. Recently, it has been shown that a high d-electron density on the metal atoms leads to a low energy difference between the different triplet states,

[a]*Section for Solid State and Theoretical Inorganic Chemistry, Institute of Inorganic Chemistry, University of Tübingen, Auf der Morgenstelle 18, 72076 Tübingen, Germany. E-mail: juergen.meyer@uni-tuebingen.de*
[b]*Institute of Physical and Theoretical Chemistry, University of Tübingen, Auf der Morgenstelle 18, 72076 Tübingen, Germany*
[c]*Department of Chemical Engineering, Münster University of Applied Science, Stegerwaldstraße 39, 48565 Steinfurt, Germany*
[d]*Department of Materials, ETH Zurich, Wolfgang-Pauli-Strasse 27, 8093 Zurich, Switzerland*

†Electronic supplementary information (ESI) available. CCDC 2115682 and 2152223. For ESI and crystallographic data in CIF or other electronic format see DOI: https://doi.org/10.1039/d2dt04063h

while a low density leads to a large difference.[14] Thus, the lower the d-electron density, the bigger the energetic splitting and the lower the thermal population of the highest triplet state. This results in long triplet lifetimes in the solid state even at room temperature, especially for iodide clusters bearing strong electron withdrawing ligands. An example is $(TBA)_2[Mo_6I_8(CO_2C_3F_7)_6]$ with lifetimes of around 235 μs at room temperature.[15] The long decay time is a result of low thermal population of the highest triplet sublevel. For the analogous species with tungsten $(TBA)_2[W_6I_8(CO_2C_3F_7)_6]$ a similar reason for its long triplet lifetime of up to 55 μs (ref. 12*b*) can be assumed.

In general, the aforementioned investigations of the photophysical properties of tungsten and molybdenum halide clusters have been carried out on anionic species ($[M_6X_8L_6]^{2-}$). While neutral and cationic clusters are reported to exist with various different solvents as ligands,[16] only a few crystal structures[17] are reported, and for only three compounds, namely $[M_6I_8(DMSO)_6](NO_3)_4$ (M = Mo, W) and $[Mo_6I_8(pyridine)_2]I_4$ have the luminescence properties been studied.[17*b*,*d*] Therefore, our aim was to synthesize new cationic tungsten halide clusters and characterize their photoluminescence properties. Recently we discovered the cationic tungsten iodide cluster species $[(W_6I_8)I_3(CH_3CN)_3]I_9$, which features a black body color due to the high iodine content.[17*c*]

On the basis of aforementioned research, we report on the synthesis of the novel cationic tungsten halide cluster species $[(W_6I_8)I(CH_3CN)_5](I_3)_2(BF_4)$ (**I**), $[(W_6I_8)(CH_3CN)_6](I_3)(BF_4)_3{\cdot}(H_2O)$ (**II**) and $[(W_6I_8)(CH_3CN)_6](BF_4)_4{\cdot}(CH_3CN)_2$ (**III**) and their crystal structures. Additionally, we investigated the photoluminescence properties and the electron localization function of (**III**) and compare it to previously reported results for different anionic tungsten halide cluster species.

Results and discussion

The recently reported compound $[(W_6I_8)I_3(CH_3CN)_3]I_9$ is formed by reaction of W_6I_{22} in acetonitrile (1).[17*c*]

$$W_6I_{22} \xrightarrow{CH_3CN} \left[(W_6I_8)I_3(CH_3CN)_3\right]I_9 + I_2 \quad (1)$$

W_6I_{22} on the other hand, is obtained from the reaction of W_6I_{12} with iodine,[18] whereby the connectivity between adjacent clusters softens up due to the incorporation of iodine molecules into the structure, leading to an overall increase of the solubility.

General attempts to synthesize isolated or dissolved clusters can depart from common methods used in cluster synthesis and may involve a significant number of reaction steps.[11*a*,*b*,17*b*,19]

Moreover, individual attempts may be required for different metal halide systems, as Köckerling has shown for a vast number of cluster compounds.[20] A general attempt includes the extraction in an appropriate solvent in the presence of a Lewis acid ($ZnCl_2$, $AlCl_3$, or $SbCl_5$) as exemplified with MCl_3 for the conversion of $K_2[(Zr_6B)Cl_{15}]$ into $[Zr_6BCl_{12}(CH_3CN)_6]$ MCl_4 (M = Al, Ga, In).[21] Another general attempt, which was adopted on the reactions presented here, is the employment of silver salts ($AgBF_4$) and subsequent precipitation of silver halide.[22]

After the discovery of the mixed ligand cluster $[(W_6I_8)I_3(CH_3CN)_3]^-$, a whole series of cluster species can be regarded to exist as $[(W_6I_8)I_{6-n}(CH_3CN)_n]^{(n-2)+}$, where n may range between zero and six.

Acetonitrile-rich members with n = 5 and 6 are obtained in reactions departing from $[(W_6I_8)I_3(CH_3CN)_3]I_9$ (n = 3) with acetonitrile and $Ag(BF_4)$ exemplified in reaction (2).

$$\left[(W_6I_8)I_3(CH_3CN)_3\right]I_9 + 3AgBF_4 \xrightarrow{CH_3CN} \left[(W_6I_8)(CH_3CN)_6\right](I_3)(BF_4)_3 + 3AgI + \frac{6}{2}I_2 \quad (2)$$

The heteroleptic cluster $[(W_6I_8)I(CH_3CN)_5](I_3)_2(BF_4)$ **I** (n = 5) and the homoleptic acetonitrile cluster $[(W_6I_8)(CH_3CN)_6](I_3)(BF_4)_3{\cdot}(H_2O)$ **II** (n = 6) are obtained in similar reactions crystallizing as deep-red crystals. Dark reddish or brown body colors are typical for polyiodides including $(I_3)^-$ in given structures and $(I_7)^-$ contained in the structure of $[(W_6I_8)I_3(CH_3CN)_3](I_7){\cdot}I_2$ making these compounds rather unattractive for optical studies. Nevertheless, yellow crystals of $[(W_6I_8)(CH_3CN)_6](BF_4)_4{\cdot}2(CH_3CN)$ **III** showing orange luminescence were obtained following a similar synthesis (see Experimental).

Crystal structures of all three compounds were solved and refined on the basis of single-crystal X-ray diffraction data with monoclinic or triclinic space groups (Table 1).

The most interesting result of this work is the presence of the homoleptic $[(W_6I_8)(CH_3CN)_6]^{4+}$ cluster cation, shown in Fig. 1. This complements the also-obtained heteroleptic $[(W_6I_8)I(CH_3CN)_5]^{3+}$, and the recently reported $[(W_6I_8)I_3(CH_3CN)_3]^+$ cluster cations, whereas the neutral species $[(W_6I_8)I_4(CH_3CN)_2]$ remains missing. With 24 electrons per cluster, all these clusters possess the same electron count as binary W_6I_{12}.

Structures of compounds **I** and **II** reveal layered arrangements with clusters and I_3^- units alternating with layers of BF_4^- ions and H_2O, as shown for **II** in Fig. 2. The structure of **III** is also dominated by a layered arrangement of nearly spherical clusters (Fig. 1) surrounded by anions and free acetonitrile filling the voids of this arrangement as shown in Fig. 3.

The $[(W_6I_8)(CH_3CN)_6^a]^{4+}$ cluster is based on an octahedral tungsten cluster, bearing eight (i = inner) iodide ligands forming the $[W_6I_8]^{4+}$ cluster core, plus six (a = outer) acetonitrile ligands. W–W distances of the octahedral cluster cores are in the range at 265.16(5)–267.81(8) pm and appear similar to other compounds with the $[(W_6I_8)I_6]^{2-}$ cluster. The averaged $W\text{–}I^i$ distances (278.2(1) pm) of the reported compounds (**I–III**) are similar to corresponding distances in $[(W_6I_8^i)I_6]^{2-}$ (278.3(2) pm).[23]

This similarity is not unexpected since there is no change of the oxidation state of the tungsten atoms. Two of the three

Table 1 Crystal data for $[(W_6I_8)I(CH_3CN)_5](I_3)_2(BF_4)$ **I**, $[(W_6I_8)(CH_3CN)_6](I_3)(BF_4)_3{\cdot}H_2O$ **II**, and $[(W_6I_8)(CH_3CN)_6](BF_4)_4{\cdot}(CH_3CN)_2$ **III**

Compound	$[(W_6I_8)I(CH_3CN)_5](I_3)_2(BF_4)$	$[(W_6I_8)(CH_3CN)_6](I_3)(BF_4)_3{\cdot}H_2O$	$[(W_6I_8)(CH_3CN)_6](BF_4)_4{\cdot}(CH_3CN)_2$
CCDC code	2064394 [b]	2115682	2152223
Formula weight (g mol^{-1})	3298.68	3023.77	2793.97
Temperature (K)	100.0(1)	100.0(1)	150.0(1)
Wavelength (pm)	71.073	71.073	71.073
Space group	$P2_1/c$	$C2/c$	$P2_1/n$
Lattice parameters (a, b, c, in pm; β in degree)	1226.89(3)	1834.07(1)	1366.22(3)
	1226.89(3)	2205.46(2)	2189.26(4)
	1857.87(5)	1234.68(1)	1633.92(4)
	109.093(3)	109.543(1)	94.424(2)
Volume (nm^3)	4.6236(2)	4.70653(7)	4.8725(2)
Z	4	4	4
Density (calculated)	4.739 g cm^{-3}	4.267 g cm^{-3}	3.809 g cm^{-3}
Absorption coefficient	24.914 mm^{-1}	21.890 mm^{-1}	19.263 mm^{-1}
Goddness-of-fit on F^2	1.023	1.171	1.153
R_1 [a] ($I > 2\sigma(I)$)	0.0512	0.0198	0.0371
wR_2 ($I > 2\sigma(I)$)	0.1065	0.0442	0.0973
R_1 (all data)	0.0826	0.0207	0.0435
wR_2 (all data)	0.1174	0.0445	0.0998

[a] $R_1 = \sum||F_o| - |F_c||/\sum|F_o|$, $wR_2 = (\sum w[(F_o)^2 - (F_c)^2]^2/\sum w[(F_o)^2]^2)^{1/2}$. [b] Florian Pachel, Markus Ströbele, H.-Jürgen Meyer, CCDC 2064394: *CSD Commun.*, 2022, DOI: 10.5517/ccdc.csd.cc2795c3.

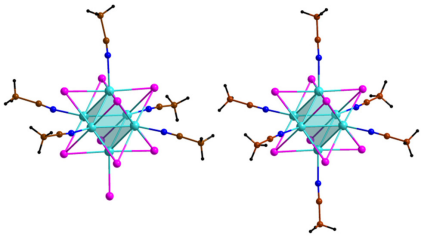

Fig. 1 Structure of $[(W_6I_8)I(CH_3CN)_5]^{3+}$ (**I**) (left) and $[(W_6I_8)(CH_3CN)_6]^{4+}$ (**II**) (right) cluster cations. Color code for W: turquoise, I: violet, N: blue, C: brown, and H: black.

$(I_3)^-$ ions in the structure of **I** are symmetric with bond lengths at 291.3(1) and 291.6(1) pm while one is nearly symmetric with 290.2(1) (I–I) and 293.4(1) pm (I···I–I). Compound **II** also shows a symmetric $(I_3)^-$ anion with a bond length of 292.2(1). For octahedral tungsten iodide clusters symmetric $(I_3)^-$ ions are unusual[24] but, in the literature, there are quite a few examples that adopt symmetrical I_3^- units with bond lengths around 290 pm.[25]

Coordinative W–N bonds range from 214.4(9) to 217.3(9) pm for the homoleptic $[(W_6I_8)(CH_3CN)_6]^{4+}$ cluster. Corresponding W–N distances with $(NCO)^-$ ligands in $(TBA)_2[W_6I_8(NCO)_6]$ were reported quite similar, with 217(1) pm (Table 2).[26]

Our research interest was first of all focused on the homoleptic compound **III**. The absence of additional I_3^- units, like in **I** or **II**, is responsible for the desirable transparency with bright yellow color of crystalline **III** and allows for the observation of a bright orange-red luminescence that is clearly visible to the naked eye (Fig. S1†). Luminescence studies of **III** should give first insights into the photophysical behavior of cationic cluster species.

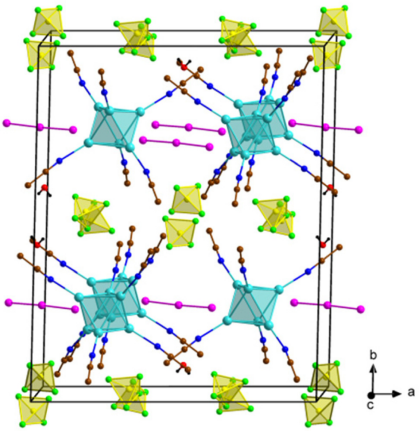

Fig. 2 Projection of the crystal structure of **II** in the ab plane. The iodide ligands and hydrogen atoms of acetonitrile are omitted for clarity. Color code for W: turquoise, I: violet, N: blue, C: brown, B: yellow, F: green, O: red and H: black.

Electron localization function

To investigate the nature of the W–N bond, the electron localization function (ELF) of **III** was calculated (Fig. 4, left). For comparison, we have also calculated the ELF of $(TBA)_2[W_6I_8(CO_2C_3F_7)_6]$ as a representative anionic tungsten

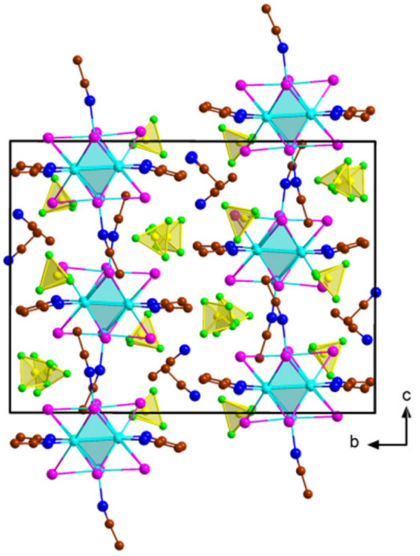

Fig. 3 Projection of the crystal structure of **III**. The $[W_6I_8(CH_3CN)_6]^{4+}$ units are showing a layered arrangement along the *b* axis with BF_4^- and free acetonitrile filling the voids. Hydrogen of clusters are omitted for clarity. Color code for W: turquoise, N: blue, C: brown, F: green, and B: yellow.

Table 2 Interatomic W–W and W–N distances (pm) for compounds **I**–**III**

Compound	W–W	W–N
$[(W_6I_8)I(CH_3CN)_5]^{3+}$ (**I**)	265.66(8)–267.81(8)	213.8(13)–225.5(1)
$[(W_6I_8)(CH_3CN)_6]^{4+}$ (**II**)	265.84(2)–267.14(2)	215.5(4)–216.3(4)
$[(W_6I_8)(CH_3CN)_6]^{4+}$ (**III**)	265.16(5)–267.63(5)	214.4(9)–217.3(9)

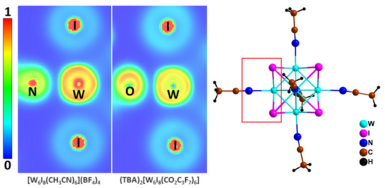

Fig. 4 Electron localization function (ELF) of **III** and $(TBA)_2[W_6I_8(CO_2C_3F_7)_6]$ (left side) and an illustration of the view on one of the clusters depicted in the ELF (right side).

iodide cluster bearing strong electron withdrawing ligands (Fig. 4).

Comparison of the ELF of **III** and $(TBA)_2[W_6I_8(CO_2C_3F_7)_6]$ shows that **III** has a higher density of localized electrons at the W site, indicating reduced ionicity.[27] Four local maxima can be found along the W–N bond of **III**, while only two are present along the W–O bond of $(TBA)_2[W_6I_8(CO_2C_3F_7)_6]$, which can be attributed to a higher covalency of **III**. However, as a nodal plane is present at the centre of both W–N/O bonds, the bond for both compounds is primarily ionic. The ELFs around the I atoms are similar for both compounds.

Photoluminescence studies

The characteristic photophysical properties of $[(W_6I_8)I_6]^{2-}$ and $[(W_6I_8)L_6]^{2-}$ clusters have been recently reported. Crystalline powders of these compounds typically appear with yellow to orange colors. Upon UV radiation or visible light photo-excitation, they emit red luminescence (phosphorescence) from excited triplet states.[8,9,11*b*,12*a*,*b*,*d*,19*b*,28]

The bonding of six apical iodide ligands in $[(W_6I_8)I_6]^{2-}$ cluster compounds is represented by covalent W–I interactions. However, it has been shown that the presence of strongly electron withdrawing ligands (L) in $[(W_6I_8)L_6]^{2-}$ clusters can lead to a blue shift of the emission maximum, which is often related to significantly increased luminescence lifetimes or quantum yields.[11*b*,*c*,12*b*,*c*]

To explain some of these observations, a model for the emitting excited triplet states developed for molybdenum and tungsten halide clusters can be employed. Kitamura *et al.* used a model with four different emitting excited triplet state sublevels to explain the cluster emission.[13] They further noted that the highest lying sublevel can couple with the ground state by an electronically allowed dipole transition, giving rise to an intense and short-lived emission. Emission from the other spin sublevels is forbidden. Studies on molybdenum halide clusters having different d-electron densities revealed splittings between these spin-triplet sublevels, whereas a low density led to a high splitting and *vice versa*.[14] Additional investigations on the temperature dependence of the emission of $(TBA)_2[Mo_6X_8(CO_2C_3F_7)_6]$ (X = Cl, Br, I) revealed smaller full width at half maximum (FWHM) values and changes in the emission lifetime between 3 K and 300 K by switching inner ligands from Cl to I. This is attributed to a growing splitting between spin sublevels. Furthermore, increasing the temperature from 3 K to 300 K leads to a red shift of the emission for $(TBA)_2[Mo_6I_8(CO_2C_3F_7)_6]$ instead of the observed blue shift for the species bearing Cl and Br ligands.[15] The different thermal behavior of the emission is observed for clusters with different inner halide ligands as well as for different organic outer ligands.[29]

The herein monitored excitation and emission spectra of $[(W_6I_8)(CH_3CN)_6](BF_4)_4{\cdot}2(CH_3CN)$ powder show a broad excitation feature between 275 and 500 nm (λ_{em} = 630 nm) and a broad emission band between 500 and 800 nm (λ_{exc} = 390 nm), presented in Fig. 5. Interestingly, this emission of **III** is not very different from that of $[(W_6I_8)(CO_2C_3F_7)_6]^{2-}$ ($\lambda_{em,max} \approx$

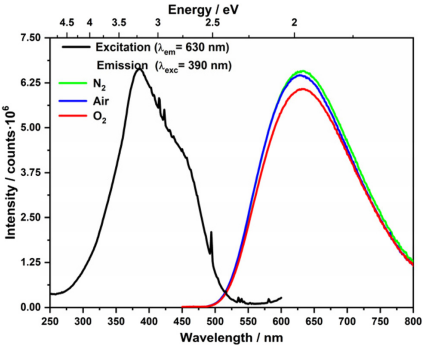

Fig. 5 Excitation (black) and emission (red, blue, green) spectra of crystalline $[(W_6I_8)(CH_3CN)_6](BF_4)_4{\cdot}2(CH_3CN)$ (**III**) powder.

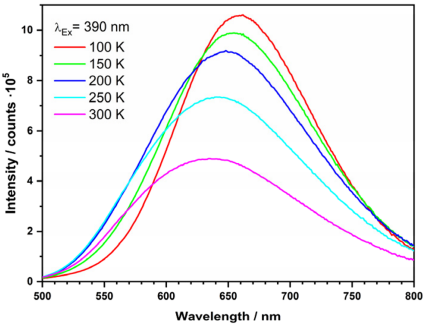

Fig. 6 Temperature-dependent photoluminescence spectra of **III** in the temperature range of 100 K to 300 K.

630 nm) carrying a strongly electron withdrawing ligand. However, a comparison of the emission lifetimes reveals a significantly shorter lifetime of **III** (τ = 11 µs, Fig. S2†) compared to $(TBA)_2[(W_6I_8)(CO_2C_3F_7)_6]$.[12b] Specifically, the original work reported a biexponential decay with τ = 27 and 55 µs, and our own lifetime measurements of $(TBA)_2[(W_6I_8)(CO_2C_3F_7)_6]$ yield a monoexponential decay with τ = 36 µs (Fig. S3†). Likewise, the behavior in the presence of molecular oxygen is also very different (Fig. 5 and S4†), with **III** showing nearly no quenching of the emission, while $(TBA)_2[(W_6I_8)(CO_2C_3F_7)_6]$ quenches strongly. In general, tungsten iodide compounds featuring strong oxygen quenching of the emission usually exhibit long emission lifetimes. This supports the fact that the quenching is related to the lifetime of the emission process in tungsten iodide clusters.

A comparison of the d-electron density in **III** (Fig. 4) and $(TBA)_2[W_6I_8(CO_2C_3F_7)_6]$ shows a higher density for **III** and a less ionic bonding between tungsten and the ligand atom. The consideration of our observations and those of Kitamura *et al.*[14,15] lead to the conclusion that the very short emission lifetime of **III** could stem from a low energetic splitting of the spin sublevels and therefore strong thermal population of the highest level responsible for a short emission lifetime. For $(TBA)_2[W_6I_8(CO_2C_3F_7)_6]$, a high energetic splitting can be expected, leading to a long lifetime.

Temperature-dependent photoluminescence studies of **III** (Fig. 6) show a blue shift of the emission with increasing temperature from 100 K to 300 K. This is in contrast to the red shift reported for $(TBA)_2[Mo_6I_8(CO_2C_3F_7)_6]$[15] and the steady emission of $(TBA)_2[W_6I_8(CO_2C_3F_7)_6]$ (Fig. S5†). The same applies for the FWHM values observed, which are ~3100 cm^{-1} at 100 K and ~4100 cm^{-1} at 300 K for **III** and ~2800 cm^{-1} at 100 K and ~3600 cm^{-1} at 300 K for $(TBA)_2[W_6I_8(CO_2C_3F_7)_6]$. In the case of $(TBA)_2[Mo_6I_8(CO_2C_3F_7)_6]$, ~1500 cm^{-1} at 3 K and ~2400 cm^{-1} at 300 K are reported. Both, the blue shift and the large FWHM value for **III** compared to $(TBA)_2[W_6I_8(CO_2C_3F_7)_6]$ or the molybdenum species could stem from strong contribution of the energetically highest emissive triplet sublevel to the photoluminescence.

Excited state studies

We investigated the excited state properties of **III** in acetonitrile solution by femtosecond and nanosecond transient absorption measurements. To observe the fast dynamics, we excited the sample with 90 fs laser pulses at a wavelength of 300 nm (1 µJ per pulse). Sequential global fitting analysis found three different components, with decay times of 2.2 ps, 87 ps and a decay significantly longer than the measurement window of 7.5 ns (Fig. 7 and S7†). These observations are in good agreement with previously reported data obtained for $(TBA)_2[Mo_6X_8Y_6]$ (X = Cl, Br, I; Y = Cl, Br, I, CO_2CF_3).[30] We attribute component 2 and 3 to the excited triplet states of the cluster since the obtained spectra are in accordance with

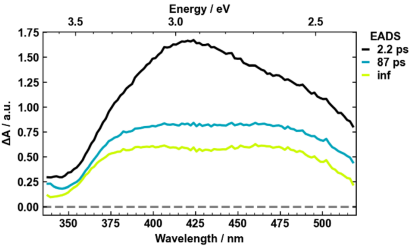

Fig. 7 Evolution-associated difference spectra (EADS) resulting from the global analysis of III in acetonitrile after excitation at 300 nm. The black spectrum forms instantaneously at time zero and evolves in 2.2 ps into the blue component which decays in 87 ps into the yellow component with a lifetime longer than the measurement window.

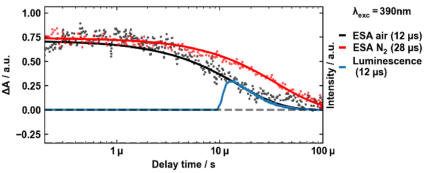

Fig. 8 Kinetic trace of III, measured at the excited-state absorption (ESA) feature at 470 nm after excitation at 390 nm in acetonitrile, revealing a mono exponential decay with a lifetime of 28 µs under N_2 (red) and 12 µs under ambient conditions (black). The photoluminescence decay spectrum is shown in blue (λ_{exc} = 390 nm, λ_{em} = 630 nm).

spectra obtained on the microsecond timescale (Fig. S8†). As described for molybdenum compounds, the second component is probably related to a hot triplet state, while component 1 has a different shape and is likely due to an excited singlet state which decays *via* intersystem crossing into the hot triplet state (component 2).

The observed lifetime of 2.2 ps for the singlet state deviates slightly from the reported lifetimes for molybdenum iodide clusters, which are typically between 0.5 ps and 1.7 ps.[30] Moreover, the 87 ps lifetime of the hot triplet is about one order of magnitude larger than the reported lifetimes for molybdenum iodide clusters. We conclude that the decay of the various excited states of **III** is generally slower than that of the corresponding excited states in molybdenum iodide clusters. A definitive attribution of this finding to the effect of the metal atom or the different apical ligands would require additional transient absorption data, *e.g.* of the molybdenum analogues with the same apical ligands, which is currently not available. To study the slower dynamics beyond 7.5 ns, *e.g.* the broad excited-state absorption feature (ESA) between 350 and 530 nm, we conduct nanosecond transient absorption spectroscopy at an excitation wavelength of 390 nm (2 µJ per pulse) (Fig. 8). We find a mono-exponential decay with a lifetime of 28 µs under nitrogen (red) and 12 µs (component 3) under ambient conditions (black) over the whole spectral range. This is in excellent agreement with time-resolved photoluminescence decay studies in acetonitrile solution (12 µs, blue curve), indicating that the long-lived ESA signal corresponds to the excited triplet state responsible for the emission.

Experimental section

Synthetic procedures

Synthesis of $[(W_6I_8)I(CH_3CN)_5](I_3)_2(BF_4)$ (I). The preparation of the starting material $[W_6I_{11}(CH_3CN)_3](I_7)\cdot I_2$ was previously reported.[17c]

A 4 ml screwcap vial was filled with 25.0 mg (6.6 mmol) $[W_6I_{11}(CH_3CN)_3](I_7)\cdot I_2$ and 1.3 mg (6.6 mmol) $AgBF_4$ and 3 ml acetonitrile. The vial was placed in a furnace at 85 °C for 2 weeks. Afterwards it was removed from the furnace for cooling to room temperature. Clear dark red plate-shaped crystals had formed on the wall of the vial (estimated yield of single crystals: 5%).

Synthesis of $[(W_6I_8)(CH_3CN)_6](I_3)(BF_4)_3\cdot(H_2O)$ (II). Similar to **I**, a 4 ml screwcap vial was filled with 25.0 mg (6.6 mmol) $[W_6I_{11}(CH_3CN)_3](I_7)\cdot I_2$ and 3.9 mg (19.9 mmol) $AgBF_4$ and 3 ml acetonitrile. The vial was placed in a furnace at 85 °C for 2 weeks. Afterwards it was removed from the furnace for cooling to room temperature. Clear red plate-shaped crystals had formed on the wall of the vial (estimated yield of single crystals: 5%).

Synthesis of $[(W_6I_8)(CH_3CN)_6](BF_4)_4\cdot(CH_3CN)_2$ (III). A thimble was filled with 150 mg (39.9 mmol) $[W_6I_{11}(CH_3CN)_3](I_7)\cdot I_2$ and 33 mg (159.4 mmol) $AgBF_4$ and placed in a Soxhlet extractor. A round flask with 120 ml of acetonitrile was connected to the extractor. The flask with acetonitrile was heated under reflux for 16 h and then cooled to room temperature. After the extraction the solvent showed a yellow color, white and small amounts of yellow precipitate were at the bottom of the flask. The yellow solution was collected and the acetonitrile evaporated to give a yellow crystalline powder and small plate-shaped crystals (yield: 74 mg; 34.0 µmol; 67%). Both the powder and the crystals showed orange luminescence when irradiated with UV light. $[(W_6I_8)(CH_3CN)_6](BF_4)_4\cdot 2(CH_3CN)$ could be handled in air but showed a slight color change after remaining in air for two weeks. ^{1}H-NMR ($[W_6I_8(CH_3CN)_6]^{4+}$, 400 MHz, CD_3CN) δ 2.77 (3H, s, CH_3). Elemental analysis for **III**: 0.69 H, 3.18 N, 5.39 C; calculated with co-crystallized solvent 0.86 H, 4.01 N, 6.87 C without solvent 0.67 H, 3.10 N, 5.32 C. IR: 2999 (C–H), 2937 (C–H); 2312 (C≡N), 2281 (C≡N); 1660 (C≡N), 1564 (C≡N); 1410 (C–H), 1367 (C–H), 1284 (C–H); 1055 (C–H); 519 (W–N).[31]

Single-crystal X-ray diffraction

The single-crystal X-ray diffraction (XRD) studies on the obtained compounds $[(W_6I_8)I(CH_3CN)_5](I_3)_2(BF_4)$, $[(W_6I_8)(CH_3CN)_6](I_3)(BF_4)_3\cdot H_2O$, $[(W_6I_8)(CH_3CN)_6](BF_4)_4\cdot(CH_3CN)_2$ were performed using a Rigaku XtaLab Synergy-S diffractometer with Mo-K_α radiation (λ = 0.71073 Å) and a mirror monochromator. Yellow or red plate-shaped single-crystals were used for the measurement under N_2 cooling at 100 K. Corrections for absorption effects were applied with CrysAlisPro 1.171.41.65a (Rigaku Oxford Diffraction, 2020). The structure was solved by direct methods (SHELXT),[32] and full-matrix least-squares structure refinements were performed with SHELXL-2014[33] implemented in Olex2 1.3-ac4.

Luminescence studies

Excitation and emission spectra of powder samples of $[(W_6I_8)(CH_3CN)_6](BF_4)_4\cdot(CH_3CN)_2$ were collected by using a fluorescence spectrometer *FLS920* (*Edinburgh Instruments*) equipped with a 450 W xenon discharge lamp (*OSRAM*) and a cryostat "*MicrostatN*" from *Oxford Instruments* as the sample chamber for adjusting the atmosphere during the measurements and to adjust the temperature. Additionally, a mirror optic for powder samples was applied. For detection, an

R2658P single-photon-counting photomultiplier tube (*Hamamatsu*) was used. All photoluminescence spectra were recorded with a spectral resolution of 1 nm, a dwell time of 0.5 s in 1 nm steps and 2 repeats.

Density functional theory

Density functional theory (DFT) was used to calculate the ELF of **III** and $(TBA)_2[W_6I_8(CO_2C_3F_7)_6]$ within the Abinit software package.[34] Calculations were performed using a 36 Ha plane-wave basis set energy cutoff and 2 × 1 × 2 (**III**) and 2 × 2 × 2 ($(TBA)_2[W_6I_8(CO_2C_3F_7)_6]$) Monkhorst–Pack grids[35] of k points. Norm-conserving pseudopotentials were used as received from the Abinit library. Example input files are available as part of the ESI.†

Transient absorption spectroscopy

Pump probe spectroscopy was conducted using a femtosecond transient absorption spectrometer (HELIOS Fire) and a nanosecond transient absorption spectrometer (EOS Fire) from Ultrafast Systems. 90 fs excitation laser pulses at 1 kHz repetition rate and 800 nm wavelength were generated with an Astrella-F ultrafast Ti:sapphire amplifier from Coherent and split into a pump and probe beam. The pump beam wavelength was varied by nonlinear frequency mixing and second harmonic generation in an Apollo-T optical parametric amplifier from Ultrafast Systems, from which monochromatic 300 nm or 390 nm pulses with approximately 1 μJ per pulse or 2 μJ per pulse were obtained. For the femtosecond experiments, a broadband probe spectrum from 320 to 640 nm was generated by focusing the 800 nm probe beam onto a CaF_2 crystal by nonlinear processes, while a mechanical delay stage controlled the pump–probe delay. For the nanosecond experiments, a photonic crystal fiber-based white-light probe continuum from 380 to 800 nm was generated and the pump–probe delay was controlled electronically.

All samples were prepared in dry acetonitrile under inert conditions in a quartz glass microcuvette with an optical path length of 2 mm and an optical density of 0.2 and 0.4 at 300 nm.

Global analysis was performed using the free software program Glotaran.[36]

NMR studies

The ^{1}H-NMR spectrum was recorded from acetonitrile-d_3 solution at room temperature on a Bruker AVII+ 400 spectrometer.

IR Studies

FTIR spectra of **III** and acetonitrile were recorded on a Bruker vertex 70 spectrometer. For solid III a KBr disk and for liquid acetonitrile a drop between two KBr disks was measured.

Elemental analyses

Elemental Analyses was obtained using a UNICUBE apparatus from ELEMENTAR.

Conclusions

Solvated $[W_6I_8]^{4+}$ clusters were synthesised in three different compounds. Among them is the homoleptic $[(W_6I_8)(CH_3CN)_6]^{4+}$ cluster cation, having the same electron cluster count as $[(W_6I_8)I_6]^{2-}$. The excited state properties were investigated by photoluminescence and transient absorption measurements. The emission maximum of solid $[(W_6I_8)(CH_3CN)_6](BF_4)_4{\cdot}2(CH_3CN)$ is observed at $\lambda_{em,max}$ = 630 nm and therefore in a quite similar range as $[W_6I_8L_6]^{2+}$ clusters bearing electron withdrawing ligands. Results of the transient absorption measurements revealed excited state absorption with three different components. Two of them featuring short decay times on the picosecond scale, while the short one is attributed to an excited singlet state and the longer one to a hot triplet state. This is in good agreement with a previous report on octahedral molybdenum halide clusters.[30]

Observations of longer time scales reveal a single component absorption with a lifetime of 12 μs, which we attribute to the excited triplet state of **III** which are supporting the results of the decay measurements for solid **III** (11 μs) and in acetonitrile solution (12 μs). Compared to other clusters like $(TBA)_2[W_6I_8(CO_2C_3F_7)_6]$ with reported lifetimes being up to 55 μs, these photoluminescence lifetimes appear short. In contrast to the behavior of $(TBA)_2[W_6I_8(CO_2C_3F_7)_6]$ the quenching of the luminescence in presence of molecular oxygen is low.

Additionally, the photoluminescence studies on **III** showed a higher FWHM of the emission compared to $(TBA)_2[W_6I_8(CO_2C_3F_7)_6]$ and a blue shift of the emission going to higher temperatures, indicating stronger participation of higher lying triplet sublevels. A comparison of the ELF of **III** and $(TBA)_2[W_6I_8(CO_2C_3F_7)_6]$ revealed higher electron density on the tungsten atoms and a less ionic bonding in **III**. This observation suggests a strong influence of the metal-to-L bond polarity on the photoluminescence properties of octahedral molybdenum or tungsten halide clusters. High bond polarity is achieved using strong electron withdrawing ligands such as fluorinated ligands, leading to tungsten or molybdenum halide clusters with long lasting luminescence and strong oxygen quenching.

Conflicts of interest

There are no conflicts to declare.

Acknowledgements

Funding by the Deutsche Forschungsgemeinschaft (DFG) *via* grant ME 914/31-1 and SCHE1905/9-1 is gratefully acknowledged. The pump–probe measurements were enabled by the DFG under grant INST 37/1160-1 FUGG. CPR was supported by ETH Zurich and by the European Union and Horizon 2020 through a Marie Sklodowska-Curie Fellowship, Grant Agreement No. 101030352. Computational resources were provided by ETH Zurich.

References

1 (*a*) A. W. Maverick, J. S. Najdzionek, D. Mackenzie, D. G. Nocera and H. B. Gray, *J. Am. Chem. Soc.*, 1983, **105**, 1878–1882; (*b*) T. C. Zietlow, D. G. Nocera and H. B. Gray, *Inorg. Chem.*, 1986, **25**, 1351–1353.

2 T. C. Zietlow, M. D. Hopkins and H. B. Gray, *J. Solid State Chem.*, 1985, **57**, 112–119.

3 J. A. Jackson, C. Turro, M. D. Newsham and D. G. Nocera, *J. Phys. Chem.*, 1990, **94**, 4500–4507.

4 D. J. Osborn, G. L. Baker and R. N. Ghosh, *J. Sol-Gel Sci. Technol.*, 2005, **36**, 5–10.

5 P. Kumar, S. Kumar, S. Cordier, S. Paofai, R. Boukherroub and S. L. Jain, *RSC Adv.*, 2014, **4**, 10420–10423.

6 M. Feliz, M. Puche, P. Atienzar, P. Concepcion, S. Cordier and Y. Molard, *ChemSusChem*, 2016, **9**, 1963–1971.

7 A. O. Solovieva, Y. A. Vorotnikov, K. E. Trifonova, O. A. Efremova, A. A. Krasilnikova, K. A. Brylev, E. V. Vorontsova, P. A. Avrorov, L. V. Shestopalova and A. F. Poveshchenko, *J. Mater. Chem. B*, 2016, **4**, 4839–4846.

8 D. V. Evtushok, A. R. Melnikov, N. A. Vorotnikova, Y. A. Vorotnikov, A. A. Ryadun, N. V. Kuratieva, K. V. Kozyr, N. R. Obedinskaya, E. I. Kretov, I. N. Novozhilov, Y. V. Mironov, D. V. Stass, O. A. Efremova and M. A. Shestopalov, *Dalton Trans.*, 2017, **46**, 11738–11747.

9 T. Hummel, D. Dutczak, A. Y. Alekseev, L. S. Adamenko, A. M. Shestopalov, Y. V. Mironov, D. Enseling, T. Jüstel and H.-J. Meyer, *RSC Adv.*, 2020, **10**, 22257–22263.

10 H. Schäfer, H. G. von Schnering, J. Tillack, F. Kuhnen, H. Wöhrle and H. Baumann, *Z. Anorg. Allg. Chem.*, 1967, **353**, 281–310.

11 (*a*) W. Preetz, P. Braack, K. Harder and G. Peters, *Z. Anorg. Allg. Chem.*, 1992, **612**, 7–13; (*b*) L. Riehl, A. Seyboldt, M. Ströbele, D. Enseling, T. Jüstel, M. Westberg, P. R. Ogilby and H.-J. Meyer, *Dalton Trans.*, 2016, **45**, 15500–15506; (*c*) K. Kirakci, P. Kubat, M. Dusek, K. Fejfarova, V. Sicha, J. Mosinger and K. Lang, *Eur. J. Inorg. Chem.*, 2012, 3107–3111.

12 (*a*) M. A. Mikhailov, A. L. Gushchin, M. R. Gallyamov, A. V. Virovets, M. N. Sokolov, D. G. Sheven and V. V. Pervukhin, *Russ. J. Coord. Chem.*, 2017, **43**, 172–180; (*b*) M. N. Sokolov, K. A. Brylev, P. A. Abramov, M. R. Gallyamov, I. N. Novozhilov, N. Kitamura and M. A. Mikhaylov, *Eur. J. Inorg. Chem.*, 2017, **2017**, 4131–4137; (*c*) M. A. Mikhailov, K. A. Brylev, P. A. Abramov, E. Sakuda, S. Akagi, A. Ito, N. Kitamura and M. N. Sokolov, *Inorg. Chem.*, 2016, **55**, 8437–8445; (*d*) A. Seyboldt, D. Enseling, T. Jüstel, M. Ivanovic, H. Peisert, T. Chassé and H.-J. Meyer, *Eur. J. Inorg. Chem.*, 2017, **2017**, 5387–5394.

13 N. Kitamura, Y. Kuwahara, Y. Ueda, Y. Ito, S. Ishizaka, Y. Sasaki, K. Tsuge and S. Akagi, *Bull. Chem. Soc. Jpn.*, 2017, **90**, 1164–1173.

14 S. Akagi, S. Fujii and N. Kitamura, *J. Phys. Chem. A*, 2018, **122**, 9014–9024.

15 S. Akagi, E. Sakuda, A. Ito and N. Kitamura, *J. Phys. Chem. A*, 2017, **121**, 7148–7156.

16 (*a*) F. A. Cotton and N. F. Curtis, *Inorg. Chem.*, 1965, **4**, 241–244; (*b*) W. M. Carmichael and D. A. Edwards, *J. Inorg. Nucl. Chem.*, 1967, **29**, 1535–1538; (*c*) J. E. Fergusson, B. H. Robinson and C. J. Wilkins, *J. Chem. Soc. A*, 1967, 486–490; (*d*) R. D. Hogue and R. E. McCarley, *Inorg. Chem.*, 1970, **9**, 1354–1360.

17 (*a*) G. M. Ehrlich, C. J. Warren, R. C. Haushalter and F. J. DiSalvo, *Inorg. Chem.*, 1995, **34**, 4284–4286; (*b*) E. V. Svezhentseva, Y. A. Vorotnikov, A. O. Solovieva, T. N. Pozmogova, I. V. Eltsov, A. A. Ivanov, D. V. Evtushok, S. M. Miroshnichenko, V. V. Yanshole, C. J. Eling, A. M. Adawi, J. S. G. Bouillard, N. V. Kuratieva, M. S. Fufaeva, L. V. Shestopalova, Y. V. Mironov, O. A. Efremova and M. A. Shestopalov, *Chem. – Eur. J.*, 2018, **24**, 17915–17920; (*c*) F. Pachel, J. Händel, M. Ströbele and H.-J. Meyer, *Eur. J. Inorg. Chem.*, 2020, **2020**, 3987–3990; (*d*) M. V. Marchuk, Y. A. Vorotnikov, A. A. Ivanov, I. V. Eltsov, N. V. Kuratieva and M. A. Shestopalov, *Symmetry*, 2022, **14**, 2117.

18 M. Ströbele and H.-J. Meyer, *Inorg. Chem.*, 2019, **58**, 12867–12872.

19 (*a*) K. Kirakci, S. Cordier and C. Perrin, *Z. Anorg. Allg. Chem.*, 2005, **631**, 411–416; (*b*) T. Hummel, M. Ströbele, D. Schmid, D. Enseling, T. Jüstel and H.-J. Meyer, *Eur. J. Inorg. Chem.*, 2016, **2016**, 5063–5067.

20 (*a*) A. Flemming and M. Köckerling, *Z. Anorg. Allg. Chem.*, 2008, **634**, 2309–2315; (*b*) A. Flemming, J. König and M. Köckerling, *Z. Anorg. Allg. Chem.*, 2013, **639**, 2527–2531; (*c*) E. Sperlich and M. Köckerling, *Z. Naturforsch., B: Chem. Sci.*, 2020, **75**, 173–181; (*d*) A. Flemming and M. Köckerling, *Angew. Chem., Int. Ed.*, 2009, **48**, 2605–2608; (*e*) I. Dartsch, J. König and M. Köckerling, *J. Cluster Sci.*, 2018, **29**, 319–323; (*f*) J. König and M. Köckerling, *Z. Anorg. Allg. Chem.*, 2020, **646**, 1–7; (*g*) D. H. Weiß and M. Köckerling, *Chem. – Eur. J.*, 2018, **24**, 18613–18617; (*h*) D. H. Weiß, F. Schröder and M. Köckerling, *Z. Anorg. Allg. Chem.*, 2017, **643**, 345–351.

21 A. Bernsdorf and M. Köckerling, *Eur. J. Inorg. Chem.*, 2011, **2011**, 4057–4062.

22 Z. Zheng, J. R. Long and R. H. Holm, *J. Am. Chem. Soc.*, 1997, **119**, 2163–2171.

23 T. Hummel, A. Mos-Hummel, A. Merkulova, M. Ströbele, A. Krishnamurthy, S. Kroeker and H.-J. Meyer, *Inorg. Chem.*, 2018, **57**, 2570–2576.

24 M. Ströbele and H.-J. Meyer, *Dalton Trans.*, 2019, **48**, 1547–1561.

25 (*a*) A. A. Ordinartsev, A. A. Petrov, K. A. Lyssenko, A. V. Petrov, E. A. Goodilin and A. B. Tarasov, *Acta Crystallogr., Sect. E: Crystallogr. Commun.*, 2021, **77**, 692–695; (*b*) F. Demartin, P. Deplano, F. A. Devillanova, F. Isaia, V. Lippolis and G. Verani, *Inorg. Chem.*, 1993, **32**, 3694–3699; (*c*) T. Bernstein and F. H. Herbstein, *Acta Crystallogr., Sect. B: Struct. Crystallogr. Cryst. Chem.*, 1968, **24**, 1640–1645; (*d*) R. Slater, *Acta Crystallogr.*, 1959, **12**, 187–196; (*e*) M. E. Kamminga, M. C. Gélvez-Rueda, S. Maheshwari, I. S. van Droffelaar, J. Baas, G. R. Blake, F. C. Grozema and T. T. M. Palstra, *J. Solid State Chem.*, 2019, **270**, 593–600; (*f*) B. F. Ali, R. Al-Far and S. F. Haddad, *Main Group Chem.*,

2009, **8**, 177–187; (*g*) E. Fialho De Assis, R. A. Howie and J. L. Wardell, *Acta Crystallogr., Sect. C: Cryst. Struct. Commun.*, 1996, **52**, 955–957; (*h*) R. J. Webb, T. Y. Dong, C. G. Pierpont, S. R. Boone, R. K. Chadha and D. N. Hendrickson, *J. Am. Chem. Soc.*, 1991, **113**, 4806–4812; (*i*) P. K. Hon and T. C. W. Mak, *Z. Kristallogr. - Cryst. Mater.*, 1982, **158**, 213–220.

26 A.-D. Fuhrmann, F. Pachel, M. Ströbele, D. Enseling, T. Jüstel and H.-J. Meyer, *Z. Anorg. Allg. Chem.*, 2020, **646**, 1650–1654.

27 A. Savin, R. Nesper, S. Wengert and T. F. Fässler, *Angew. Chem., Int. Ed. Engl.*, 1997, **36**, 1808–1832.

28 (*a*) D. V. Evtushok, N. A. Vorotnikova, V. A. Logvinenko, A. I. Smolentsev, K. A. Brylev, P. E. Plyusnin, D. P. Pishchur, N. Kitamura, Y. V. Mironov, A. O. Solovieva, O. A. Efremova and M. A. Shestopalov, *New J. Chem.*, 2017, **41**, 14855–14861; (*b*) T. Hummel, M. Ströbele, A. D. Fuhrmann, D. Enseling, T. Jüstel and H.-J. Meyer, *Eur. J. Inorg. Chem.*, 2019, **2019**, 4014–4019; (*c*) M. Bregnhoj, K. Strunge, R. J. Sorensen, M. Ströbele, T. Hummel, H.-J. Meyer, F. Jensen and P. R. Ogilby, *J. Phys. Chem. A*, 2019, **123**, 1730–1739; (*d*) M. Ströbele, D. Enseling, T. Jüstel and H.-J. Meyer, *Z. Anorg. Allg. Chem.*, 2016, **642**, 1435–1438.

29 S. Akagi, T. Horiguchi, S. Fujii and N. Kitamura, *Inorg. Chem.*, 2019, **58**, 703–714.

30 K. Kirakci, P. Kubat, J. Langmaier, T. Polivka, M. Fuciman, K. Fejfarova and K. Lang, *Dalton Trans.*, 2013, **42**, 7224–7232.

31 (*a*) M. F. Farona, J. G. Grasselli and B. L. Ross, *Spectrochim. Acta, Part A*, 1967, **23**, 1875–1881; (*b*) E. M. Kosower, G. Markovich and G. Borz, *ChemPhysChem*, 2007, **8**, 2513–2519; (*c*) S. Thomas, C. G. Young and E. R. T. Tiekink, *Organometallics*, 1998, **17**, 182–189; (*d*) J. Reedijk, A. P. Zuur and W. L. Groeneveld, *Recl. Trav. Chim. Pays-Bas*, 1967, **86**, 1127–1137.

32 G. M. Sheldrick, *Acta Crystallogr. A*, 2015, **71**, 3–8.

33 C. B. Huebschle, G. M. Sheldrick and B. Dittrich, *J. Appl. Crystallogr.*, 2011, **44**, 1281–1284.

34 X. Gonze, B. Amadon, G. Antonius, F. Arnardi, L. Baguet, J.-M. Beuken, J. Bieder, F. Bottin, J. Bouchet, E. Bousquet, N. Brouwer, F. Bruneval, G. Brunin, T. Cavignac, J.-B. Charraud, W. Chen, M. Côté, S. Cottenier, J. Denier, G. Geneste, P. Ghosez, M. Giantomassi, Y. Gillet, O. Gingras, D. R. Hamann, G. Hautier, X. He, N. Helbig, N. Holzwarth, Y. Jia, F. Jollet, W. Lafargue-Dit-Hauret, K. Lejaeghere, M. A. L. Marques, A. Martin, C. Martins, H. P. C. Miranda, F. Naccarato, K. Persson, G. Petretto, V. Planes, Y. Pouillon, S. Prokhorenko, F. Ricci, G.-M. Rignanese, A. H. Romero, M. M. Schmitt, M. Torrent, M. J. van Setten, B. Van Troeye, M. J. Verstraete, G. Zérah and J. W. Zwanziger, *Comput. Phys. Commun.*, 2020, **248**, 107042.

35 H. J. Monkhorst and J. D. Pack, *Phys. Rev. B: Solid State*, 1976, **13**, 5188–5192.

36 J. J. Snellenburg, S. Laptenok, R. Seger, K. M. Mullen and I. H. M. van Stokkum, *J. Stat. Softw.*, 2012, **49**, 1–22.

Electronic Supplementary Material (ESI) for Dalton Transactions.

Supporting Information for:

Preparation and Luminescence of the Homoleptic Cluster Cation $[(W_6I_8)(CH_3CN)_6]^{4+}$

Florian Pachel,[a] Philipp Frech,[b] Markus Ströbele,[a] David Enseling,[c] Carl P. Romao,[d] Thomas Jüstel,[c] Marcus Scheele[b] and Hans-Jürgen Meyer[a*]

[a] Section for Solid State and Theoretical Inorganic Chemistry, Institute of Inorganic Chemistry, University of Tübingen, Auf der Morgenstelle 18, 72076 Tübingen, Germany.

[b] Institute of Physical and Theoretical Chemistry, University of Tübingen, Auf der Morgenstelle 18, 72076 Tübingen, Germany.

[c]Department of Chemical Engineering, Münster University of Applied Science, Stegerwaldstraße 39, 48565 Steinfurt, Germany.

[d]Department of Materials, ETH Zurich, Wolfgang-Pauli-Straße 27, 8093 Zurich, Switzerland.

Figure S1. Crystals of **III** under VIS (left side) and UV (right side) irradiation

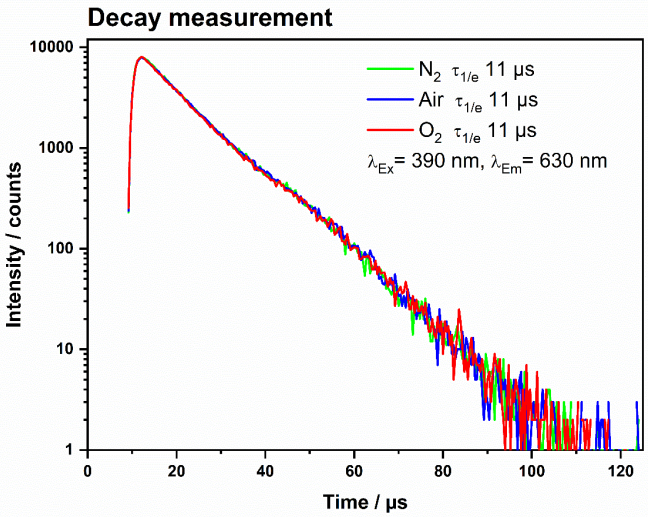

Figure S2. Decay measurement of solid **III**.

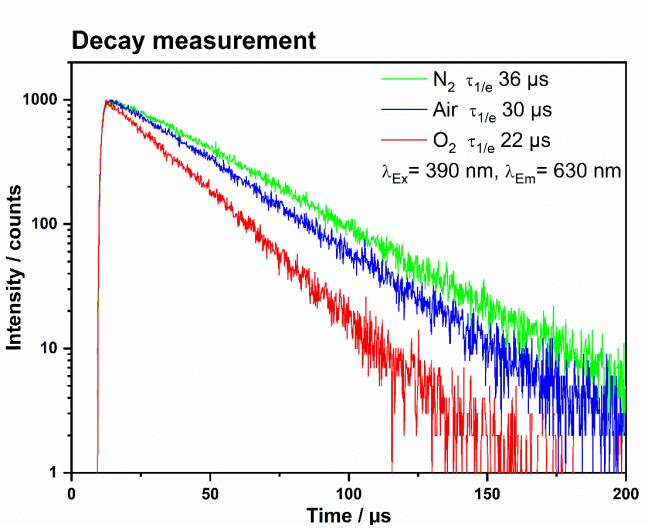

Figure S3. Decay measurement of solid $(TBA)_2[W_6I_8(CO_2C_3F_7)_6]$.

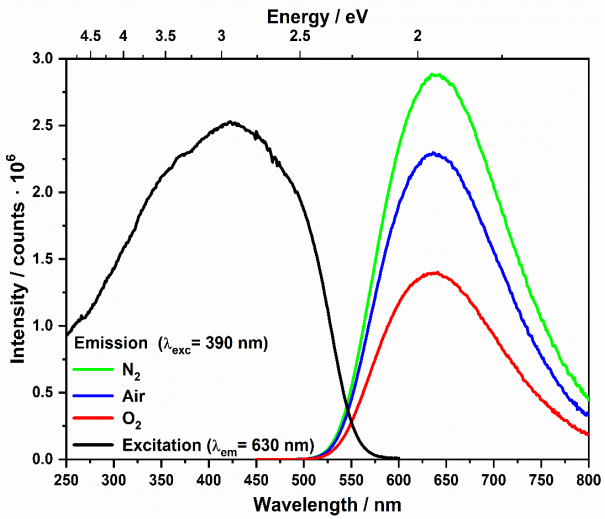

Figure S4. Excitation and emission spectra of solid $(TBA)_2[W_6I_8(CO_2C_3F_7)_6]$ under nitrogen, air and oxygen atmosphere.

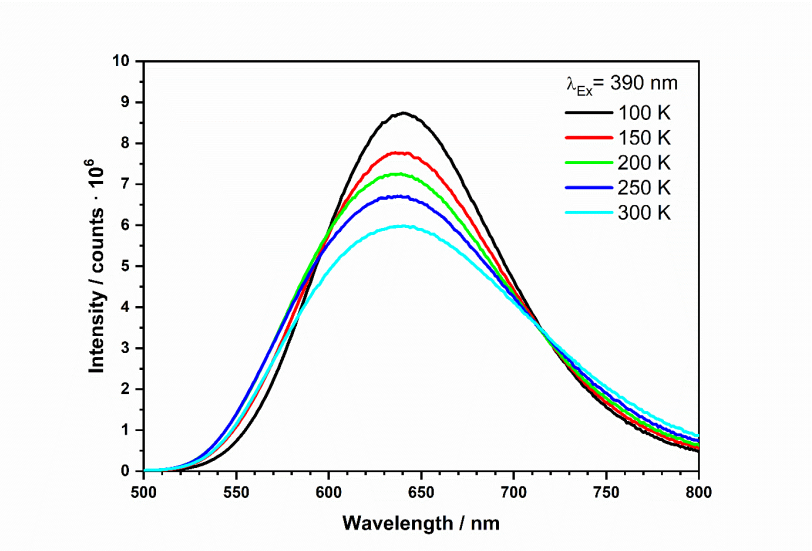

Figure S6. Emission spectra of solid $(TBA)_2[W_6I_8(CO_2C_3F_7)_6]$ at different temperatures.

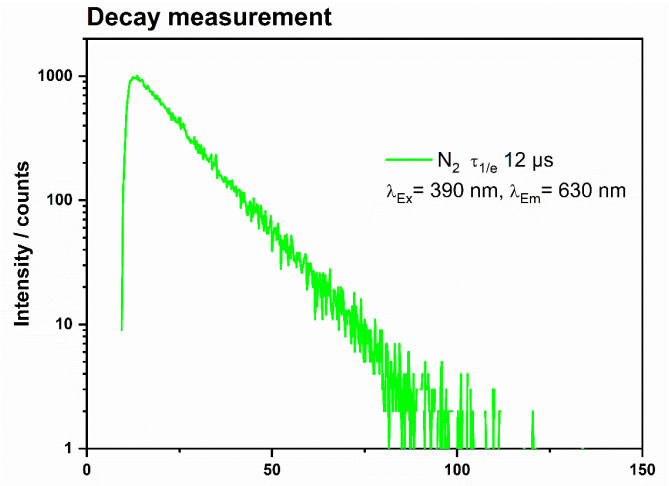

Figure S5. Decay measurement of **III** in acetonitrile.

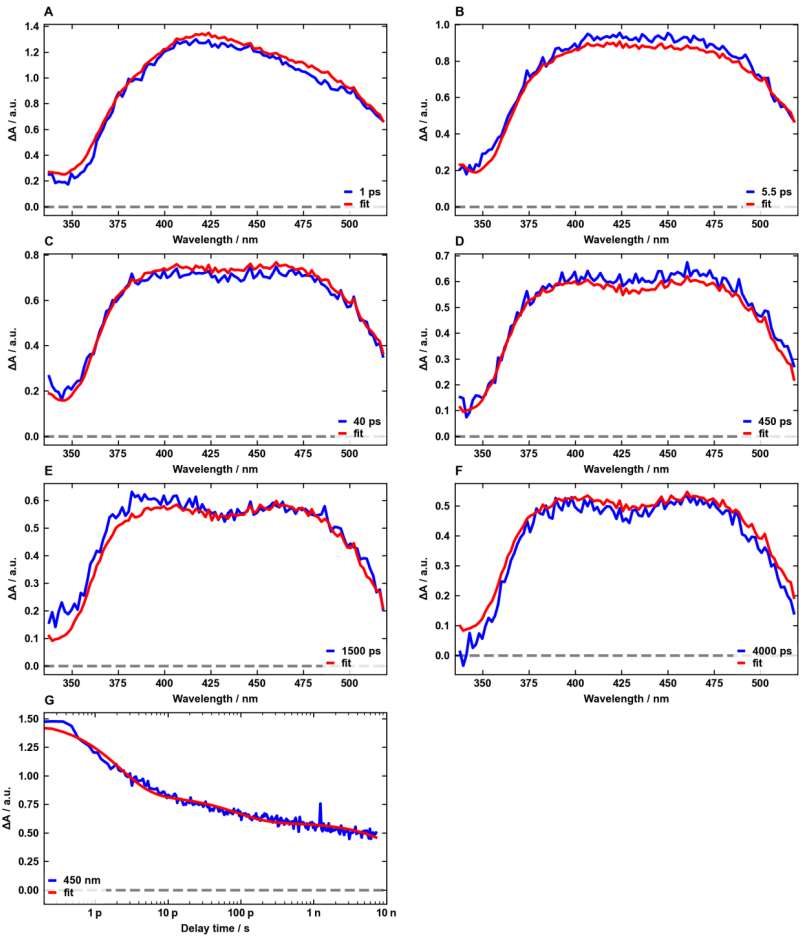

Figure S7. Selected ΔA spectra (A-F) of **III** at different time delays (blue) after excitation at 300 nm and kinetic trace at 450 nm (G). The corresponding fit spectra and traces of the global analysis are shown in red.

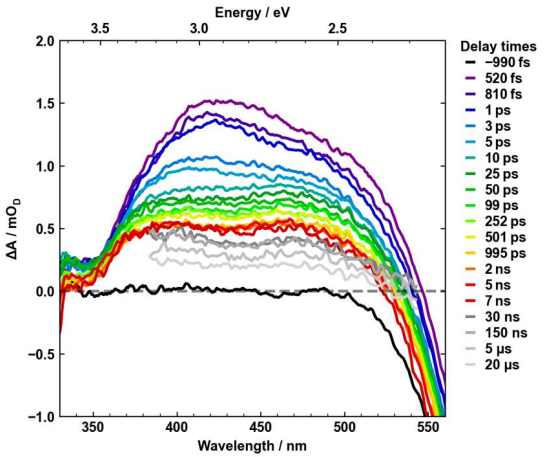

Figure S8. Selected ΔA spectra of **III** at different delay times after excitation at 300 nm. A femtosecond transient absorption spectrometer was used for delay times up to 7.5 ns. For the long-lived species longer than 7 ns, a different nanosecond pump probe spectrometer was used (grey scale). The negative signals at wavelengths higher than 520 nm are due to strong luminescence.

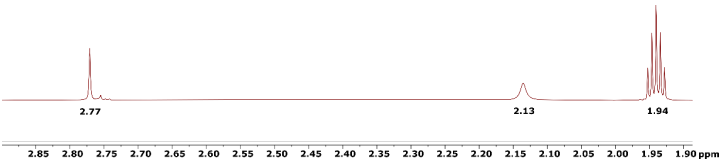

Figure S9. Section of the ^{1}H-NMR of **III** in CD_3CN showing the signal for the CH_3-group at 2.77 ppm and a signal of H_2O at 2.13 ppm.

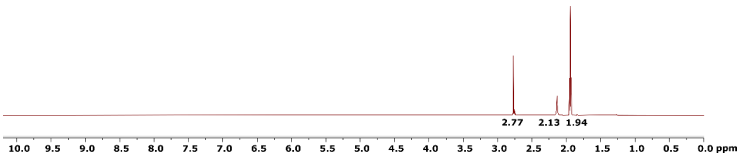

Figure 10. Greater section of the ^{1}H-NMR of **III** in CD_3CN between 0.0 and 10 ppm.

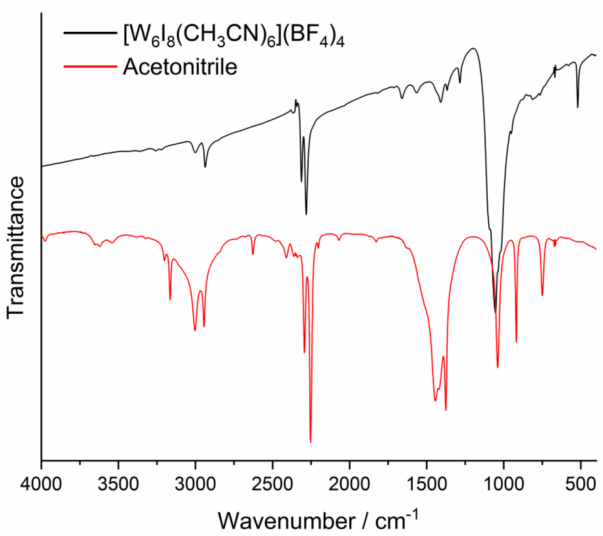

Figure 11. Infrared spectrum of **III** in black and of acetonitrile in red.

Publication 3

The Remarkable Robust, Photoactive Tungsten Iodide Cluster $[W_6I_{12}(NCC_6H_5)_2]$

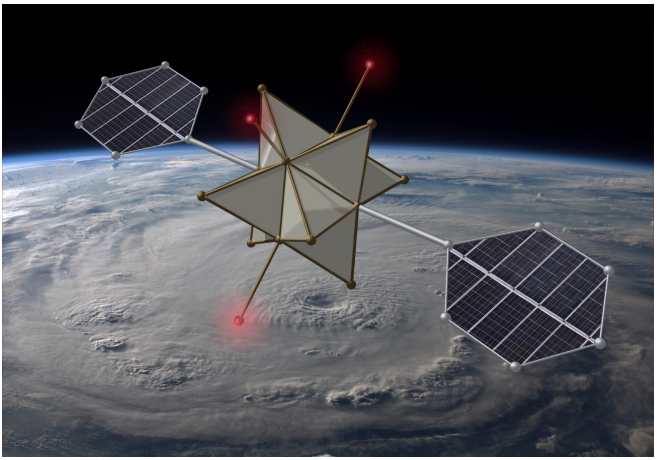

https://doi.org/10.1002/ejic.202300096

Reprinted with permission from

Eur. J. Inorg. Chem. **2023**, *26*, e202300096

EurJIC
European Journal of Inorganic Chemistry

Research Article
doi.org/10.1002/ejic.202300096

Chemistry Europe
European Chemical Societies Publishing

www.eurjic.org

The Remarkably Robust, Photoactive Tungsten Iodide Cluster $[W_6I_{12}(NCC_6H_5)_2]$

Florian Pachel,[a] Markus Ströbele,[a] Carl P. Romao,[b] David Enseling,[c] Thomas Jüstel,[c] and Hans-Jürgen Meyer*[a]

The new heteroleptic tungsten iodide cluster compound $[W_6I_{12}(NCC_6H_5)_2]$ is presented. The synthesis is carried-out from $Cs_2W_6I_{14}$ and ZnI_2 under solvothermal conditions in benzonitrile solution, yielding red cube-shaped crystals. $[W_6I_{12}(NCC_6H_5)_2]$ represents a heteroleptic $[W_6I_8]$-type cluster bearing four apical iodides and two benzonitrile ligands. Molecular $[W_6I_{12}(NCC_6H_5)_2]$ clusters form a robust hydrogen bridged crystal structure with high thermal stability and high resistibility against hydrolysis. The electronic structure is analyzed by quantum chemical methods of the calculated electron localization function (ELF) and the band structure. Photoluminescence measurements are performed to verify and describe the photophysical properties of $[W_6I_{12}(NCC_6H_5)_2]$. Finally, the photocatalytic properties of $[W_6I_{12}(NCC_6H_5)_2]$ are evaluated as a proof-of-concept.

Introduction

Metal halide clusters M_6X_{12} (M = Mo, W; X = Cl, Br, I) consist of an octahedral metal core surrounded by eight inner halide ligands located above the faces of the octahedron, and six apical halide ligands above the edges (four of them shared between clusters). The structure of these binary metal halides was first reported in the 1960s by Schäfer et al. for Mo_6Cl_{12}.[1] Based on this work, structures have also been reported for other octahedral tungsten and molybdenum metal halides.[2] Since then, it has been discovered that these clusters show a bright red to orange luminescence based on their $[M_6X_8]$ moieties, which is caused by excitation of an electron from the ground state S_0 into an excited singlet state S_n, followed by intersystem crossing (ISC) into excited triplet states and subsequent relaxation into the ground state through phosphorescence.[3] Continuing research discovered the energy transfer from these excited triplet states onto molecular oxygen to form singlet oxygen.[4] These and other optical properties make cluster compounds based on the $[M_6X_8]$ type interesting for applications in various different fields like in medicine (photodynamic therapy,[5] X-ray contrast agent, surface disinfection[6]), photocatalysis,[7] solar energy harvesting,[8] oxygen sensing[9] and so on.

Typically, these octahedral metal halide clusters are semiconductors featuring optical bandgaps around 2 eV,[7d,10] qualifying them for applications in photocatalysis. Their potential in this field has been proven by water purification from organic dyes, as has been reported for two cluster species, showing good activity in the decomposition of rhodamine B.[7c,d,10c] However, stability is always a concern when using tungsten or molybdenum halide clusters in reactions or applications involving aqueous media. Thus, the field of possible candidates is limited. Species bearing organic anions are prone to undergo ligand exchange with OH^-.[5,11]

Research into the photophysical properties of the octahedral metal halide clusters has mostly been undertaken on anionic cluster species of the form $[M_6X_8L_6]^{2-}$ (M = Mo, W; X = Cl, Br, I; L = Cl, Br, I, organic anions)[10a,12] accompanied by large organic cations like tetrabutylammonium (TBA), triphenyl phosphonium (PPh_4) or bis(triphenylphosphine)iminium (PPN).[13] However, investigations regarding the luminescence of neutral and cationic cluster species are scarce, even though first examples were reported decades ago.[14] To the best of our knowledge, only a few compounds have known crystal structures and have been characterized in regard to their photophysical properties.[5,10b,15]

Herein we report on the synthesis and structure of the new neutral octahedral tungsten iodide cluster $[W_6I_{12}(NCC_6H_5)_2]$, which bears two benzonitrile ligands, and subsequent investigations into it's thermal stability and stability in aqueous media, bonding and electronic conditions, photoluminescence studies and on the photophysical decomposition of rhodamine B.

[a] F. Pachel, Dr. M. Ströbele, Prof. Dr. H.-J. Meyer
Section for Solid State and Theoretical Inorganic Chemistry
Institute of Inorganic Chemistry
Eberhard Karls Universität Tübingen
Auf der Morgenstelle 18, D-72076 Tübingen (Germany)
E-mail: juergen.meyer@uni-tuebingen.de
[b] C. P. Romao
Department of Materials
ETH Zürich
Wolfgang-Pauli-Strasse 27, CH-8093 Zurich (Switzerland)
[c] D. Enseling, T. Jüstel
Department of Chemical Engineering
Münster University of Applied Science
Stegerwaldstraße 39, D-48565 Steinfurt (Germany)

Supporting information for this article is available on the WWW under https://doi.org/10.1002/ejic.202300096

Research Article
doi.org/10.1002/ejic.202300096

Chemistry Europe
European Chemical Societies Publishing

Results and Discussion

The synthesis of the title compound was first achieved in an approach analogous to that reported for the cationic cluster species $[W_6I_{11}(CH_3CN)_3]I_7 \cdot I_2$ featuring acetonitrile as a ligand, departing from W_6I_{22}.[15b] Reactions starting from the soluble cluster species W_6I_{22} under solvothermal conditions in benzonitrile, performed in a fused quartz ampoule yielded $[W_6I_{12}(NCC_6H_5)_2]$ (**1**, Figure 1, left side) as black cube-shaped crystals (Figure 1, middle). We attributed the black body color to the excess of iodine in the reaction and thus tried to remove it by rinsing or redissolving the crystals. Unfortunately, the compound is insoluble in all common solvents including benzonitrile. Subsequent synthesis approaches departed from $Cs_2W_6I_{14}$ in benzonitrile, which could be expected to form $[W_6I_{12}(NCC_6H_5)_2]$ plus CsI straight forwardly. However, the resulting product was not our desired compound **1** and remained unidentified. Trying to capture CsI, we added ZnI_2 to obtain Cs_2ZnI_4 as byproduct. The reaction mixture of $Cs_2W_6I_{14}$, ZnI_2 in benzonitrile (solvothermal conditions at 200 °C) yielded **1** as orange cube-shaped crystals with a red to orange photoluminescence (Figure 1, right side) and Cs_2ZnI_4 as by-product.

Like other octahedral tungsten halide compounds, **1** features the characteristic $[W_6X_8]$-type cluster with six ligands attached at the corners of the octahedral tungsten core (Figure 1, left side). Four iodide and two benzonitrile ligands in these positions represent a heteroleptic cluster species. The only other reported crystal structure of an heteroleptic tungsten iodide cluster is $[W_6I_{11}\{CH_3CN\}_3]I_7 \cdot I_2$.[15b] $[W_6I_{12}(NCC_6H_5)_2]$ crystallizes in the monoclinic space group $P2_1/c$, with the clusters oriented in layers in the *bc* plane (Figure 2, left side). The isolated cluster units are alternately tilted to the right and left (Figure 2, right side), to allow a tight packing arrangement of molecular clusters without the presence of any co-crystallized solvent. Some crystallographic data are presented in Table 1.

Observed W–W distances range between 265.88(3)–267.42(3) pm and appear similar to values obtained in compounds with the $[W_6I_8I_6]^{2-}$ cluster (Table 2).[16] Averaged interatomic distances for W–I (280.15(4) pm within the $[W_6I_8]$ core and W–I 281.49(4) pm for apical iodides) are also in agreement to previously reported ones.[16] The coordinative W–N distance of 217.2(5) pm found for **1** corresponds well with literature data obtained for $(TBA)_2[W_6I_8(NCO)_6]$ with distances of 217(1) pm.[17]

Depicted in Figure 3 is the crystal structure of **1** showing isolated clusters with short distances between hydrogen and the apical iodide ligands of adjacent units. Observed H···I distances of 301.83 pm (I6···H7) and 306.56 pm (I5···H6) are far below the sum of the van der Waals radii (3.35 Å),[18] indicating H···I bonds between clusters.[18]

Table 1. Selected crystallographic data of **1**.

Compound		$[W_6I_{12}(NCC_6H_5)_2]$
CCDC code		2084368
Formula weight (g/mol)		2832.1
Temperature (K)		100.0(1)
Wavelength (pm)		71.073
Space group		$P\,1\,2_1/c\,1$
Unit cell dimensions (pm, degree)	*a*	968.78(1)
	b	1437.70(1)
	c	1362.18(1)
	β	104.961(1)°
Volume (nm^3)		4.6236(2)
Z		2
Density (calculated)		5.131 g/cm^3
Absorption coefficient		28.868 mm^{-1}
Goodness-of-fit on F^2		1.118
Final R indices ($I > 2\sigma(I)$)[a]		$R1 = 0.0160$, $wR2 = 0.0372$
R indices (all data)		$R1 = 0.0160$, $wR2 = 0.0372$

[a] $R_1 = \Sigma||F_o| - |F_c||/\Sigma|F_o|$, $wR_2 = (\Sigma w[(F_o)^2 - (F_c)^2]^2/\Sigma w[(F_o)^2]^2)^{1/2}$.

Table 2. Interatomic distances in **1**.

	W–W in pm
W–W	265.88(3)–267.42(3)
W–I[i]	278.22(4)–282.09(4)
W–I[a]	281.46(4)–281.52(4)
W–N	217.2(5)

[i] inner iodides of $[W_6I_8]$ core; [a] apical contact with the $[W_6I_8]$ core.

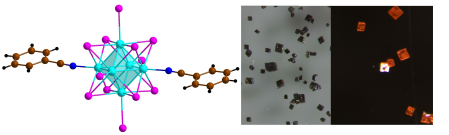

Figure 1. Structure of the neutral tungsten iodide cluster **1** (left side) with tungsten atoms as turquoise, iodine as pink, nitrogen as blue, carbon as brown, and hydrogen as black balls. Single crystals of **1** resulting from the synthesis from $[W_6I_{22}]$ (middle) and from $Cs_2W_6I_{14}$ with addition of ZnI_2 (right side).

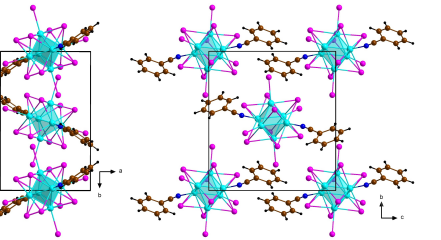

Figure 2. Projection of the crystal structure of **1** in the *ab* (left side) and *bc* plane (right side) with W atoms as turquoise, I as pink, carbon as brown, nitrogen as blue and hydrogen as black spheres.

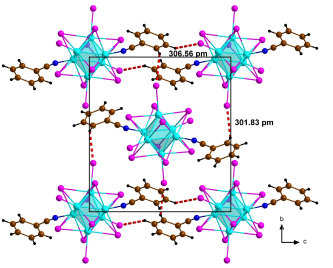

Figure 3. Projection of the crystal structure of **1** on the *bc* plane with close contacts between hydride and iodide marked as red dashed bonds. W atoms are displayed as turquoise, I as pink, carbon as brown, nitrogen as blue and hydrogen as black spheres.

Electron localization function and band structure

The photophysical properties of $[W_6I_8]$-type clusters are strongly influenced by apical cluster ligands.[10a,12c,19] For this reason we had a closer look at the nature of the bonding with apical ligands. For this purpose, the electron localization function (ELF) was calculated to investigate the W–N bonding of **1** and compared with the W–I bonding in $(TBA)_2[W_6I_{14}]$ and the W–O bonding in $(TBA)_2[W_6I_8(CO_2C_3F_7)_6$ (Figure 4). The surfaces of the ELF show high values about the metal centers for both **1** and $(TBA)_2[W_6I_{14}]$. Significantly lower values are obtained in $(TBA)_2[W_6I_8(CO_2C_3F_7)_6]$ featuring a strong electron withdrawing ligand, implying a reduced ionicity in **1** and $(TBA)_2[W_6I_{14}]$.

Along the W–N bond four local maxima are visible, while in case of the W–O bond only two are present, and the W–I bond shows three. The number of local maxima is related to the degree of covalency,[20] and suggests higher covalency in **1**. Nevertheless, all shown bonds between W–N/O/I are primarily ionic, as evidenced by the presence of a nodal plane at the midpoint between the atomic centers.

The calculated electronic band structure of **1** (Figure S1) shows it to be a semiconductor with an indirect band gap of 1.9 eV, corresponding well with the experimental optical band gap of 2.17 eV. Note, the value derived from DFT is likely an underestimate, due to the well-known band gap problem.

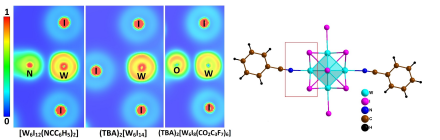

Figure 4. Electron localisation functions of **1**, $(TBA)_2[W_6I_{14}]$ and $(TBA)_2[W_6I_8(CO_2C_3F_7)_6]$ (from left to right) and an illustration of the observed area (right side).

Stability

The employment of a given material, like octahedral metal halide clusters in fields like oxygen sensing,[9b,21] photocatalysis[7,22] or solar cells[8b,23] requires long-term stability. Particularly three key aspects need to be avoided, namely thermal decomposition, oxidation in air, and hydrolysis. Therefore, one important property is thermal stability. Binary tungsten or molybdenum halides M_6X_{12} (X = Cl, Br, I) are stable at high temperatures.[1,24] This changes after outer halide ligands are substituted by organic ligands. Investigations into the thermal stability of **1** by thermogravimetric (TG) analysis under argon (Figure 5) shows the compound to be stable until 400 °C without any mass loss beforehand. Above 400 °C a mass loss of around 7% occurs, which corresponds to the mass of benzonitrile (7.3%). The remaining W_6I_{12} begins to decompose around 650 °C.

Stability up to 400 °C is previously unreported in any tungsten halide cluster bearing organic ligands. Related molybdenum cluster compounds have shown lower stabilities.[25] For example $(pyridineH)_{0.2}[Mo_6I_8(pyridine)_{1.8}I_{4.2}]$ was reported to show a gradual mass loss starting above 100 °C until 350 °C followed by a strong mass loss at 400 °C, corresponding to the formation of $[Mo_6I_{12}]$.[10b]

Aside from temperature, stability against hydrolysis is also a concern for octahedral metal halide clusters. Exposed to aqueous media the octahedral tungsten and molybdenum iodide cluster species tend to partially exchange apical ligands by hydroxyl groups.[5,11] With the goal of long-term stability and retention of the clusters photophysical properties this is disadvantageous. Therefore, it was interesting to see if the cluster can remain intact upon continuous contact with water. For that purpose, a small amount of **1** was dispersed into water for over a month. Afterwards the body color of the powder was unchanged, the PXRD pattern showed phase pure **1** (Figure S3), suggesting hydrolytic stability in aqueous media.

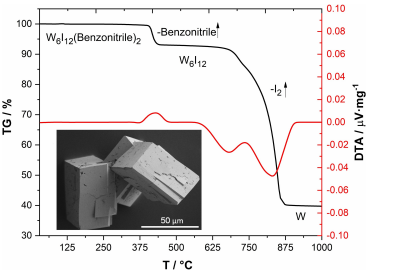

Figure 5. Thermal analysis of crystalline material of **1** (see inset of a SEM micrograph) under argon flow with the thermogravimetric (TG) curve displayed in black and the differential thermal analysis (DTA) curve in red.

Luminescence studies

In general, compounds containing $[M_6X_8L_6]^{2-}$ clusters (with M = Mo or W; X = Cl, Br, or I; L = Cl, Br, I or organic anions) are widely known for their strong red photoluminescence, long luminescence decay times, high quantum yields, and their quenching of the luminescence in the presence of molecular oxygen to produce singlet oxygen.[4,10a,12,19,26] Typically, these clusters are anionic species and only few examples exist for neutral or cationic species. Hence investigations concerning their luminescence are rare. However, it is assumed that $[Mo_6Cl_{12}(CH_3CN)_2]$ is an intermediate in the production of the oxygen sensor made from $[Mo_6Cl_{12}]$.[9] Recently, luminescence properties of the neutral molybdenum cluster species $(PyridineH)_{0.2}[Mo_6I_8(pyridine)_{1.8}I_{4.2}]$ were reported to show negligible photoluminescence in the solid-state.[10b]

Like other octahedral metal halide clusters, **1** shows a broad excitation band between 250 nm and 550 nm (18200 cm^{-1}) and a broad emission band peaking at around 630 nm (15900 cm^{-1}) with a FWHM of 3000 cm^{-1} (Figure 6). The photoluminescence emission is rather weak with a low quantum yield (0.4%) and short lifetimes of $\tau_1 = 0.48$ µs (29%) and $\tau_2 = 1.57$ µs (71%) (Figure S6). We attributed the short triplet lifetimes to a small energetic splitting between the emitting triplet sublevels with the highest lying sublevel possessing an allowed transition towards the ground state.[27] Low energetic splitting is explained to be a consequence of high d-electron density on the metal atoms.[27] The observed electron density in the ELF is comparable to the one of $(TBA)_2[W_6I_{14}]$ and far higher than for $(TBA)_2[W_6I_8(CO_2C_3F_7)_6]$ (Figure 4). Additionally, due to the observed dense packing of cluster units, very short decay times and low intensities can be expected. Due to the low distances between adjacent cluster units the efficiency of non-radiative energy transfer can be higher than for species featuring large cations and ligands.[15a,28]

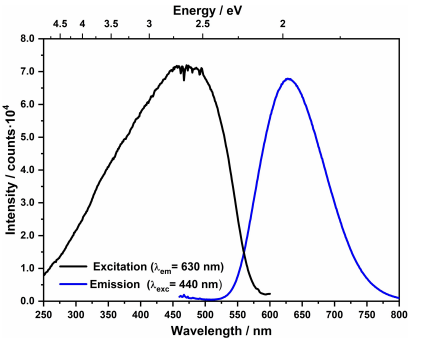

Figure 6. Excitation (black curve) and emission (blue curve) spectrum of crystalline **1** recorded at room temperature.

Photocatalysis

Purifying wastewater from persistent organic pollutants is an extensively investigated topic. Many studies deal with removing or breaking down organic pollutants for example, estrogen or triclosan.[29] Heterogenous photocatalysis is considered as a promising approach using TiO_2 or other semiconducting materials as catalysts. Upon irradiation with UV radiation or visible light these materials produce reactive oxygen species.[30] Ideally, the pollutant is completely broken down to CO_2 and H_2O. However, TiO_2 with a band gap of about 3.2 eV uses only a small portion of the solar light spectrum.[31] Octahedral metal halide clusters (metal = Mo, W) feature reported band gaps around 2 eV.[7d,10] Consequently, they can potentially be used for photocatalytic applications. It has been shown that some compounds are active in the photocatalytic decomposition of rhodamine B (RhB). For example, this is reported for $Na_2[Mo_6Br_8(N_3)_6]$,[7d] nanocomposites out of gold nanoparticles, graphene oxide and $Na_2[Mo_6Br_8(N_3)_6]$[7c] and $[Mo_6I_8(H_2O)_2(OH)_4]$ supported on h–BN.[10c] Different studies also showed the potential of these clusters in the photocatalytic water reduction.[22]

As has been mentioned, stability is a concern for molybdenum and tungsten halide clusters. From this perspective the durability of **1** in the presence of water or temperature is remarkable and make it a suitable candidate for photocatalytic applications. Thus, we attempted, in a proof of concept, to photocatalytically decompose RhB in water with **1** as a photocatalyst. During the experiment we used the decay of the absorption band of RhB at ca. 554 nm to monitor the decomposition of the dye against irradiation time. We recorded the changes during a time span of 180 min, while we stirred the suspension/solution in the dark for 30 min to establish an adsorption and desorption equilibrium and subsequent UV irradiation for 150 min. The control experiment, with a pure RhB solution showed less then 10% degradation after 150 min irradiation with UV radiation and otherwise identical conditions.

Figure 7a shows the recorded UV/Vis spectra of the RhB solution with **1** as photocatalyst during the experiment. The decreasing intensity of the rhodamine B absorption and the characteristic hypsochromic shift of the absorption maximum over time are clearly visible. This shift can be observed due to

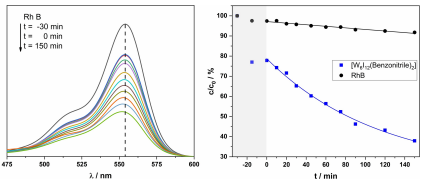

Figure 7. UV/Vis absorption spectra of the photocatalytic decomposition of RhB with **1** as catalyst starting from −30 min to 150 min irradiation time (left side). Time-dependent course of the RhB concentration during the photocatalysis experiment with and without **1** as photocatalyst.

the stepwise de-ethylation of the RhB-molecule. In Figure 7b the change of concentration is plotted in dependence of the irradiation time. After 30 min without irradiation, an equilibrium of desorption and adsorption of the dye on the particle surface of **1** is achieved. Around 22 % of the dye is adsorbed onto the particle surface. Over the 150 min of irradiation time a continuous decrease of the rhodamine B absorption is visible. Afterwards, more than 40 % of the dye have been decomposed.

Decomposition was also observed in an additional experiment using small screwcap vials filled with a suspension of 5 mg of **1** in 10 mL of the RhB solution (Figure S4). During the experiment the vials were placed in front of the window in the daylight (conducted during winter). After 2–3 days the solution was completely colorless, indicating complete decomposition of the RhB molecules. This was repeated for two times with similar results. The decomposition of RhB is reported to show three different stages of decomposition, with the first being formation of de-ethylated rhodamine B species, the second features different compounds resulting from a cleaved chromophore system and the third with complete cleavage into different aliphatic alcohols and carboxylic acids.[32] A cleavage of the chromophore structure is reported to be the dominant step. The decomposition can be attributed to the presence of multiple reactive oxygen species (ROS) involved in the decomposition of dyes in photocatalytic processes.[7d,30] The process may involve hydroxyl radicals (OH•), superoxide radicals ($O_2^{\bullet-}$) or singlet oxygen.

Conclusions

The new $[W_6I_{12}(NCC_6H_5)_2]$ is a remarkable compound because it demonstrates a number of important features in cluster chemistry. Due to the neutral charge of this species the crystal structure shows molecular clusters. Despite this molecular appearance, these clusters are densely packed and strongly interconnected via hydrogen bonding in the crystal. This bridging of adjacent clusters adds to the stability of the compound and allows decomposition temperatures above 400 °C.

Normally, ligand substituted tungsten or molybdenum halide clusters show low stability against water. However, $[W_6I_{12}(NCC_6H_5)_2]$ displays no sign of hydrolysis, even after being suspended into water for over a month. Thermal and hydrolytic stability and a narrow band gap of 2.17 eV allow for the compound to be used as a photocatalyst for excitation at wavelengths below 570 nm.

$[W_6I_{12}(NCC_6H_5)_2]$ successfully acts as a photocatalyst in the decomposition of rhodamine B in water. Repeated photocatalysis experiments using solar light demonstrate continuous activity without visible hydrolysis.

Experimental Section

All chemicals were used without further purification. Benzonitrile (99 %, extra pure) and WCl_6 (99.9 %+) were obtained from Acros Organics, diethylether from VWR chemicals (Chromanorm), SiI_4 (99 %) from ChemPur, CsI (99 %), ZnI_2 (99.999 %), acetone (99.8 %, Chromasolv) from SigmaAldrich, and I_2 (99.8 %) from AlfaAesar.

The preparation of the starting materials $Cs_2W_6I_{14}$[12c] or W_6I_{22}[33] is reported elsewhere.

A reaction mixture of 100.0 mg $Cs_2W_6I_{14}$ (31.8 μmol), 10.1 mg ZnI_2 (31.8 μmol) and 0.8 mL benzonitrile (7.76 mmol) was fused together into a homemade silica ampoule with 70 mm length and 10 mm inner diameter. The ampoule was placed upright in an oven and heated to 200 °C with 2 °C/min and kept at the temperature for 3 d. Afterwards the reaction was cooled to RT with 0.5 °C/min. After removing the solvent and rinsing with diethylether and acetone each three times, the product remained as red, cube-shaped crystals (yield: 65 mg, 22.95 μmol, 72.2 %). Elemental analysis: 0.951 N, 5.848 C, 0.325 H; calculated: 0.989 N, 5.937, 0.356 H. EDX: W/I ratio 1 : 2. IR: 548 (C═C), 675 (C═C), 756 (C–H), 1440 (C═C), 1589 (C═C), 1629 (C═C), 2245 (C ≡ N).[34]

The parent reaction departing from W_6I_{22} (without ZnI_2) was carried out analogous to the described synthesis.

Thermoanalysis. Differential thermal analysis (DTA) was performed with a STA 449F3 Jupiter apparatus (Netzsch, Selb, Germany). Samples were filled into corundum containers and analyzed between room temperature and 1000 °C with a heating and cooling rate of 2 °C/min under argon stream.

Single-crystal X-ray Diffraction. The single-crystal X-ray diffraction (XRD) study on $[W_6I_{12}(NCC_6H_5)_2]$ was performed using a Rigaku XtaLab Synergy-S diffractometer with Mo–K_α radiation (λ = 0.71073 Å) and a mirror monochromator. A cube-shaped single-crystal was used for the measurement under N_2 cooling at 100 K. Corrections for absorption effects were applied with CrysAlisPro 1.171.41.65a (Rigaku Oxford Diffraction, 2020). The structure was solved by direct methods (SHELXS),[35] and full-matrix least-squares structure refinements were performed with SHELXL-2014[36] implemented in Olex2 1.3-ac4.

Deposition Number 2084368 (for **1**) contains the supplementary crystallographic data for this paper. These data are provided free of charge by the joint Cambridge Crystallographic Data Centre and Fachinformationszentrum Karlsruhe Access Structures service.

Powder X-ray diffraction (PXRD). PXRD experiments were carried out with a powder diffractometer (STOE Darmstadt, STADI-P, Ge-monochromator) using Cu–$K_{\alpha1}$ (λ = 1.540598 Å) radiation in the range of $3 < 2\theta < 70°$. The purity of $[W_6I_{12}(NCC_6H_5)_2]$ was checked and confirmed as single-phase, according to the PXRD pattern.

Luminescence. Excitation and emission spectra of $[W_6I_{12}(NCC_6H_5)_2]$ were recorded by using a fluorescence spectrometer FLS920 (Edinburgh Instruments) equipped with a 450 W xenon discharge lamp (OSRAM). Additionally, a mirror optic for powder samples was mounted inside the sample chamber. For detection, an R2658P single-photon-counting photomultiplier tube (Hamamatsu) was used. All photoluminescence spectra were recorded with a spectral resolution of 1 nm, a dwell time of 0.5 s in 1 nm steps and 2 repeats. The photoluminescence decay curve was measured with the same spectrometer using a 445 nm picosecond laser.

Photocatalysis. The photocatalysis experiments were carried out with a standard UV radiation with a wavelength of 395 nm (5 W). 40 mL of a 40 μmol/l solution of rhodamine B dissolved in distilled water was transferred into a beaker and 20 mg of $[W_6I_{12}(NCC_6H_5)_2]$ powder was added. After −30, −15, 0, 10, 20, 30, 45, 60, 75, 90, 120 and 150 min of irradiation time a sample of 3 mL was centrifuged, transferred into a glass cuvette and UV/Vis spectra were recorded in the range between 200 nm and 800 nm. For recording the

spectra, a Cary 60 UV–Vis spectrophotometer from Agilent was used. Photocatalysis experiments with solar light were carried out by dispersing 5 mg of **1** in 10 mL of the rhodamine B solution in a screwcap vial placed in front of the window.

UV–Vis in diffuse reflectance. For recording the spectra a Maya 2000 Pro spectrometer from OceanOptics equipped with a praying mantis sample chamber from Harrick and a DH-2000-BAL (Deuterium-Tungsten-Lamp) as a light source from OceanOptics. As a software OceanView 1.6.7 (lite) from OceanOptics was used with following settings: scans to average = 10, boxcarwidth = 5 and integration time = 115 ms. The band gap E_g of **1** was calculated using following equation $(\alpha h\nu)^{1/n} = A \cdot (h\nu - E_g)$, where α is the absorption coefficient, h is the Planck constant, A is a material related constant and $h\nu$ is the photon energy. For an indirect band gap n = 2.

DFT. Density functional theory (DFT) was used to calculate the ELF of **1** and $(TBA)_2[W_6I_{14}]$, using the Abinit software package.[37] Calculations were performed using a 36 Ha plane-wave basis set energy cutoff and 4×4×4 (**1**), and 2×2×1 $(TBA)_2[W_6I_{14}]$ Monkhorst–Pack grids[38] of k points. Norm-conserving pseudopotentials were used as received from the Abinit library. Example input files are available as part of the Supporting Information.

Elemental analyses. Elemental Analyses (C, H, N) was obtained using a UNICUBE apparatus from ELEMENTAR.

EDX Measurement. The EDX spectroscopy data was collected using a Hitachi SU8030 scanning electron microscope equipped with a Bruker QUANTAX 6G EDX detector.

Electron Microscopy. Scanning electron microscopy (SEM) was carried out on a Hitachi SU8030 scanning electron microscope equipped with a Bruker QUANTAX 6G EDX detector.

The authors declare no competing financial interest.

Acknowledgements

This work was supported by the Deutsche Forschungsgemeinschaft (DFG) via funding ME 914/31-1. CPR was supported by ETH Zurich and by the European Union and Horizon 2020 through a Marie Sklodowska-Curie Fellowship, Grant Agreement No. 101030352. The authors would like to thank Peter Janoschek for the UV/Vis measurement in diffuse reflection, Fabian Grahlow for his contribution to the TOC graphic, Marcus Scheele for the opportunity to use the Cary 60 UV/Vis spectrophotometer, Philipp Frech for his instructions on using this device and Elke Nadler for recording the SEM images and EDX data. Computational resources were provided by ETH Zurich. Open Access funding enabled and organized by Projekt DEAL.

Conflict of Interests

The authors declare no conflict of interest.

Data Availability Statement

The data that support the findings of this study are available from the corresponding author upon reasonable request.

Keywords: Cluster compounds · Crystal structure · Electronic structure · Photocatalytic decomposition · Thermal analysis · Tungsten

[1] H. Schäfer, H. G. von Schnering, J. Tillack, F. Kuhnen, H. Wöhrle, H. Baumann, *Z. Anorg. Allg. Chem.* **1967**, *353*, 281–310.
[2] H. Schäfer, R. Siepmann, *Z. Anorg. Allg. Chem.* **1968**, *357*, 273–288.
[3] a) A. W. Maverick, H. B. Gray, *J. Am. Chem. Soc.* **1981**, *103*, 1298–1300; b) T. C. Zietlow, M. D. Hopkins, H. B. Gray, *J. Solid State Chem.* **1985**, *57*, 112–119.
[4] J. A. Jackson, C. Turro, M. D. Newsham, D. G. Nocera, *J. Phys. Chem.* **1990**, *94*, 4500–4507.
[5] E. V. Svezhentseva, Y. A. Vorotnikov, A. O. Solovieva, T. N. Pozmogova, I. V. Eltsov, A. A. Ivanov, D. V. Evtushok, S. M. Miroshnichenko, V. V. Yanshole, C. J. Eling, A. M. Adawi, J. S. G. Bouillard, N. V. Kuratieva, M. S. Fufaeva, L. V. Shestopalova, Y. V. Mironov, O. A. Efremova, M. A. Shestopalov, *Chem. Eur. J.* **2018**, *24*, 17915–17920.
[6] T. Hummel, D. Dutczak, A. Y. Alekseev, L. S. Adamenko, A. M. Shestopalov, Y. V. Mironov, D. Enseling, T. Jüstel, H.-J. Meyer, *RSC Adv.* **2020**, *10*, 22257–22263.
[7] a) M. Feliz, M. Puche, P. Atienzar, P. Concepción, S. Cordier, Y. Molard, *ChemSusChem* **2016**, *9*, 1963–1971; b) P. Kumar, S. Kumar, S. Cordier, S. Paofai, R. Boukherroub, S. L. Jain, *RSC Adv.* **2014**, *4*, 10420–10423; c) A. Barras, M. R. Das, R. R. Devarapalli, M. V. Shelke, S. Cordier, S. Szunerits, R. Boukherroub, *Appl. Catal. B* **2013**, *130 (131)*, 270–276; d) A. Barras, S. Cordier, R. Boukherroub, *Appl. Catal. B* **2012**, *123*, 1–8.
[8] a) A. M. Steiner, F. Lissel, A. Fery, J. Lauth, M. Scheele, *Angew. Chem. Int. Ed.* **2021**, *60*, 1152–1175; *Angew. Chem.* **2021**, *133*, 1168–1194; b) A. Renaud, F. Grasset, B. Dierre, T. Uchikoshi, N. Ohashi, T. Takei, A. Planchat, L. Cario, S. Jobic, F. Odobel, S. Cordier, *ChemistrySelect* **2016**, *1*, 2284–2289.
[9] a) D. J. Osborn, G. L. Baker, R. N. Ghosh, *J. Sol-Gel Sci. Technol.* **2005**, *36*, 5–10; b) R. N. Ghosh, G. L. Baker, C. Ruud, D. G. Nocera, *Appl. Phys. Lett.* **1999**, *75*, 2885–2887.
[10] a) A. Seyboldt, D. Enseling, T. Jüstel, M. Ivanovic, H. Peisert, T. Chassé, H.-J. Meyer, *Eur. J. Inorg. Chem.* **2017**, *2017*, 5387–5394; b) M. V. Marchuk, Y. A. Vorotnikov, A. A. Ivanov, I. V. Eltsov, N. V. Kuratieva, M. A. Shestopalov, *Symmetry* **2022**, *14*, 2117; c) M. N. Ivanova, Y. A. Vorotnikov, E. E. Plotnikova, M. V. Marchuk, A. A. Ivanov, I. P. Asanov, A. R. Tsygankova, E. D. Grayfer, V. E. Fedorov, M. A. Shestopalov, *Inorg. Chem.* **2020**, *59*, 6439–6448.
[11] a) A. M. Cheplakova, A. O. Solovieva, T. N. Pozmogova, Y. A. Vorotnikov, K. A. Brylev, N. A. Vorotnikova, E. V. Vorontsova, Y. V. Mironov, A. F. Poveshchenko, K. A. Kovalenko, M. A. Shestopalov, *J. Inorg. Biochem.* **2017**, *166*, 100–107; b) K. Kirakci, P. Kubat, M. Kucerakova, V. Sicha, H. Gbelcova, P. Lovecka, P. Grznarova, T. Ruml, K. Lang, *Inorg. Chim. Acta.* **2016**, *441*, 42–49; c) Y. A. Vorotnikov, O. A. Efremova, I. N. Novozhilov, V. V. Yanshole, N. V. Kuratieva, K. A. Brylev, N. Kitamura, Y. V. Mironov, M. A. Shestopalov, *J. Mol. Struct.* **2017**, *1134*, 237–243.
[12] a) K. Kirakci, P. Kubat, M. Dusek, K. Fejfarova, V. Sicha, J. Mosinger, K. Lang, *Eur. J. Inorg. Chem.* **2012**, *2012*, 3107–3111; b) O. A. Efremova, Y. A. Vorotnikov, K. A. Brylev, N. A. Vorotnikova, I. N. Novozhilov, N. V. Kuratieva, M. V. Edeleva, D. M. Benoit, N. Kitamura, Y. V. Mironov, M. A. Shestopalov, A. J. Sutherland, *Dalton Trans.* **2016**, *45*, 15427–15435; c) L. Riehl, A. Seyboldt, M. Ströbele, D. Enseling, T. Jüstel, M. Westberg, P. R. Ogilby, H.-J. Meyer, *Dalton Trans.* **2016**, *45*, 15500–15506.
[13] T. Hummel, M. Ströbele, A. D. Fuhrmann, D. Enseling, T. Jüstel, H.-J. Meyer, *Eur. J. Inorg. Chem.* **2019**, *2019*, 4014–4019.
[14] a) F. A. Cotton, N. F. Curtis, *Inorg. Chem.* **1965**, *4*, 241–244; b) W. M. Carmichael, D. A. Edwards, *J. Inorg. Nucl. Chem.* **1967**, *29*, 1535–1538; c) J. E. Fergusson, B. H. Robinson, C. J. Wilkins, *J. Chem. Soc. A* **1967**, 486–490.
[15] a) M. V. Marchuk, N. A. Vorotnikova, Y. A. Vorotnikov, N. V. Kuratieva, D. V. Stass, M. A. Shestopalov, *Dalton Trans.* **2021**, *50*, 8794–8802; b) F. Pachel, J. Händel, M. Ströbele, H.-J. Meyer, *Eur. J. Inorg. Chem.* **2020**, *2020*, 3987–3990; c) G. M. Ehrlich, C. J. Warren, R. C. Haushalter, F. J. DiSalvo, *Inorg. Chem.* **1995**, *34*, 4284–4286.
[16] T. Hummel, A. Mos-Hummel, A. Merkulova, M. Ströbele, A. Krishnamurthy, S. Kroeker, H.-J. Meyer, *Inorg. Chem.* **2018**, *57*, 2570–2576.
[17] A.-D. Fuhrmann, F. Pachel, M. Ströbele, D. Enseling, T. Jüstel, H.-J. Meyer, *Z. Anorg. Allg. Chem.* **2020**, *646*, 1650–1654.

[18] a) C. L. D. Gibb, E. D. Stevens, B. C. Gibb, *J. Am. Chem. Soc.* **2001**, *123*, 5849–5850; b) L. Garzón-Tovar, Á. Duarte-Ruiz, K. Wurst, *Inorg. Chem. Commun.* **2013**, *32*, 64–67.
[19] M. N. Sokolov, K. A. Brylev, P. A. Abramov, M. R. Gallyamov, I. N. Novozhilov, N. Kitamura, M. A. Mikhaylov, *Eur. J. Inorg. Chem.* **2017**, *2017*, 4131–4137.
[20] A. Savin, R. Nesper, S. Wengert, T. F. Fässler, *Angew. Chem. Int. Ed. Engl.* **1997**, *36*, 1808–1832.
[21] P. Zhang, D. J. Osborn, G. L. Baker, R. N. Ghosh, *IEEE Sens. 2005, 4th* **2005**, *1 (2)*, 628–631.
[22] a) M. Puche, R. García-Aboal, M. A. Mikhaylov, M. N. Sokolov, P. Atienzar, M. Feliz, *Nanomaterials* **2020**, *10*, 1259; b) M. Feliz, P. Atienzar, M. Amela-Cortés, N. Dumait, P. Lemoine, Y. Molard, S. Cordier, *Inorg. Chem.* **2019**, *58*, 15443–15454; c) M. Feliz, M. Puche, P. Atienzar, P. Concepcion, S. Cordier, Y. Molard, *ChemSusChem* **2016**, *9*, 1963–1971.
[23] A. Renaud, P.-Y. Jouan, N. Dumait, S. Ababou-Girard, N. Barreau, T. Uchikoshi, F. Grasset, S. Jobic, S. Cordier, *ACS Appl. Mater. Interfaces* **2022**, *14*, 1347–1354.
[24] a) M. Ströbele, H.-J. Meyer, *Dalton Trans.* **2019**, *48*, 1547–1561; b) H. Schäfer, H. G. Schulz, *Z. Anorg. Allg. Chem.* **1984**, *516*, 196–200.
[25] J. Kraft, H. Schäfer, *Z. Anorg. Allg. Chem.* **1985**, *524*, 137–143.
[26] M. A. Mikhailov, K. A. Brylev, P. A. Abramov, E. Sakuda, S. Akagi, A. Ito, N. Kitamura, M. N. Sokolov, *Inorg. Chem.* **2016**, *55*, 8437–8445.
[27] S. Akagi, S. Fujii, N. Kitamura, *J. Phys. Chem. A* **2018**, *122*, 9014–9024.
[28] a) N. Kitamura, Y. Kuwahara, Y. Ueda, Y. Ito, S. Ishizaka, Y. Sasaki, K. Tsuge, S. Akagi, *Bull. Chem. Soc. Jpn.* **2017**, *90*, 1164–1173; b) K. Costuas, A. Garreau, A. Bulou, B. Fontaine, J. Cuny, R. Gautier, M. Mortier, Y. Molard, J. L. Duvail, E. Faulques, S. Cordier, *Phys. Chem. Chem. Phys.* **2015**, *17*, 28574–28585.
[29] a) W. Zhang, Y. Li, Q. Wu, H. Hongying, *Environ. Eng. Sci.* **2012**, *29*, 195–201; b) H. S. Kushwaha, G. Parmesh, R. Vaish, K. B. R. Varma, *J. Non-Cryst. Solids* **2015**, *408*, 13–17; c) M. J. Arlos, R. Liang, M. M. Hatat-Fraile, L. M. Bragg, N. Y. Zhou, M. R. Servos, S. A. Andrews, *J. Hazard. Mater.* **2016**, *318*, 541–550; d) I. Köwitsch, M. Mehring, *J. Mater. Sci.* **2021**, *56*, 18608–18624; e) J. Zhang, D. Li, J. Qiu, Z. Wen, X. Luo, C. Bian, J. Chen, M. Luo, *Mater. Res. Express* **2020**, *7*, 115502.
[30] M. Pelaez, N. T. Nolan, S. C. Pillai, M. K. Seery, P. Falaras, A. G. Kontos, P. S. M. Dunlop, J. W. J. Hamilton, J. A. Byrne, K. O'Shea, M. H. Entezari, D. D. Dionysiou, *Appl. Catal. B* **2012**, *125*, 331–349.
[31] W. F. Yao, H. Wang, X. H. Xu, J. T. Zhou, X. N. Yang, Y. Zhang, S. X. Shang, M. Wang, *Chem. Phys. Lett.* **2003**, *377*, 501–506.
[32] K. Yu, S. Yang, H. He, C. Sun, C. Gu, Y. Ju, *J. Phys. Chem. A* **2009**, *113*, 10024–10032.
[33] M. Ströbele, H.-J. Meyer, *Inorg. Chem.* **2019**, *58*, 12867–12872.
[34] R. E. Clarke, P. C. Ford, *Inorg. Chem.* **1970**, *9*, 227–235.
[35] G. Sheldrick, *Acta Crystallogr. Sect. A* **2015**, *71*, 3–8.
[36] C. B. Huebschle, G. M. Sheldrick, B. Dittrich, *J. Appl. Crystallogr.* **2011**, *44*, 1281–1284.
[37] X. Gonze, B. Amadon, G. Antonius, F. Arnardi, L. Baguet, J.-M. Beuken, J. Bieder, F. Bottin, J. Bouchet, E. Bousquet, N. Brouwer, F. Bruneval, G. Brunin, T. Cavignac, J.-B. Charraud, W. Chen, M. Côté, S. Cottenier, J. Denier, G. Geneste, P. Ghosez, M. Giantomassi, Y. Gillet, O. Gingras, D. R. Hamann, G. Hautier, X. He, N. Helbig, N. Holzwarth, Y. Jia, F. Jollet, W. Lafargue-Dit-Hauret, K. Lejaeghere, M. A. L. Marques, A. Martin, C. Martins, H. P. C. Miranda, F. Naccarato, K. Persson, G. Petretto, V. Planes, Y. Pouillon, S. Prokhorenko, F. Ricci, G.-M. Rignanese, A. H. Romero, M. M. Schmitt, M. Torrent, M. J. van Setten, B. Van Troeye, M. J. Verstraete, G. Zérah, J. W. Zwanziger, *Comput. Phys. Commun.* **2020**, *248*, 107042.
[38] H. J. Monkhorst, J. D. Pack, *Phys. Rev. B* **1976**, *13*, 5188–5192.

Manuscript received: February 22, 2023
Revised manuscript received: April 17, 2023
Accepted manuscript online: April 18, 2023

European Journal of Inorganic Chemistry

Supporting Information

The Remarkably Robust, Photoactive Tungsten Iodide Cluster $[W_6I_{12}(NCC_6H_5)_2]$

Florian Pachel, Markus Ströbele, Carl P. Romao, David Enseling, Thomas Jüstel, and Hans-Jürgen Meyer*

Index

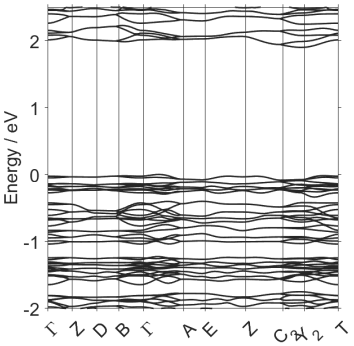

Figure S1. The calculated electronic band structure of $[W_6I_{12}(NCC_6H_5)_2]$.

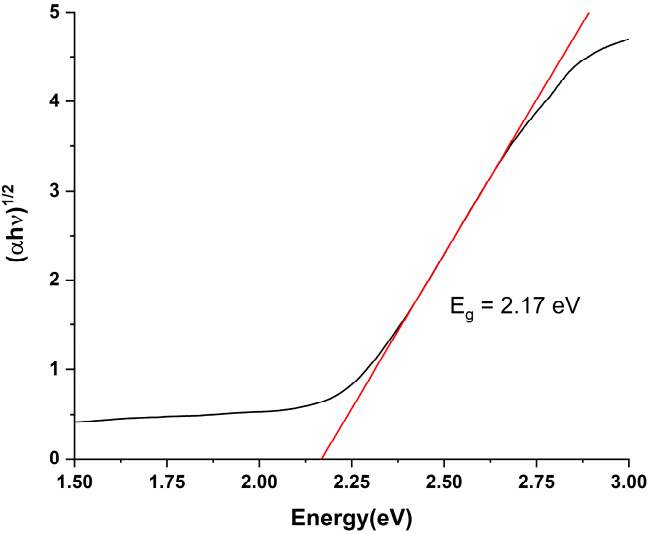

Figure S2. Tauc plot of a UV-Vis reflectance measurement of $[W_6I_{12}(NCC_6H_5)_2]$ indicating a indirect band gap of 2.17 eV. α corresponds to the absorption coefficient, h is the Planck´s constant and v is the frequency.

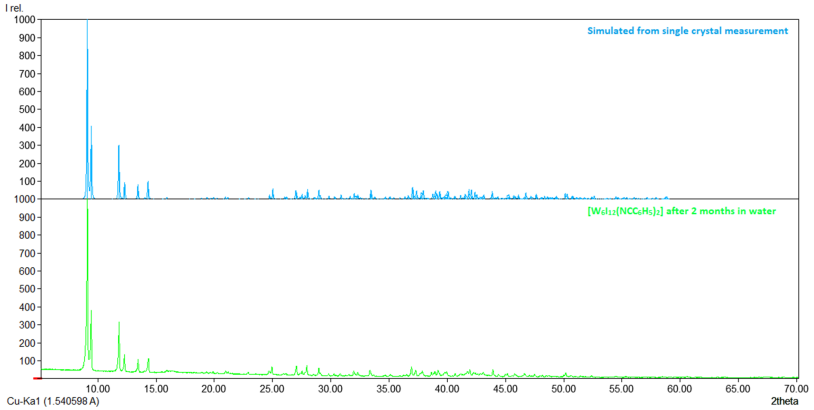

Figure S3. Powder pattern of $[W_6I_{12}(NCC_6H_5)_2]$ simulated from single crystal measurement (blue, top) and powder pattern of the compound after two months storage in water (green, bottom).

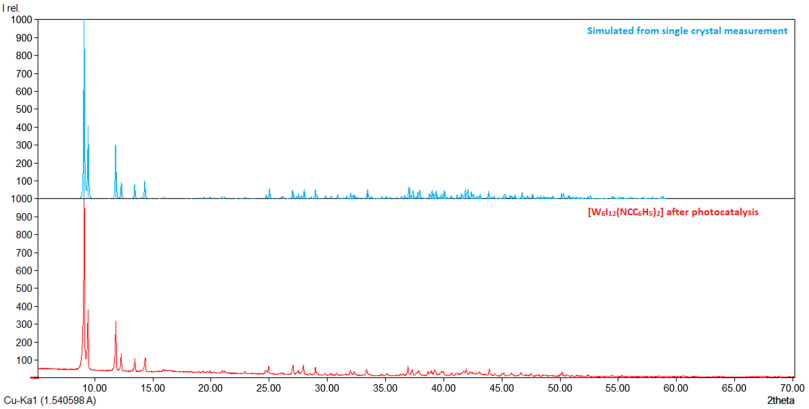

Figure S4. Powder pattern of $[W_6I_{12}(NCC_6H_5)_2]$ simulated from single crystal measurement (blue, top) and powder pattern of the compound after photocatalysis (red, bottom).

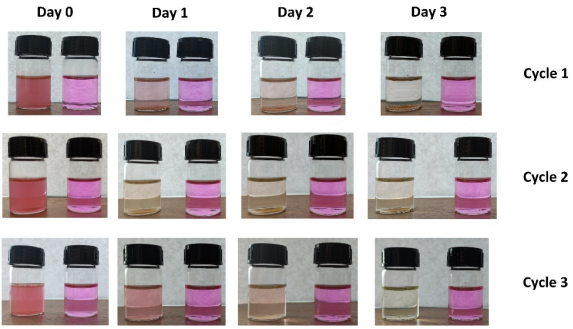

Figure S5. Photocatalysis experiments carried out in the sunlight. 5 mg of $[W_6I_{12}(NCC_6H_5)_2]$ were dispersed in 10 ml of Rhodamine B solution (right side) and placed in front of the window. Additionally, pure Rhodamine B solution was also kept under the same condition as a standard (left side). After three days the solution was clear and the experiment was repeated two times with the same result. The resulting solution showed green fluorescence upon irradiation with UV light (bottom), while the powder of the cluster species kept it´s orange phosphorescence.

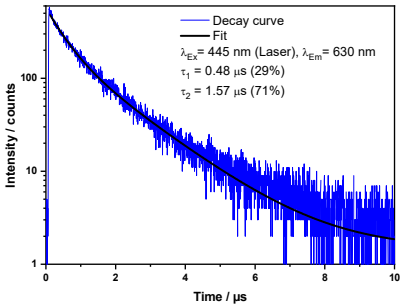

Figure 6. Decay curve with a biexponential fit of $[W_6I_{12}(NCC_6H_5)_2]$ under 445 nm excitation (emission monitored at 630 nm).

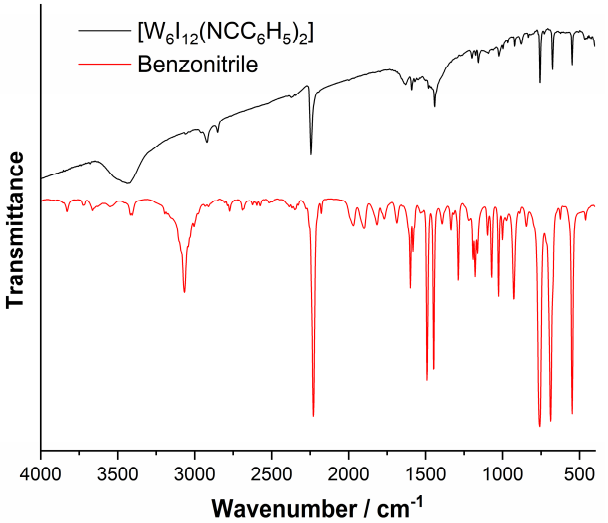

Figure S7. Recorded FTIR spectra of $[W_6I_{12}(NCC_6H_5)_2]$ (black) and benzonitrile (red).

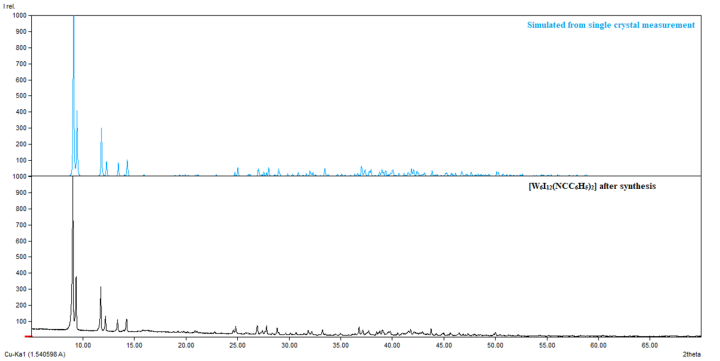

Figure S8. Powder pattern of $[W_6I_{12}(NCC_6H_5)_2]$ simulated from single crystal measurement (blue, top) and powder pattern of the freshly synthesized compound (black, bottom).

Publication 4

Synthesis, Crystal Structure, and Luminescence of Metal Iodide Cluster Compounds $(^{n}Bu_4N)_2[M_6I_8(NCO)_6]$ with M = Mo, W

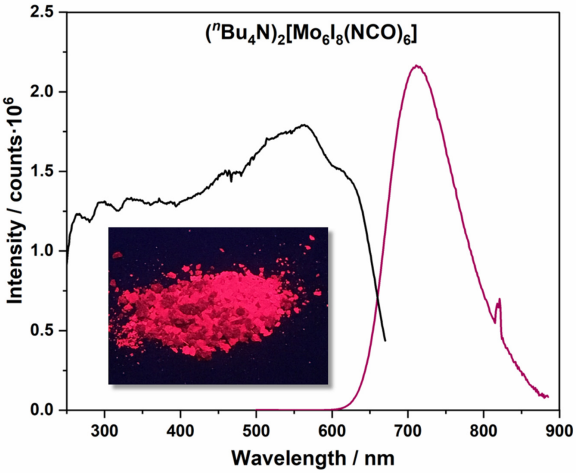

https://doi.org/ 10.1002/zaac.202000209

Reprinted with permission from

Z. Anorg. Allg. Chem. ***2020****, 646, 1650–1654*

Journal of Inorganic and General Chemistry
ZAAC
Zeitschrift für anorganische und allgemeine Chemie
DOI: 10.1002/zaac.202000209
ARTICLE

Synthesis, Crystal Structure, and Luminescence of Metal Iodide Cluster Compounds $(^nBu_4N)_2[M_6I_8(NCO)_6]$ with M = Mo, W

Arin-Daniel Fuhrmann,[a] Florian Pachel,[a] Markus Ströbele,[a] David Enseling,[b] Thomas Jüstel,[b] and Hans-Jürgen Meyer*[a]

Abstract. Molybdenum and tungsten iodide clusters with the $[M_6I_8]$ cluster core show versatile photophysical properties that strongly depend on the nature of six apical ligands (L) in $[M_6I_8L_6]^{2-}$. In course of our syntheses we report a new efficient preparation of $Cs_2[Mo_6I_{14}]$ as precursor. Target compounds $(^nBu_4N)_2[M_6I_8(NCO)_6]$ with M = Mo, W with cyanate ligands were synthesized and structurally characterized to study their photophysical properties. $(^nBu_4N)_2[M_6I_8(NCO)_6]$ compounds appear as deep red (Mo) and light yellow (W) crystal powders showing strong phosphorescence. Compared to other cluster compounds of this type there is no significant concentration quenching obtained by the presence of molecular oxygen.

Introduction

Hexanuclear metal halide clusters derived from Mo_6I_{12} and W_6I_{12} are based on the remarkable robust octahedral $[M_6I_8]$ cluster core and six apical iodine atoms. Various cluster compounds with the $[M_6I_8]$ core have been prepared as crystalline powders, which can be dissolved into polar organic solvents as $[M_6I_{14}]^{2-}$, or $[M_6I_8L_6]^{2-}$ with L being terminal ligands, making these compounds or ions of interest for optical studies in solid state and solution.[1]

The occupied metal–metal bonding states of $[M_6I_8I_6]^{2-}$ molybdenum and tungsten clusters contain 24 electrons in cluster based molecular orbitals including the HOMO. Their bandgaps have been determined to be in the order of 2–3 eV.[2]

Photoexcitation in the UV/Vis range (typically between 250 and 450 nm) result in a deep red phosphorescence in solid state and in solution.[1c,1r,3]

The nature of apical cluster ligands (L) have shown to strongly influence the photophysical properties of $[M_6I_8L_6]^{2-}$. Extensive investigations in this field have led to the development of various compounds with mostly organic, electron withdrawing ligands, with maximum luminescence quantum yields up to unity.[3b] Another remarkable feature of compounds is the ability to generate singlet oxygen, if an energy exchange between cluster triplet states and molecular oxygen is possible to occur.[1n,1r] To this end, various ligands (L) were explored with respect to their influence on the photophysical properties of $[M_6I_8L_6]^{2-}$ in solid state and in solution.

Herein we describe the preparation, crystal structure and solid-state luminescence of purely inorganic cluster anions in $(^nBu_4N)_2[M_6I_8(NCO)_6]$ with M = Mo, W.

Results and Discussion

Preparations of cluster compounds of the general formula $A_2[M_6I_8L_6]$ with A being an organic cation, M = Mo, W, and L being a monovalent anion have been successfully performed as described elsewhere.[1a] The corresponding reaction sequence usually involves the preparation of (insoluble) $Cs_2[M_6I_{14}]$ followed by cation exchange to obtain (soluble) $(^nBu_4N)_2[M_6I_{14}]$ to finally exchange six terminal iodido ligands of the cluster by a reaction with Ag(NCO) in solution. The products, $(^nBu_4N)_2[M_6I_8(NCO)_6]$ with M = Mo, W were obtained as bright colored crystal powders.

A challenge is the preparation of the binary MoI_2 as starting material, that is either obtained from the elements reacted in a silica tube (typically at 700 °C, 7 d) under a latent critically high iodine pressure on heating, or via a halide exchange from $MoCl_5$ and SiI_4.[4] It has to be noted that the latter reaction yields MoI_3 which first has to be transferred to MoI_2. As MoI_2 is afterwards converged into $Cs_2[Mo_6I_{14}]$ with CsI (700 °C, 4 d) we aimed to combine both reactions into one, in which the moderate melting point of CsI (626 °C) could be beneficial for the reaction. Hence, CsI, Mo, and I were combined in stoichiometric proportions (for $Cs_2[Mo_6I_{14}]$) and reacted at 700 °C for 72 h (in which one compartment of the reaction tube was initially kept near the outside area of the tube furnace to control the I_2 pressure). $Cs_2[Mo_6I_{14}]$ obtained from this reaction appeared in high yield (> 95%) and involves immense time savings and safer handling.

Crystal structures of $(^nBu_4N)_2[M_6I_8(NCO)_6]$ with M = Mo, W were refined on basis of single-crystal data obtained from X-ray single-crystal diffraction. The structure is isotypic to the

* Prof. Dr. H.-J. Meyer
E-Mail: juergen.meyer@uni-tuebingen.de
[a] Section for Solid State and Theoretical Inorganic Chemistry
Institute of Inorganic Chemistry
University of Tübingen
Auf der Morgenstelle 18
72076 Tübingen, Germany
[b] Department of Chemical Engineering
Münster University of Applied Sciences
Stegerwaldstraße 39
48565 Steinfurt, Germany
Supporting information for this article is available on the WWW under **http://dx.doi.org/10.1002/zaac.202000209** or from the author.

Journal of Inorganic and General Chemistry
ZAAC
Zeitschrift für anorganische und allgemeine Chemie

already reported structure of $(^nBu_4N)_2[Mo_6X_8(NCO)_6]$ with X = Cl, Br and consists of the cation $(^nBu_4N)^+$ and the anionic building block $[M_6I_8(NCO)_6]^{2-}$ in a 2 : 1 ratio (Tables S1 and S2, Supporting Information).[5] The cluster core is located at the cell edges while the center of gravity of the cation is located in a strongly distorted tetrahedral environment which could be expected for this cluster type (Figure 1).

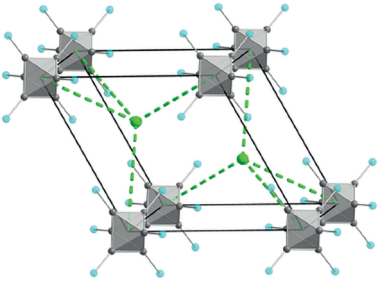

Figure 1. Unit cell arrangement for the structure of $(^nBu_4N)_2[Mo_6I_8(NCO)_6]$ emphasizing the tetrahedral environment of $^nBu_4N$ cations. Grey atoms represent Mo or W, light blue represent NCO^- ligands, and green atoms mark the centres of gravity of nBu$_4$N cations. Inner iodido ligands are omitted for clarity.

The most important feature of crystal structures with M = Mo and W is the characteristic $[M_6I_8(NCO)_6]^{2-}$ ion, resembling the octahedral metal cluster with eight face-capping iodido and six apical isocyanato ligands (Figure 2). The cyanate ion is an ambidentate ligand that acts as a base in aqueous media, forming isocyanic acid (HNCO). Although the vast majority of compounds with the $[M_6I_8L_6]^{2-}$ cluster contain terminal ligands connected via oxygen, this is not the case here. Corresponding compounds $(^nBu_4N)_2[Mo_6X_8(NCO)_6]$ with X = Cl, Br and $(^nBu_4N)_2[W_6Cl_8(NCO)_6]$ were already reported by *Simsek* et al. and analyzed for their spectroscopic properties.[5,6] Crystal structure refinements revealed Mo–N distances of 204.4–217.7 pm, similar to corresponding distances in hexaazido clusters (209.0–215.3 pm).[7] These findings agree with the nitrogen atom of the cyanate ion coordinating the cluster with M–N distances of 212.1–213.8 pm (M = Mo) and 216–218 pm (M = W) in $[M_6I_8(NCO)_6]^{2-}$ clusters (Table 1). Corresponding results are given in theoretical studies on reported and perspective $[Mo_6X_8(NCS)_6]$ compounds (X = Cl, Br, I).[8]

Infrared spectra of $(^nBu_4N)_2[M_6I_8(NCO)_6]$ compounds show intrinsic vibrations of cyanato ligands in the expected regions. The N–C valance vibrations are found at 2210 cm^{-1} (M = W) and 2200 (M = Mo) those of C–O at 1379 cm^{-1} and 1344 cm^{-1} (M = W), and 1338 and 1379 cm^{-1} (M = Mo). Deformation vibrations appear at 605 cm^{-1} (M = W) and 604 cm^{-1} (M = Mo).

The bright body color that is evident for the crystalline powders of $(^nBu_4N)_2[M_6I_8(NCO)_6]$ with M = Mo, W, and the strong phosphorescence obtained under UV irradiation (Figure 3) indicate some promising properties that are investigated in some detail by photoluminescence spectroscopy.

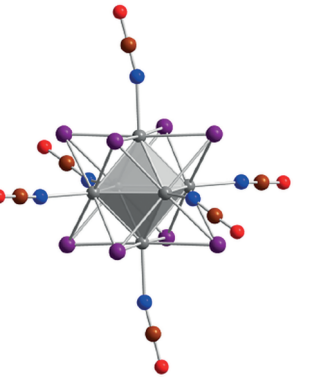

Figure 2. The $[Mo_6X_8(NCO)_6]^{2-}$ cluster from the crystal structure of $(^nBu_4N)_2[Mo_6X_8(NCO)_6]$. Grey atoms represent molybdenum atoms, blue nitrogen, brown carbon, red oxygen, and violet iodine.

Table 1. Selected average interatomic distances /Å in $[M_6I_8(NCO)_6]^{2-}$ with M = Mo, W.

	Mo	W
M–M	2.6726(4)	2.6690(7)
M–I	2.7971(4)	2.810(4)
M–N	2.131(3)	2.17(1)
N–C	1.162(5)	1.06(2)
C–O	1.203(5)	1.25(2)

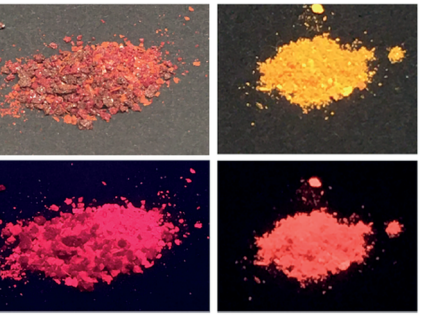

Figure 3. Red (Mo) and bright yellow (W) crystal powders of $(^nBu_4N)_2[M_6X_8(NCO)_6]$ under daylight (top) and under UV irradiation (bottom, 366 nm).

Photoluminescence Studies

Clusters with the $[M_6I_8L_6]^{2-}$ anion have been shown to exhibit various luminescence (respectively phosphorescence) properties.[1a] Most of them show luminescence quenching in the

presence of molecular oxygen, due to an energy transfer from excited cluster triplet states to the triplet state of oxygen.[1r,9] There are few examples reported on related pseudo halide cluster compounds that have been studied for their photophysical properties. These include water-soluble compounds $Na_2[Mo_6I_8(N_3)_6]$,[1j] $Na_2[Mo_6I_8(NCS)_6]$,[1j] $(^nBu_4N)_2[Mo_6X_8(N_3)_6]$[10] and $Na_2[Mo_6Br_8(N_3)_6]$[11] that, however, gradually hydrolyze into hydroxido derivatives. The latter compound has been verified for its photocatalytic activity, due to the generation of a hole in the valence band subsequent to visible light excitation and an electron/hole charge separation allowing for a photo catalytic surface process to degrade rhodamine B.[11] Another attempt explored the formation of singlet oxygen in aqueous solution to serve as luminescent probe or singlet oxygen sensitizer in living cells.[12]

Photoluminescence spectra of solid samples of $(^nBu_4N)_2[M_6I_8(NCO)_6]$ with M = Mo, W reveal a broad excitation spectrum, expanding between 350 and 650 nm for the Mo compound with an emission maximum centered at 712 nm (Figure 4). Quite similar emission maxima at 687 and 672 nm are reported for $Na_2[Mo_6I_8(N_3)_6]$ and $Na_2[Mo_6I_8(NCS)_6]$ in water.[1j] The shift in the maximum emission could be due to partial hydrolysis.[12c] The emission of the M = tungsten compound is significantly broader, as typical for tungsten clusters of this type, with an emission maximum near 692 nm (Figure 4). Luminescence measurements under variable oxygen gas partial pressure indicate only little quenching behavior, due to the presence of oxygen, in the order of 3 % for the tungsten and 10 % for the molybdenum species, showing that both compounds retain almost their full phosphorescence intensity in air, without relevant generation of singlet oxygen (Figures S1 and S2, Supporting Information). For comparison, oxygen quenching of the phosphorescence in solid $(^nBu_4N)_2[Mo_6I_8(OOCCF_3)_6]$ has been shown to be in the order of 90 %.[1r]

This weak quenching behavior is also confirmed by the recorded decay curves (Figures S1 and S2), i.e. the decay time of the molybdenum species decreases from 187 µs in pure nitrogen to 180 µs in pure oxygen. The difference in decay time for the tungsten species is even smaller, i.e. within the limits of the experimental accuracy level and thus in line with the very little photoluminescence quenching caused by oxygen.

Conclusions

The vast majority of $[M_6I_8L_6]^{2-}$ clusters with M = Mo and W are characterized by L being an organic ligand being attached to apical cluster positions by an M–O bond. The presence of a cyanato in an apical cluster position resembles a purely inorganic cluster anion, showing a M–NCO connectivity. Luminescence studies on the compounds $(^nBu_4N)_2[M_6I_8(NCO)_6]$ with M = Mo, W reveal generally similar features. The materials behave strongly luminescent with only small phosphorescence quenching by the presence of molecular oxygen. The M = Mo compound shows an extremely wide excitation spectrum into the regions of visible light with a maximum between 550 and 575 nm and strong phosphorescence centered around 700–750 nm slightly quenched by molecular oxygen.

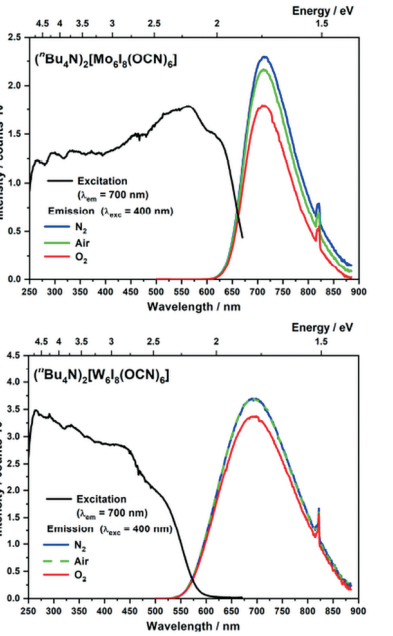

Figure 4. Excitation and emission spectra of $(^nBu_4N)_2[M_6I_8(OCN)_6]$ with M = Mo, W.

Experimental Section

$Cs_2[W_6I_{14}]$: Powder samples of $Cs_2[W_6I_{14}]$ were prepared according to literature starting from a halide exchange of WCl_6 and SiI_4 under inert gas conditions.[1q]

$Cs_2[Mo_6I_{14}]$: CsI, molybdenum, iodine and were weighed with a 2 : 6 : 12 stoichiometric ratio into a mortar and ground in an argon atmosphere (total mass 1.0 g). The mixture was transferred into an 8 cm quartz ampule (V = 10.6 mL) and sealed under vacuum under cooling. The ampule was placed horizontally into a homemade tube furnace with a temperature gradient. The part of the ampule containing the powder was exposed to 700 °C while keeping the colder side of the ampule near room temperature. The duration of this reactions was 30 minutes; the heating and cooling rates 5 K·min^{-1}. At room temperature, the ampule was gently shaken to homogenise the product. The heating and homogenization procedures were repeated three times, giving high yields (> 95 % metals basis). Unreacted iodine deposited at the cold side of the ampule.

(^{n}Bu$_4$N)$_2$[M_6I$_8$(NCO)$_6$] (M = Mo, W): 300 mg of (^{n}Bu$_4$N)$_2$[M_6I$_{14}$] were filled into an inert Schlenk flask and 6 equivalents of the Ag(NCO) were added with 5 mL of dried acetone in an argon flow. The reaction mixture was stirred for 16 h in the dark. The resulting solution was filtered through a 20 µm syringe filter and layered with 3 mL of n-pentane or diethyl ether resulting in red (Mo) and light yellow (W) powders containing single crystals of (^{n}Bu$_4$N)$_2$[M_6I$_8$(NCO)$_6$]. Yields of the crystallizations were 174 mg (70 %) for the Mo and 112 mg (44 %) for the W compound.

Single-Crystal X-ray Diffraction: Single-crystals of both compounds were selected and measured in air with a single-crystal X-ray diffractometer (Stoe, IPDS, Darmstadt, Germany), equipped with (graphite) monochromated Mo-K_α radiation (λ = 0.71073 Å) at 100 K. Crystal structure refinements and solutions were performed with direct methods (SHELXS) and least square refinements on F^2 (SHELXL[13]).

Crystallographic data (excluding structure factors) for the structures in this paper have been deposited with the Cambridge Crystallographic Data Centre, CCDC, 12 Union Road, Cambridge CB21EZ, UK. Copies of the data can be obtained free of charge on quoting the depository numbers CCDC-1903477 for (nBu$_4$N)$_2$[Mo$_6$I$_8$(NCO)$_6$] and CCDC-1983623 for (nBu$_4$N)$_2$[W$_6$I$_8$(NCO)$_6$] (Fax: +44-1223-336-033; E-Mail: deposit@ccdc.cam.ac.uk, http://www.ccdc.cam.ac.uk).

Photoluminescence Studies: Excitation and emission spectra of (^{n}Bu$_4$N)$_2$[M_6I$_8$(NCO)$_6$] with M = Mo, W were collected by using a fluorescence spectrometer FLS920 (Edinburgh Instruments) equipped with a 450 W ozone-free xenon discharge lamp (*OSRAM*) and a cryostat "MicrostatN" from Oxford Instruments as the sample chamber for adjusting the atmosphere during the measurements. Additionally, a mirror optic for powder samples was applied. For detection, an R2658P single-photon-counting photomultiplier tube (Hamamatsu) was used. All photoluminescence spectra were recorded with a spectral resolution of 1 nm, a dwell time of 0.5 s in 1 nm steps and 2 repeats.

Supporting Information (see footnote on the first page of this article): **Table S1**: Structure refinement data of (^{n}Bu$_4$N)$_2$[Mo$_6$I$_8$(OCN)$_6$]. **Table S2**: Structure refinement data of (^{n}Bu$_4$N)$_2$[W$_6$I$_8$(OCN)$_6$]. **Figure S1**: Decay measurement of solid (^{n}Bu$_4$N)$_2$[Mo$_6$I$_8$(OCN)$_6$]. **Figure S2**: Decay measurement of solid (^{n}Bu$_4$N)$_2$[W$_6$I$_8$(OCN)$_6$].

Acknowledgements

ADF thanks the Karl and Anna Buck Stiftung for financial support. Support of this research by the Deutsche Forschungsgemeinschaft (Bonn) through the project ME 914/31-1 is gratefully acknowledged. The authors like to thank *Thorsten Hummel* for his assistance. Open access funding enabled and organized by Projekt DEAL.

Keywords: Cluster; Molybdenum; Tungsten; Luminescence; Quenching by oxygen

References

[1] a) M. A. Mikhaylov, M. A. Sokolov, *Eur. J. Inorg. Chem.* **2019**, *2019*, 4181–4197; b) K. Kirakci, P. Kubat, M. Dusek, K. Fejfarova, V. Sicha, J. Mosinger, K. Lang, *Eur. J. Inorg. Chem.* **2012**, 3107–3111; c) K. Kirakci, P. Kubat, J. Langmaier, T. Polivka, M. Fuciman, K. Fejfarova, K. Lang, *Dalton Trans.* **2013**, *42*, 7224–7232; d) M. N. Sokolov, M. A. Mikhailov, K. A. Brylev, A. V. Virovets, C. Vicent, N. B. Kompankov, N. Kitamura, V. P. Fedin, *Inorg. Chem.* **2013**, *52*, 12477–12481; e) M. N. Sokolov, M. A. Mikhailov, A. V. Virovets, K. A. Brylev, R. A. Bredikhin, A. M. Maksimov, V. E. Platonov, V. P. Fedin, *Russ. Chem. Bull.* **2013**, *62*, 1764–1767; f) O. A. Efremova, M. A. Shestopalov, N. A. Chirtsova, A. I. Smolentsev, Y. V. Mironov, N. Kitamura, K. A. Brylev, A. J. Sutherland, *Dalton Trans.* **2014**, *43*, 6021–6025; g) K. Kirakci, K. Fejfarova, M. Kucerakova, K. Lang, *Eur. J. Inorg. Chem.* **2014**, *2014*, 2331–2336; h) K. Kirakci, V. Sicha, J. Holub, P. Kubat, K. Lang, *Inorg. Chem.* **2014**, *53*, 13012–13018; i) K. Kirakci, P. Kubat, K. Fejfarova, J. Martincik, M. Nikl, K. Lang, *Inorg. Chem.* **2016**, *55*, 803–809; j) K. Kirakci, P. Kubat, M. Kucerakova, V. Sicha, H. Gbelcova, P. Lovecka, P. Grznarova, T. Ruml, K. Lang, *Inorg. Chim. Acta* **2016**, *441*, 42–49; k) M. A. Mikhailov, K. A. Brylev, P. A. Abramov, E. Sakuda, S. Akagi, A. Ito, N. Kitamura, M. N. Sokolov, *Inorg. Chem.* **2016**, *55*, 8437–8445; l) M. A. Mikhailov, K. A. Brylev, A. V. Virovets, M. R. Gallyamov, I. Novozhilov, M. N. Sokolov, *New J. Chem.* **2016**, *40*, 1162–1168; m) L. Riehl, M. Ströbele, D. Enseling, T. Jüstel, H.-J. Meyer, *Z. Anorg. Allg. Chem.* **2016**, *642*, 403–408; n) A.-D. Fuhrmann, A. Seyboldt, A. Schank, G. Zitzer, B. Speiser, D. Enseling, T. Jüstel, H.-J. Meyer, *Eur. J. Inorg. Chem.* **2017**, *2017*, 4259–4266; o) E. V. Svezhentseva, A. O. Solovieva, Y. A. Vorotnikov, O. G. Kurskaya, K. A. Brylev, A. R. Tsygankova, M. V. Edeleva, S. N. Gyrylova, N. Kitamura, O. A. Efremova, M. A. Shestopalov, Y. V. Mironov, A. M. Shestopalov, *New J. Chem.* **2017**, *41*, 1670–1676; p) N. A. Vorotnikova, A. Y. Alekseev, Y. A. Vorotnikov, D. V. Evtushok, Y. Molard, M. Amela-Cortes, S. Cordier, A. I. Smolentsev, C. G. Burton, P. M. Kozhin, P. Zhu, P. D. Topham, Y. V. Mironov, M. Bradley, O. A. Efremova, M. A. Shestopalov, *Mater. Sci. Eng. C* **2019**, *105*, 110150; q) T. Hummel, M. Ströbele, D. Schmid, D. Enseling, T. Jüstel, H.-J. Meyer, *Eur. J. Inorg. Chem.* **2016**, *2016*, 5063–5067; r) L. Riehl, A. Seyboldt, M. Ströbele, D. Enseling, T. Jüstel, M. Westberg, P. R. Ogilby, H.-J. Meyer, *Dalton Trans.* **2016**, *45*, 15500–15506.

[2] T. G. Gray, *Chem. Eur. J.* **2009**, *15*, 2581–2593.

[3] a) D. V. Evtushok, A. R. Melnikov, N. A. Vorotnikova, Y. A. Vorotnikov, A. A. Ryadun, N. V. Kuratieva, K. V. Kozyr, N. R. Obedinskaya, E. I. Kretov, I. N. Novozhilov, Y. V. Mironov, D. V. Stass, O. A. Efremova, M. A. Shestopalov, *Dalton Trans.* **2017**, *46*, 11738–11747; b) A. Seyboldt, D. Enseling, T. Jüstel, M. Ivanovic, H. Peisert, T. Chasse, H.-J. Meyer, *Eur. J. Inorg. Chem.* **2017**, *2017*, 5387–5394.

[4] a) M. Ströbele, R. Thalwitzer, H.-J. Meyer, *Inorg. Chem.* **2016**, *55*, 12074–12078; b) Z. G. Aliev, L. A. Klinkova, I. V. Dubrovin, L. O. Atovmyan, *Zh. Neorg. Khim.* **1981**, *26*, 1964–1967.

[5] M. K. Simsek, W. Preetz, *Z. Anorg. Allg. Chem.* **1997**, *623*, 515–523.

[6] a) C. S. Weinert, C. L. Stern, D. F. Shriver, *Inorg. Chim. Acta* **2000**, *307*, 139–143; b) C. S. Weinert, C. L. Stern, D. F. Shriver, *Inorg. Chem.* **2000**, *39*, 240–246.

[7] D. Bublitz, W. Preetz, M. K. Simsek, *Z. Anorg. Allg. Chem.* **1997**, *623*, 1–7.

[8] R. Ramirez-Tagle, R. Arratia-Perez, *Chem. Phys. Lett.* **2008**, *455*, 38–41.

[9] a) J. Holmehave, S. K. Pedersen, H. H. Jensen, P. R. Ogilby, *Arkivoc* **2015**, 52–64; b) J. A. Jackson, M. D. Newsham, C. Worsham, D. G. Nocera, *Chem. Mater.* **1996**, *8*, 558–564; c) M. Bregnhoj, K. Strunge, R. J. Sorensen, M. Ströbele, T. Hummel, H.-J. Meyer, F. Jensen, P. R. Ogilby, *J. Phys. Chem. A* **2019**, *123*, 1730–1739.

[10] Y. A. Vorotnikov, O. A. Efremova, I. N. Novozhilov, V. V. Yanshole, N. V. Kuratieva, K. A. Brylev, N. Kitamura, Y. V. Mironov, M. A. Shestopalov, *J. Mol. Struct.* **2017**, *1134*, 237–243.

[11] A. Barras, S. Cordier, R. Boukherroub, *Appl. Catal. B* **2012**, *123*, 1–8.

[12] a) C. Neaime, M. Amela-Cortes, F. Grasset, Y. Molard, S. Cordier, B. Dierre, M. Mortier, T. Takei, K. Takahashi, H. Haneda, M. Verelst, S. Lechevallier, *Phys. Chem. Chem. Phys.*

2016, *18*, 30166–30173; b) K. Kirakci, J. Zelenka, M. Rumlova, J. Cvacka, T. Ruml, K. Lang, *Biomater. Sci.* **2019**, *7*, 1386–1392; c) E. V. Svezhentseva, Y. A. Vorotnikov, A. O. Solovieva, T. N. Pozmogova, I. V. Eltsov, A. A. Ivanov, D. V. Evtushok, S. M. Miroshnichenko, V. V. Yanshole, C. J. Eling, A. M. Adawi, J. S. G. Bouillard, N. V. Kuratieva, M. S. Fufaeva, L. V. Shestopalova, Y. V. Mironov, O. A. Efremova, M. A. Shestopalov, *Chem. Eur. J.* **2018**, *24*, 17915–17920.

[13] a) G. M. Sheldrick, University of Göttingen **1997**; b) G. M. Sheldrick, *Acta Crystallogr., Sect. A* **2008**, *64*, 112–122.

Received: May 9, 2020
Published Online: October 2, 2020

Z. Anorg. Allg. Chem. **2020** · ISSN 0044–2313

SUPPORTING INFORMATION

Title: Synthesis, Crystal Structure, and Luminescence of Metal Iodide Cluster Compounds $(n\mathrm{Bu_4N})_2[M_6\mathrm{I_8}(\mathrm{NCO})_6]$ with M = Mo, W
Author(s): A.-D. Fuhrmann, F. Pachel, M. Ströbele, D. Enseling, T. Jüstel, H.-J. Meyer*
Ref. No.: z202000209

Synthesis, Crystal Structure and Luminescence of Metal Iodide Cluster Compounds (^{n}Bu$_4$N)$_2$[M_6I$_8$(NCO)$_6$] with M = Mo, W

Arin-Daniel Fuhrmann,[a] Florian Pachel,[a] Markus Ströbele,[a] David Enseling,[b] Thomas Jüstel[b] and Hans-Jürgen Meyer[a]*

* E-Mail: juergen.meyer@uni-tuebingen.de, Prof. Dr. Hans-Jürgen Meyer

[a] Section for Solid State and Theoretical Inorganic Chemistry, Institute of Inorganic Chemistry, University of Tübingen, Auf der Morgenstelle 18, 72076 Tübingen, Germany.

[b] Department of Chemical Engineering, Münster University of Applied Science, Stegerwaldstraße 39, 48565 Steinfurt, Germany.

Table S1: Structure refinement data of $(^{n}Bu_4N)_2[Mo_6I_8(NCO)_6]$.

Identification code	CCDC 1903477
Empirical formula	$(^{n}Bu_4N)_2[Mo_6I_8(NCO)_6]$
Formula weight / g·mol^{-1}	2327.88
Temperature / K	100(2)
Wavelength / pm	71.073
Crystal system	Triclinic
Space group	$P\bar{1}$
Unit cell dimensions / pm	a = 1199.00(5)
	b = 1214.49(6)
	c = 1239.41(6)
	α = 92.366(1)°
	β = 102.280(1)°
	γ = 118.896(1)°
Volume / pm^3	1521.9(1)
Z	1
Density (calculated) / g·cm^{-3}	2.540
Absorption coefficient / mm^{-1}	5.301
F(000)	1080
Crystal size / mm^3	0.384 x 0.068 x 0.057
Theta range for data collection	1.943 to 25.022°
Index ranges	-14 ≤ h ≤ 14, -14 ≤ k ≤ 14, -14 ≤ l ≤ 14
Reflections collected	54260
Independent reflections	5375 [R(int) = 0.0289]
Completeness to theta = 25.022°	100.0 %
Absorption correction	Numerical
Max. and min. transmission	0.7458 and 0.5257
Refinement method	Full-matrix least-squares on F^2
Data / restraints / parameters	5375 / 0 / 442
Goodness-of-fit on F^2	1.121
Final R indices [I > 2σ(I)]	R_1 = 0.0231, wR_2 = 0.0550
R indices (all data)	R_1 = 0.0252, wR_2 = 0.0566
Largest diff. peak and hole / e.Å^{-3}	1.485 and -0.816

Table S2: Structure refinement data of $(^{n}Bu_4N)_2[W_6I_8(NCO)_6]$.

Identification code	CCDC 1983623
Empirical formula	$(^{n}Bu_4N)_2[W_6I_8(NCO)_6]$
Formula weight / g·mol^{-1}	2855.33
Temperature / K	296(2)
Wavelength / pm	71.073
Crystal system	Triclinic
Space group	$P\bar{1}$
Unit cell dimensions / pm	a = 1208.36(6)
	b = 1216.32(7)
	c = 1236.28(7)
	α = 92.232(1)°
	β = 102.141(1)°
	γ = 118.741(1)°
Volume / pm^3	1536.6(2)
Z	1
Density (calculated) / g·cm^{-3}	3.086
Absorption coefficient / mm^{-1}	15.246
F(000)	1272
Crystal size / mm^3	0.24 x 0.2 x 0.08
Theta range for data collection	1.991 to 25.022°
Index ranges	$-14 \le h \le 14$, $-14 \le k \le 14$, $-14 \le l \le 14$
Reflections collected	39370
Independent reflections	5432 [R(int) = 0.0546]
Completeness to theta = 25.022°	99.9 %
Absorption correction	Numerical
Max. and min. transmission	0.2063 and 0.0616
Refinement method	Full-matrix least-squares on F^2
Data / restraints / parameters	5432 / 0 / 302
Goodness-of-fit on F^2	1.104
Final R indices [I > 2σ(I)]	R_1 = 0.0454, wR_2 = 0.1101
R indices (all data)	R_1 = 0.0595, wR_2 = 0.1265
Largest diff. peak and hole / e.Å^{-3}	4.041 and -2.371

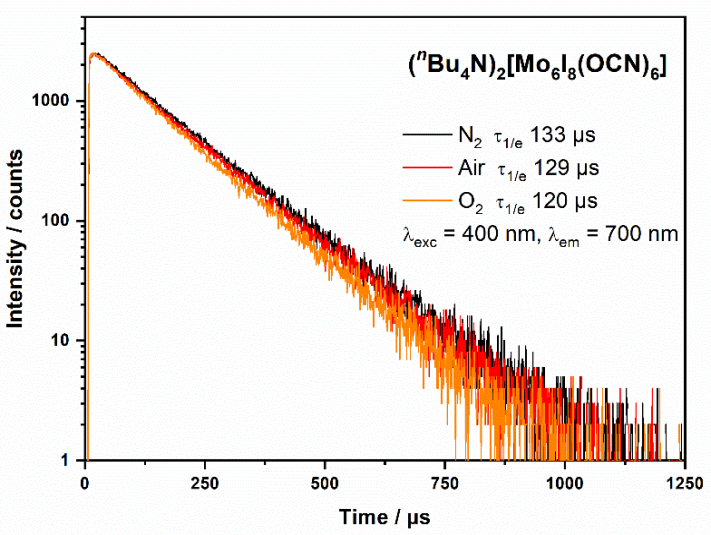

Figure S1: Decay measurement of solid $(^{n}Bu_4N)_2[Mo_6I_8(NCO)_6]$.

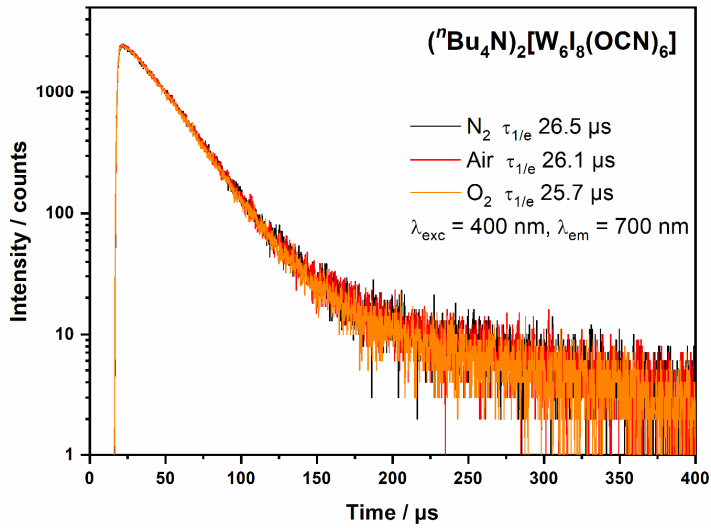

Figure S2: Decay measurement of solid $(^{n}Bu_4N)_2[W_6I_8(NCO)_6]$.

Publication 5

Crystal structure, Magnetic and Photoluminescence Properties of GdW_6Cl_{15}, TbW_6Cl_{15}, and EuW_6Cl_{14}

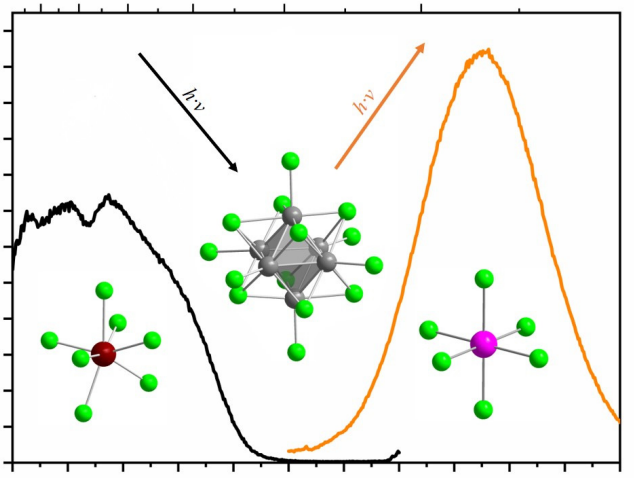

https://doi.org/10.1002/zaac.202100046

Z. Anorg. Allg. Chem. ***2021****, 647, 1392–1396*

Journal of Inorganic and General Chemistry
ZAAC
Zeitschrift für anorganische und allgemeine Chemie

DOI: 10.1002/zaac.202100046

ARTICLE

Crystal structure, Magnetic and Photoluminescence Properties of GdW_6Cl_{15}, TbW_6Cl_{15}, and EuW_6Cl_{14}

Florian Pachel,[a] Markus Ströbele,[a] David Enseling,[b] Thomas Jüstel,[b] and Hans-Jürgen Meyer*[a]

Ternary compounds with the $[M_6X_{14}]^{2-}$ (M=Mo, W; X=Cl, Br, I) cluster have been established with several counter cations. Herein, we report examples of the ternary rare-earth (RE) compounds REW_6Cl_{15} and REW_6Cl_{14}. Preparations of the compounds GdW_6Cl_{15}, TbW_6Cl_{15} and EuW_6Cl_{14} are accomplished by solid-state reactions of W_6Cl_{12} and $RECl_3$ (RE=Gd, Tb), or $EuCl_2$ at 575 °C in fused silica tubing. GdW_6Cl_{15} and TbW_6Cl_{15} crystallize in the space group $C2/c$ and EuW_6Cl_{14} in $Pn\bar{3}$, isotypic to BiW_6Cl_{15} (REW_6Cl_{15}) and $PbMo_6Cl_{15}$ (EuW_6Cl_{14}) according to X-ray powder diffraction. Crystal structures are discussed in the light of related compounds, and properties such as magnetism and photoluminescence are reported.

Introduction

Metal-rich tungsten and molybdenum(II) halides form characteristic $[M_6X_{14}]^{2-}$ cluster units (M=Mo, W; X=Cl, Br, I) which have been established in many ways.[1] Their structures are characterized by the $[M_6X_8^iX_6^a]^{2-}$ clusters with an octahedral metal cluster core M_6, surrounded by eight inner (X^i) halides as $[M_6X_8^i]$ and six outer halides (X^a) located over each cluster vertex.[2]

The most interesting feature of compounds with the $[M_6X_{14}]^{2-}$ cluster is their photoluminescence, which can be described as follows: photoexcitation involves an S_0 to S_m transition, followed by intersystem crossing (ISC) into triplet states and relaxation via phosphorescence.[1c,3] These properties are obtained for clusters in solution and in solid state. Iodide species, $[M_6I_{14}]^{2-}$ have shown the strongest emission properties among halides, and thus attracted most attention.[1e] Compounds with $[W_6I_{14}]^{2-}$ clusters typically show broad absorption bands in the region 250–500 nm and emission bands in the order of 700 nm in solid state and in solution.[1e,4]

Crystal structures of ternary compounds with the $[W_6I_{14}]^{2-}$ cluster have been reported with monovalent cations (A=Li, Na, K, Rb, Cs, Ag) as $A_2[W_6I_{14}]$,[4a,5] and divalent cations (AE=Mg, Ca, Sr, Ba) as $AE[W_6I_{14}]$.[4b]

Solid-state phosphorescence properties of alkali und alkaline earth compounds, $A_2[W_6I_{14}]$ and $AE[W_6I_{14}]$ have been reported. However, their emission intensities were rather weak, explained by the poor transparency of crystalline materials, and significant thermal quenching obtained in photoluminescence studies.[4a,b]

Significantly higher emission intensities were obtained for compounds with monovalent organic cations (TBA^+ = tetrabutylammonium, PPh_4^+ = tetraphenylphosphonium, PPN^+ = bis(triphenylphosphane)iminium).[1e,4c] These compounds, in which the clusters are well separated by the bulky organic cations, show less thermal quenching, and the luminescence quantum yield of $(PPN)_2[W_6I_{14}]$ was reported at 42 %.[4c]

The combination of an octahedral metal halide cluster with a luminescent rare earth ion was recently reported for RE=Nd and Yb in supramolecular assemblies [Crypt-RE]-$[W_6I_{14}]$, to show interesting intermolecular interactions between cluster and rare earth ion.[6]

Herein, we report on the synthesis and structural characterization of three rare-earth tungsten chloride clusters because chlorides provide higher optical transparency, when compared to iodides. Crystal structures of GdW_6Cl_{15}, TbW_6Cl_{15} and EuW_6Cl_{14} are reported with their magnetic and photoluminescence properties.

Results and Discussion

The synthesis of the title compounds was achieved by solid-state reactions between $RECl_3$ (RE=Gd, Tb) or $EuCl_2$ and W_6Cl_{12}. Products were obtained at 575 °C. Reactions of $GdCl_3$ and $TbCl_3$ with W_6Cl_{12} yielded the compounds GdW_6Cl_{15} and TbW_6Cl_{15}. Preparations with $EuCl_2$ as a starting material yielded EuW_6Cl_{14} as main product, but the formation of EuW_6Cl_{14} also took place when $EuCl_3$ was employed as reactant. Excess of rare-earth halides appeared useful to ensure complete conversions of W_6Cl_{12} in reactions, which were later removed by rinsing the reaction product with dry acetonitrile.

[a] F. Pachel, Dr. M. Ströbele, H.-J. Meyer
Section for Solid State and Theoretical Inorganic Chemistry, Institute of Inorganic Chemistry, University of Tübingen, Auf der Morgenstelle 18, 72076 Tübingen, Germany
E-mail: juergen.meyer@uni-tuebingen.de
[b] Dr. D. Enseling, Prof. Dr. T. Jüstel
Department of Chemical Engineering, Münster University of Applied Science, Stegerwaldstraße 39, 48565 Steinfurt, Germany.

Supporting information for this article is available on the WWW under https://doi.org/10.1002/zaac.202100046

The powder X-ray diffraction (PXRD) patterns for GdW_6Cl_{15} and TbW_6Cl_{15} were indexed in the monoclinic space group *C2/c* (No.13), and the PXRD pattern of EuW_6Cl_{14} was indexed in the cubic space group *Pn* $\bar{3}$ (No. 201). Crystal structures of GdW_6Cl_{15} and TbW_6Cl_{15} are found isotypic to BiW_6Cl_{15}[7] and the pattern of EuW_6Cl_{14} was refined isotypic to $PbMo_6Cl_{14}$.[8] The crystal structures were refined on the basis of PXRD data (Figure 1, S1 and S2).

The structures of the REW_6Cl_{15} compounds contain $[W_6Cl_{14}]^{2-}$ clusters and $(RECl)^{2+}$ (*RE*=Gd and Tb) units (Figure 2). Each *RE* ion is surrounded by a total of seven chloride ions; six chloride ions are outer ligands (Cl^a) of the cluster and one *lonely* chloride is linked to the *RE* cation only. Gd–Cl distances are observed in the range between 2.665(2)–2.936(2) Å, of which the shortest Gd–Cl distance represents the *lonely* chloride ion of $(GdCl)^{2+}$. For TbW_6Cl_{15} the results are similar with Tb–Cl distances in the range of 2.621(2)–2.915(1) Å. Comparable results were previously reported for Bi–Cl distances in BiW_6Cl_{15} and $BiMo_6Cl_{15}$.[7] The general arrangement of $[W_6Cl_{14}]^{2-}$ clusters and $(RECl)^{2+}$ units in the crystal structure can be derived from the motif of a distorted rock-salt super-structure (Figure 3), in the sense that the centers of gravity of RE^{3+} ions and cluster anions occupy positions similar to those of Na^+ and Cl^- in the NaCl structure.

The crystal structure of EuW_6Cl_{14} contains $[W_6Cl_{14}]^{2-}$ clusters and Eu^{2+} ions. The europium ion is coordinated by six outer chlorido ligands (Figure 2) of six different clusters. The arrangement of $[W_6Cl_{14}]^{2-}$ (centers of gravity) and Eu^{2+} ions in the structure of EuW_6Cl_{14} also follows the motif of the rock salt structure (Figure 4). Some crystallographic data are given in Table 1.

Magnetic measurements of all three compounds in the temperature region 5–300 K show linear dependencies of $1/\chi$ on T, indicating a paramagnetic behavior (Figure 5, S3 and S4). Experimental magnetic moments for TbW_6Cl_{15} 10.49 μ_B,

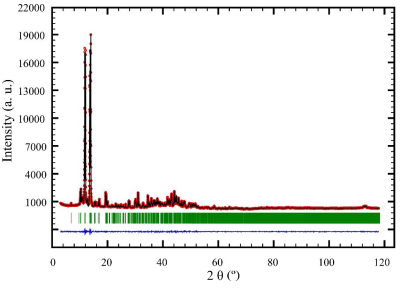

Figure 1. Refined X-ray powder XRD pattern of GdW_6Cl_{15} with space group *C2/c*. Red circles represent measured data points which are superimposed with the calculated powder pattern (black line). Green lines represent the Bragg positions; the difference curve is shown as a blue line.

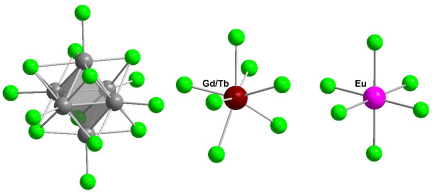

Figure 2. $[W_6Cl_{14}]^{2-}$ cluster (left side), coordination environment of the Gd^{3+} and Tb^{3+}-ions in GdW_6Cl_{15} and TbW_6Cl_{15} (center), and the coordination environment of the Eu^{2+}-ions in EuW_6Cl_{14} (right side). W atoms are displayed in grey, Gd and Tb in red, Cl in green and Eu in pink.

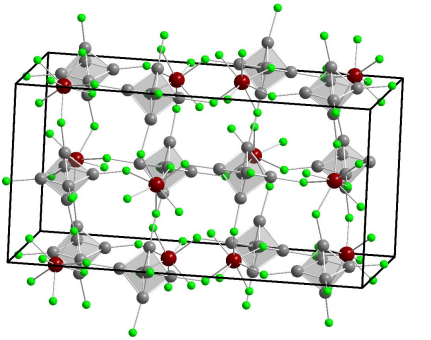

Figure 3. Unit cell of REW_6Cl_{15} (*RE* = Gd, Tb) with inner Cl ligands of the cluster (Cl^i) omitted for clarity. W atoms are displayed in dark grey, RE in red and Cl in green.

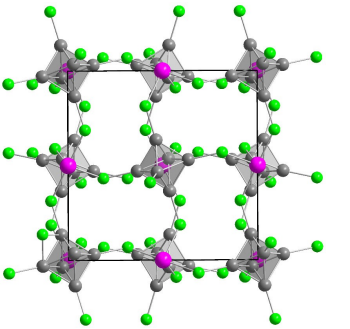

Figure 4. Projected unit cell of EuW_6Cl_{14} with Cl^i omitted for clarity. W atoms are displayed in dark grey, Eu in purple and Cl in green.

Table 1. Crystal data and structure refinement for GdW_6Cl_{15}, TbW_6Cl_{15} and EuW_6Cl_{14} measured at room temperature.

	GdW_6Cl_{15}	TbW_6Cl_{15}	EuW_6Cl_{14}
CCDC No.	1989717	1989650	2000975
Molecular mass/g·mol^{-1}	1792.085	1793.760	1751.304
Wavelength	1.54060	1.54060	1.54060
Space group	*C2/c*	*C2/c*	$Pn\bar{3}$
a/Å	12.6694(2)	12.6592(1)	12.9874(1)
b/Å	13.0418(2)	13.0337(1)	12.9874(1)
c/Å	25.7144(5)	25.6980(1)	12.9874(1)
β/°	92.0182(7)	91.9407(4)	
Volume/Å^3	4246.2(1)	4237.65(4)	2190.60(6)
Z	8	8	4
Absorption coefficient/mm^{-1}	95.408	91.768	92.241
Density (calc.)/g·cm^{-3}	5.607	5.623	5.310
Theta range for data collection/°	1.5–59	1.5–59	1.5–59
Total number of measured reflections	3241	3152	584
Refined structure parameters	79	79	18
R_p, R_{wp}	3.5168 4.5318	2.3885 3.3025	2.2179 3.0700
R_{Bragg}	1.8392	1.7645	1.3011
χ^2	1.1520	1.1465	1.0083

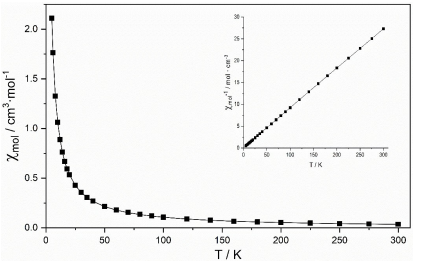

Figure 5. Magnetic susceptibility of GdW_6Cl_{15}.

GdW_6Cl_{15} 9.27 μ_B and EuW_6Cl_{14} 10.07 μ_B are somewhat above the expected values for trivalent/divalent rare earth ions (≈9.7 μ_B for Tb^{3+} and ≈7.9 μ_B for Gd^{3+} and Eu^{2+}).[9] PXRD patterns of the samples used in the magnetic measurements revealed still some small amounts of rare-earth halides (after washing). In spite of the observed deviations of magnetic moments, the presence of a Eu^{2+} ion in EuW_6Cl_{14} is clearly evidenced. The magnetic moments recorded for EuW_6Cl_{14} indicate the presence of around 6 wt% of $EuCl_2$, and some smaller amounts of about 2.5 wt% and 4.5 wt% of $TbCl_3$ and $GdCl_3$ in the crystalline samples of TbW_6Cl_{15} and GdW_6Cl_{15}. The results show no coupling between the magnetic moments of the rare-earth ions, in agreement with the refined crystal structures which show rather isolated Gd^{3+}, Tb^{3+} and Eu^{2+} cation distributions in the structures.

Photoluminescence

Octahedral tungsten halide clusters $[W_6X_{14}]^{2-}$ are known for their photophysical properties. Previously reported alkali salts $Na_{2-x}W_6I_{14}$ and $Cs_2W_6I_{14}$ showing a dark green and orange body color, respectively exhibit broad emission bands peaking at 685 nm and 708 nm. Studies of the luminescence of these compounds were performed at 100 K because of significant thermal quenching at higher temperature.[4a,5] Similar results apply to the alkaline earth salts *AE*$[W_6I_{14}]$ (*AE*=Mg, Ca, Sr, Ba) with green body colors. SrW_6I_{14} and BaW_6I_{14} show an emission band peaking at 630 nm and 644 nm, respectively. The luminescence spectra were also recorded at 100 K because of thermal quenching.[4b]

Previously reported [Crypt-*RE*]-$[W_6I_{14}]$ compounds show efficient energy transfer between the excited cluster and the rare earth ion, demonstrated by the luminescence of *RE*=Yb, Nd.[6]

Luminescence spectra recorded on crystalline powders of TbW_6Cl_{15} and EuW_6Cl_{14} under UV irradiation at λ = 360 nm, display weak deep red luminescence. The excitation and emission properties of both compounds are very similar, exhibiting broad excitation bands between 250 nm and 450 nm and a weak emission band extending from 550 nm to 800 nm, centered around 675 nm (Figure 6, S5). The obtained excitation patterns appear characteristic for $[W_6Cl_4]^{2-}$ clusters, and the weak emission intensity at room temperature can be related to thermal quenching reported earlier.[4a] Moreover, no photoluminescence of the rare earth ions is observed. This can be explained by the rather low energy of the emitting triplet state of the tungsten cluster yielding red phosphorescence as shown above.[10] Energy transfer to the emitting states of Eu^{2+} ($^5F_0$, >25,000 cm^{-1})[11] Tb^{3+} ($^5D_4$, >21,000 cm^{-1}),[12] an Gd^{3+} ($^6P_{7/2}$, >32,000 cm^{-1})[12] is unlikely, since these states are located at higher energy than the emitting triplet state of the tungsten cluster.

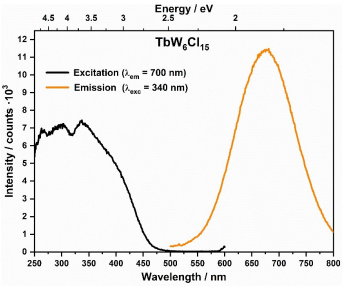

Figure 6. Excitation and emission spectra of TbW_6Cl_{15} at room temperature.

Conclusions

Solid-state syntheses of GdW_6Cl_{15} and TbW_6Cl_{15} were successfully performed to obtain tungsten chloride cluster compounds containing trivalent rare earth ions. Their crystal structures are isotypic to BiW_6Cl_{15}. Additionally, EuW_6Cl_{14} was synthesized with divalent europium having a structure isotypic to $PbMo_6Cl_{14}$. Magnetic measurements show paramagnetic behavior and no coupling between the magnetic moments of the rare earth ions. This can be explained due to the separation of *RE* ions in the crystal structures. Luminescence studies on compounds with *RE*=Tb, Eu reveal broad excitation bands between 250 and 450 nm and weak emission intensities centered around 675 nm. The obtained excitation and emission properties are characteristic for octahedral tungsten halide clusters and comparable to other compounds in the literature, revealing strong thermal quenching at room temperature.[4b]

Experimental Section

W_6Cl_{12} was synthesized according to literature[7] starting from WCl_6 and bismuth powder. BiW_6Cl_{15} was dissolved in concentrated HCl to form $(H_3O)_2W_6Cl_{14}$ and then thermally treated to yield W_6Cl_{12}. $GdCl_3$ powder was purchased from Sigma Aldrich (99.99%), $TbCl_3$ powder (99.9%) from ABCR, $EuCl_2$ powder (99.99%) from Sigma Aldrich, WCl_6 powder (99.9%+) from Acros Organics and bismuth powder (99.99%) from Evochem. The three compounds GdW_6Cl_{15}, TbW_6Cl_{15} and EuW_6Cl_{14} were synthesized starting from 0.1 g W_6Cl_{12} (65 mmol) and 35 mg $GdCl_3$ (130 mmol), 35 mg $TbCl_3$ (130 mmol), 39 mg $EuCl_2$ (130 mmol). W_6Cl_{12} and $RECl_3$ (*RE*=Gd, Tb), or $EuCl_2$ were ground together in a mortar under argon (glovebox) and subsequently sealed in homemade silica ampules under vacuum. Afterwards the ampule was placed in a furnace and heated with a rate of 5 °C/min to 575 °C, kept at this temperature for 24 h before cooling to RT with a rate of 0.5 °C/min. The resulting powder was rinsed with dry acetonitrile under argon (Schlenk technique) to remove the excess of $RECl_3$. The products appeared with beige body colours. Yields after rinsing were 90 mg (77%) for GdW_6Cl_{15}, 94 mg (81%) for TbW_6Cl_{15} and 92 mg (81%) for EuW_6Cl_{14}.

X-Ray Diffraction Studies: Powder XRD patterns of crystalline products were collected with an X-ray diffractometer (Stoe STADI-P, Ge monochromator) using Cu–$K_{\alpha1}$ radiation ($\lambda = 1.540598$ Å) in the range of $3 < 2\theta < 120°$ and a Mythen I Detector. GdW_6Cl_{15} and TbW_6Cl_{15} were indexed isotypically to BiW_6Cl_{15}. EuW_6Cl_{14} was indexed isotypic to $PbMo_6Cl_{14}$. Crystal structures were refined by global refinement (Fullprof Suite[13]). CCDC 1989717 (GdW_6Cl_{15}), 1989650 (TbW_6Cl_{15}) and 2000975 (EuW_6Cl_{14}) contain the supplementary crystallographic data for this paper. These data can be obtained free of charge via www.ccdc.cam.ac.uk/data_request/cif, or by emailing data_request@ccdc.cam.ac.uk, or by contacting The Cambridge Crystallographic Data Centre, 12 Union Road, Cambridge CB2 1EZ, UK; fax: +44 1223 336033.

Magnetic Studies: Magnetic susceptibility measurements of crystalline powders were performed in gelatine capsules between 5 and 300 K with a Quantum design SQUID magnetometer equipped with a 2010 squid controller, a 2000 VHF squid amplifier, a 1802 R/G bridge and a 1822 MDMS controller. The amount of material used for the measurements was 46.4 mg (GdW_6Cl_{15}), 56.2 mg (TbW_6Cl_{15}) and 68.6 mg (EuW_6Cl_{14}).

Photoluminescence Studies: Excitation and emission spectra of TbW_6Cl_{15} and EuW_6Cl_{14} were collected by using a fluorescence spectrometer FLS920 (Edinburgh Instruments) equipped with a 450 W ozone-free xenon discharge lamp (OSRAM). Additionally, a mirror optic for powder samples was applied. For detection, an R2658P single-photon-counting photomultiplier tube (Hamamatsu) was used. All photoluminescence spectra were recorded with a spectral resolution of 1 nm, a dwell time of 0.5 s in 1 nm steps and 2 repeats.

Acknowledgements

Support of this research by the Deutsche Forschungsgemeinschaft (Bonn) through the project ME 914/31-1 is gratefully acknowledged. Open access funding enabled and organized by Projekt DEAL.

Keywords: Tungsten chloride · Cluster · Rare earth · Paramagnetism · Luminescence

[1] a) A. Renaud, F. Grasset, B. Dierre, T. Uchikoshi, N. Ohashi, T. Takei, A. Planchat, L. Cario, S. Jobic, F. Odobel, S. Cordier, *ChemistrySelect* **2016**, *1*, 2284–2289; b) P. Zhang, D. J. Osborn, G. L. Baker, R. N. Ghosh, *IEEE Sens. J.* **2005**, *1–2*, 628–631; c) A. W. Maverick, J. S. Najdzionek, D. Mackenzie, D. G. Nocera, H. B. Gray, *J. Am. Chem. Soc.* **1983**, *105*, 1878–1882; d) J. A. Jackson, C. Turro, M. D. Newsham, D. G. Nocera, *J. Phys. Chem.* **1990**, *94*, 4500–4507; e) T. C. Zietlow, D. G. Nocera, H. B. Gray, *Inorg. Chem.* **1986**, *25*, 1351–1353; f) K. Kirakci, P. Kubat, M. Dusek, K. Fejfarova, V. Sicha, J. Mosinger, K. Lang, *Eur. J. Inorg. Chem.* **2012**, 3107–3111; g) M. A. Mikhailov, K. A. Brylev, P. A. Abramov, E. Sakuda, S. Akagi, A. Ito, N. Kitamura, M. N. Sokolov, *Inorg. Chem.* **2016**, *55*, 8437–8445; h) A. O. Solovieva, Y. A. Vorotnikov, K. E. Trifonova, O. A. Efremova, A. A. Krasilnikova, K. A. Brylev, E. V. Vorontsova, P. A. Avrorov, L. V. Shestopalova, A. F. Poveshchenko, *J. Mater. Chem. B* **2016**, *4*, 4839–4846; i) E. V. Svezhentseva, Y. A. Vorotnikov, A. O. Solovieva, T. N. Pozmogova, I. V. Eltsov, A. A. Ivanov, D. V. Evtushok, S. M. Miroshnichenko, V. V. Yanshole, C. J. Eling, A. M. Adawi, J. S. G. Bouillard, N. V. Kuratieva, M. S. Fufaeva, L. V. Shestopalova, Y. V. Mironov, O. A. Efremova, M. A. Shestopalov, *Chem. Eur. J.* **2018**, *24*, 17915–17920.

[2] H. Schäfer, H. G. von Schnering, J. Tillack, F. Kuhnen, H. Wöhrle, H. Baumann, *Z. Anorg. Allg. Chem.* **1967**, *353*, 281–310.

[3] a) A. W. Maverick, H. B. Gray, *J. Am. Chem. Soc.* **1981**, *103*, 1298–1300; b) T. Azumi, Y. Saito, *J. Phys. Chem.* **1988**, *92*, 1715–1721.

[4] a) T. Hummel, M. Ströbele, D. Schmid, D. Enseling, T. Jüstel, H.-J. Meyer, *Eur. J. Inorg. Chem.* **2016**, *2016*, 5063–5067; b) T. Hummel, A. Mos-Hummel, M. Ströbele, H.-J. Meyer, *Z. Anorg. Allg. Chem.* **2019**, *645*, 831–834; c) T. Hummel, M. Ströbele, A. D. Fuhrmann, D. Enseling, T. Jüstel, H.-J. Meyer, *Eur. J. Inorg. Chem.* **2019**, *2019*, 4014–4019.

[5] T. Hummel, A. Mos-Hummel, A. Merkulova, M. Ströbele, A. Krishnamurthy, S. Kroeker, H.-J. Meyer, *Inorg. Chem.* **2018**, *57*, 2570–2576.

[6] T. Hummel, W. Leis, A. Eckhardt, M. Ströbele, D. Enseling, T. Jüstel, H.-J. Meyer, *Dalton Trans.* **2020**.

[7] M. Ströbele, T. Jüstel, H. Bettentrup, H.-J. Meyer, *Z. Anorg. Allg. Chem.* **2009**, *635*, 822–827.

[8] a) S. Böschen, H. L. Keller, *Z. Kristallogr.* **1992**, *200*, 305–315; b) M. Potel, C. Perrin, A. Perrin, M. Sergent, *Mat. Res. Bull.* **1986**,

21, 1239–1245; c) S. Ihmaine, C. Perrin, M. Sergent, E. H. El Ghadraoui, *Ann. Chim. Sci. Mat.* **1998**, *23*, 187–190.

[9] a) S. Arajs, R. Colvin, *J. Appl. Phys.* **1961**, *32*, 336–337; b) W. Klemm, H. Bommer, *Z. Anorg. Allg. Chem.* **1937**, *231*, 138–171; c) F. Spedding, S. Legvold, A. Daane, L. Jennings, in *Progress in low temperature physics, Vol. 2*, Elsevier, **1957**, pp. 368–394.

[10] L. Riehl, A. Seyboldt, M. Ströbele, D. Enseling, T. Jüstel, M. Westberg, P. R. Ogilby, H.-J. Meyer, *Dalton Trans.* **2016**, *45*, 15500–15506.

[11] M. J. Freiser, S. Methfessel, F. Holtzberg, *J. Appl. Phys.* **1968**, *39*, 900–902.

[12] G. Blasse, B. C. Grabmaier, in *Luminescent materials*, 1 ed., Springer, Heidelberg-Berlin, **1994**, pp. 25–27.

[13] T. Roisnel, J. Rodriguez-Carvajal, *Proceedings of the Seventh European Powder Diffraction Conference (EPDIC7)* **2000**, *118*.

Manuscript received: February 11, 2021
Revised manuscript received: March 22, 2021

Zeitschrift für anorganische und allgemeine Chemie

Supporting Information

Crystal structure, Magnetic and Photoluminescence Properties of GdW_6Cl_{15}, TbW_6Cl_{15}, and EuW_6Cl_{14}

Florian Pachel, Markus Ströbele, David Enseling, Thomas Jüstel, and Hans-Jürgen Meyer*

Crystal structure, Magnetic and Photoluminescence properties of GdW_6Cl_{15}, TbW_6Cl_{15} and EuW_6Cl_{14}

Florian Pachel,[a] Markus Ströbele,[a] David Enseling,[b] Thomas Jüstel[b] and Hans-Jürgen Meyer*[a]

* Prof. Dr. Hans-Jürgen Meyer, E-Mail: juergen.meyer@uni-tuebingen.de

[a] Section for Solid State and Theoretical Inorganic Chemistry, Institute of Inorganic Chemistry, University of Tübingen, Auf der Morgenstelle 18, 72076 Tübingen, Germany.

[b] Department of Chemical Engineering, Münster University of Applied Science, Stegerwaldstraße 39, 48565 Steinfurt, Germany.

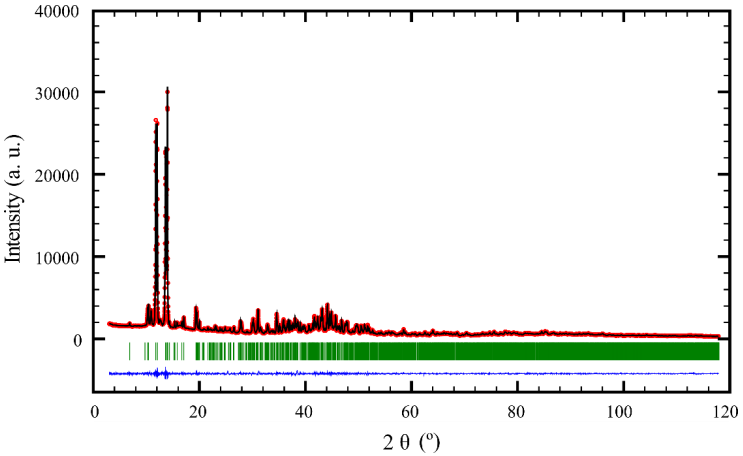

Figure S1. Fitted powder XRD pattern of TbW_6Cl_{15} with space group *C2/c*. Red circles represent measured data points which are superimposed with the calculated powder pattern (black line). Green lines represent the Bragg positions; the difference curve is shown as a blue line.

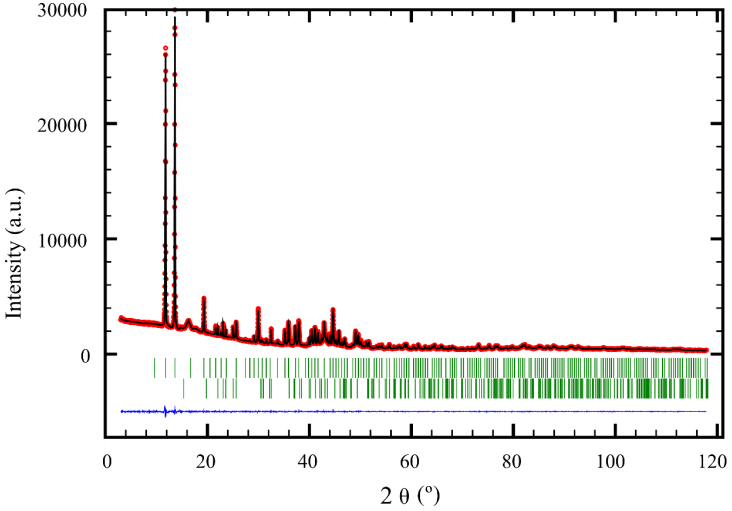

Figure S2. Fitted powder XRD pattern of EuW_6Cl_{14} with space group *Pn-3.* Red circles represent measured data points which are superimposed with the calculated powder pattern (black line). Green lines represent the Bragg positions of EuW_6Cl_{14} (top) and $EuCl_2$ (bottom); the difference curve is shown as a blue line.

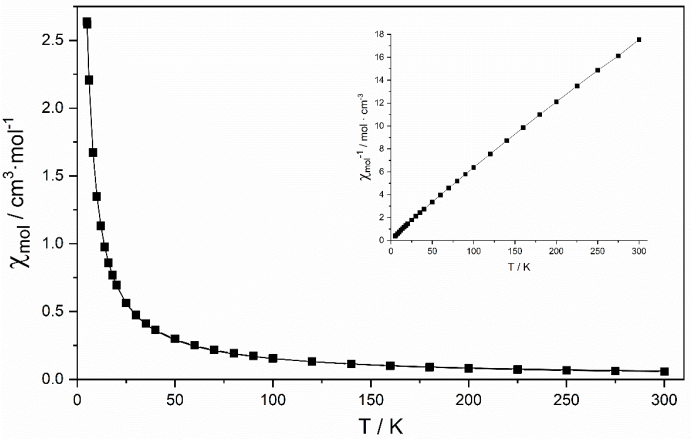

Figure S3. Magnetic susceptibility of TbW_6Cl_{15}.

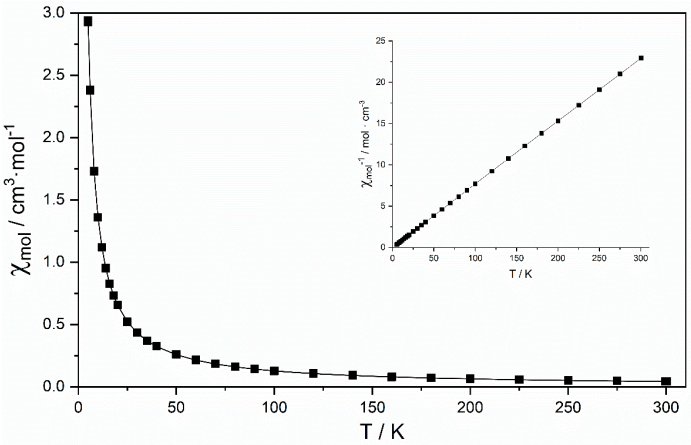

Figure S4. Magnetic susceptibility of EuW_6Cl_{14}.

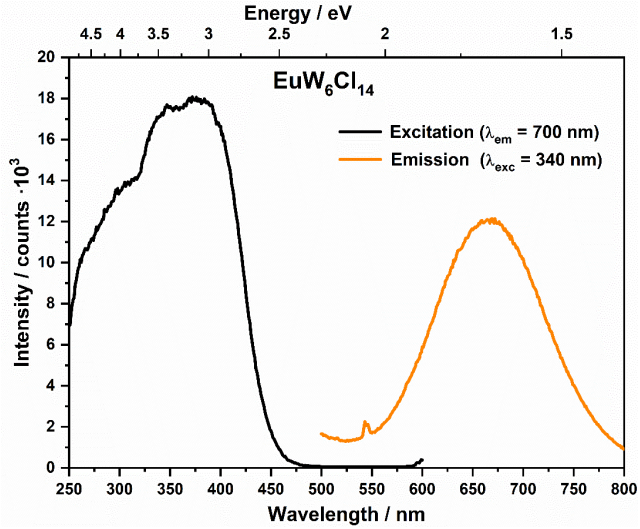

Figure S5. Excitation and emission spectra of EuW_6Cl_{14}.